IEEE Access
Multidisciplinary ⋮ Rapid Review ⋮ Open Access Journal

Received 30 June 2023, accepted 25 July 2023, date of publication 1 August 2023, date of current version 11 August 2023.

Digital Object Identifier 10.1109/ACCESS.2023.3300475

SURVEY

A Comprehensive Review of the Recent Development of Wireless Power Transfer Technologies for Electric Vehicle Charging Systems

AMRITANSH SAGAR[1], (Student Member, IEEE), ARUN KASHYAP[2], MORTEZA AZIMI NASAB[3], (Member, IEEE), SANJEEVIKUMAR PADMANABAN[3], (Senior Member, IEEE), MANUELE BERTOLUZZO[1], ABHAY KUMAR[1], AND FREDE BLAABJERG[4], (Fellow, IEEE)

[1]Department of Industrial Engineering, University of Padua, 35131 Padua, Italy
[2]Department of Applied Computational Science and Engineering, GL Bajaj Institute of Technology and Management, Greater Noida 201306, India
[3]Department of Electrical Engineering, IT and Cybernetic, University of South-Eastern Norway, 3918 Porsgrunn, Norway
[4]Centre for Reliable Power Electronics (CoRPE), Department of Energy Engineering, Aalborg University, 9220 Aalborg, Denmark

Corresponding authors: Amritansh Sagar (amritansh.sagar@studenti.unipd.it) and Manuele Bertoluzzo (manuele.bertoluzzo@unipd.it)

This work was supported by the Università degli Studi di Padova.

ABSTRACT The expanding Electric vehicle (EV) market is fueled by the need for more efficient and dependable ways to recharge the battery. By eradicating the necessity for direct physical interaction between vehicles and charge equipment, the Wireless Power Transfer (WPT) methodology eliminates the drawbacks and risks associated with the conventional conductive system. The innovative WPT technique replaces the conductive charging system to keep a similar power rating and efficiency. Numerous strategies have been created to improve the effectiveness and dependability of the WPT model. As a result, this review article thoroughly analyses current major research literatures that describe WPT technologies for EV charging. The papers are classified based on various coupling types along with magnetic couplers and shielding, compensation, misalignment tolerance and control methods in WPT systems. In addition, the possible research gaps and the challenges associated with the existing works of WPT systems are discussed. The reviewed results are analyzed based on performance metrics and implementation tools attained using above classifications and EMF exposure references employed in the WPT system. The comparative effectiveness is presented in the tables, diagrams, as well as interconnections for ease of presentation and conceptual understanding. The core asset of this article lies in the fact that the findings offer a good ''one-stop'' resource including both aspects of the system and with regard to the power stage. This review article also emphasizes the potential and obstacles of inductive wireless EV battery chargers. A developer can find this study will contribute substantially to selecting an optimum design for the enhancement of the WPT system.

INDEX TERMS Capacitive power transfer, compensation, control, coupling, electric vehicle charging, inductive resonant power transfer, wireless power transfer.

NOMENCLATURE

Abbreviations	Descriptions
AC	Alternating Current.
ARIB	Association of Radio Industries and Businesses.
BMS	Battery Management Systems.
CC	Constant Current.
CISPR	International Special Committee on Radiofrequency Interference.
CPT	Capacitive Power Transfer.
CV	Constant Voltage.
DC	Direct Current.
DSP	Digital Signal Processor.

The associate editor coordinating the review of this manuscript and approving it for publication was Luyu Zhao.

DWPT	Dynamic Wireless Power Transfer.
EMF	Electromagnetic Field.
FHA	Fundamental Harmonic Approximation.
FWNC	Fermat-Weber Problem with Norm Constraints.
HAR	Half Active Rectifier.
IM	Impedance Matching Algorithm.
IPT	Inductive Power Transfer.
ISM	Industrial Scientific and Medical Frequency Band.
MRC	Magnetic Resonant Coupling.
PFC	Power-Factor-Correction.
PI	Proportional Integral.
PTE	Power Transfer Efficiency.
Qi	Standard Of Wireless Power Consortium.
RF	Radio Frequency.
Rx	Receiver.
SAE	Society Of Automotive Engineers.
SN	Series-None.
TTA	Telecommunication Technology Association.
Tx	Transmitter.
WEV	Wireless Electric Vehicle.
WPT	Wireless Power Transfer.
ZPA	Zero Phase Angle.

I. INTRODUCTION

Development and testing of EV systems have increased because of the demand for a responsible transport mode brought on by the shortage of fossil fuels and also the marked rise in carbon emissions that heavily pollute our atmosphere [1]. The limited battery range of traditional EVs is an acknowledged barrier for consumers who have not wholeheartedly embraced environmentally sustainable motorization [2]. Additionally, concerns with present battery techniques, such as bulky cells, expensive costs, and long recharging periods, are difficult to resolve [3]. Nikola Tesla produced the idea for the WPT employing magnetic resonance over a generation back. It has only been apparent that a WPT system can be developed affordably sufficiently to benefit from advancements in power electronics technologies [4], [5], [6], [7], [8]. Many industries, such as WiTricity, Evatran, Qualcomm, etc., have already created a few solutions to deliver power via a particular air gap with an appropriate range of power and efficiency [1]. A WPT system, which includes transmitting coils for sending power and receiving coils for collecting power, would produce some EMF. However, this value needs to be carefully controlled to protect users. To limit magnetic leakage flux, the main cause of the EMF, it is a smart option to boost the magnetic coupling factor of the WPT by suitable coil construction [9], [10]. This technique could not be widely provided to WPT having a greater air gap between transmitting and receiving coils in which the magnetic coupling factor is lesser, except for contact type WPT, where the strong magnetic coupling is attainable [11]. Access to public charging stations will need to expand in order to accommodate growing EV markets. The majority of electric vehicle charging takes place today

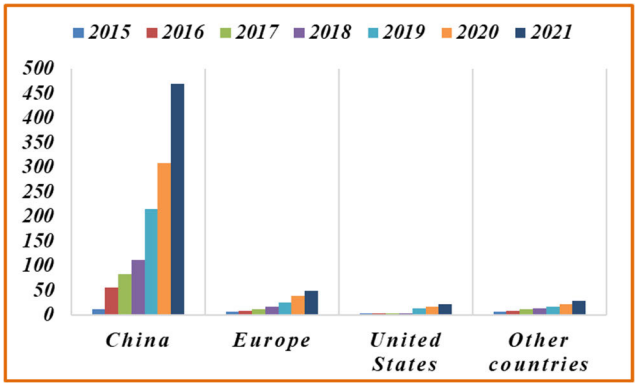

FIGURE 1. Globally available EVs fast charging stations in thousands, 2015-2021.

in private homes and workplaces. Consumers will have a growing expectation that electric vehicles (EVs) will provide the same services, simplicity, and autonomy that conventional vehicles do. By 2021, the number of publicly accessible chargers around the world was getting close to 1.8 million charging points, of which one-third were fast chargers as shown in Fig. 1 [12]. The total number of public charging stations in 2017 was less than the number of chargers that were installed in 2021, which brought the total to nearly 500,000. The increase in the number of publicly accessible chargers was 37% in 2021, which is lower than the growth rate in 2020 (45%), which was also lower than the rollout rates before the pandemic. Between the years 2015 and 2019, the average annual growth rate came in at almost 50%. In 2021, the rate of increase for fast charging was slightly higher than in 2020 (48%) versus 43%), while the rate of increase for slow charging was significantly lower (33% versus 46%). The projected uptake of electric vehicles (EVs) across transport modes and regions is evaluated to determine the best course of action for electrifying road transport in the vital ten years to 2030 [13]. The report afterward digs into the effects of electrical vehicles on charging stations, battery requirements, energy requirements, carbon dioxide emissions, and sales from highway fuel taxation. Stated Policies and Sustainable Development Scenarios are used to create this perspective for electrical vehicles, which is based on the most up-to-date industry analysis, regulation, and technological outlooks as shown in Fig. 2.

Amidst the Covid-19 pandemic and distribution network difficulties, such as scarcities of semiconductor chips, the number of electric vehicles purchased in 2021 approached an all-high and set a new record [12], [14]. In retrospect, approximately 120000 electric cars were sold across the globe in the year 2012. In 2021, that quantity was purchased in a single week. The sales of electric cars, including battery electric vehicles (BEVs) and plug-in hybrid electric vehicles (PHEVs), nearly doubled year-on-year to 6.6 million in 2021 after increasing in 2020 despite a depressed car market as depicted in Fig. 3. Because of this, the total number

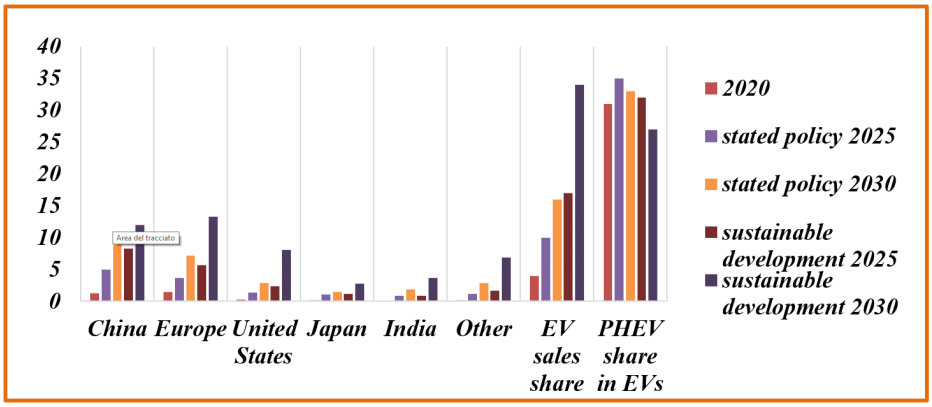

FIGURE 2. EVs sales around the world in millions by scenario-based approach, 2020– 2030.

of electric cars currently operating on the road surpassed 16.5 million. As was the case in prior years, BEVs were responsible for the majority of the increase (approximately 70%). The markets for electric vehicles are growing rapidly. In 2021, sales of electric cars made up 9% of the global market for automobiles, which was four times as much as their market share in 2019.

The IPT and the CPT are the common techniques to realize WPT. To create the electromagnet for the IPT technology, a large current must flow through the path, which results in ohmic loss and decreased efficiency. Efficiency can be increased by distributing corner section lines or numerous coils. There is a demand for additional converters for power electronics with even more segments or coils. CPT uses an electric field to deliver power, unlike IPT [15], [16], [17], [18], [19], [20], [21]. The stray capacitance between the sending plates and ground contributes to the consumption of certain capacitive currents necessary to sustain a high frequency emf. There continues to be stray capacitance between the sending plates and the shielding, although this capacitor is also insulated. If the stray capacitance is kept to a minimum, it can stimulate a high-frequency electric field down an extended path with minimal energy loss. The CPT system provides more advantages than the IPT system [22], [23]. A cheap, thin metal plate serves as the coupler in a CPT system. Additionally, metallic objects do not affect the CPT system. The framework of a car is typically built of metal. When using CPT, dealing with the EV is simple [24]. If your paper is intended for a conference, please contact your conference editor concerning acceptable word processor formats for your particular conference. The demands of the BMS can only be met with the help of an appropriate control strategy. Furthermore, operating with enhanced efficiency is critical for WPT systems because even a minor decrease in efficiency in such a system results in significant power loss. As a result, the key control objectives are to regulate the voltage and current at the output while also maximizing efficiency. The dynamic impedance matching approach is often employed in high frequencies and low power conditions. This plan requires a variety of capacitors, which could increase the device's mass, volume, and control strategy. By impedance modification, the DC-DC conversion can reduce the system's impact from changeable loads, allowing the WPT system to operate at a particular frequency. It is possible to minimize the necessity for a tunable impedance-matching network by modifying it.

Additionally, another classification for the closed-loop control methods is transmitting side control [25], receiving side control [26] and dual side control [27]. Receiving side control, as opposed to transmitting and dual side control, prevents power flow interaction between the primary and secondary sides, ensuring control speeds and stability of delivered power. The secondary side control of the Buck converter is intended to meet the charging current adjustment objective [28].

Fig. 4 shows the taxonomy of the WPT system for EV charging involving different approaches. Research into WPT mainly focused on three sections: (1) Coupling topology; (2) Compensation techniques; and (3) Control methods. The contribution of the paper is:

- To analyze and review current major research articles on wireless power transfer for EV charging.
- To categorize the articles based on different coupling strategies including different magnetic couplers design and shielding, compensation methods, misalignment tolerance and control methods of the WPT system used in the recent works of literature.
- To analyze the performance of the various research articles on the basis of the efficiency, power, tool used and frequency range.

The organization of this paper is as follows: chapter I presents a brief introduction to WPT in EVs; state-of-art coupling methods and magnetic couplers of WPT are presented in chapter II; research on different compensation techniques, misalignment tolerance and control methods are presented in chapter III, IV and V respectively; analysis and discussion of current practices and performances of different WPT systems

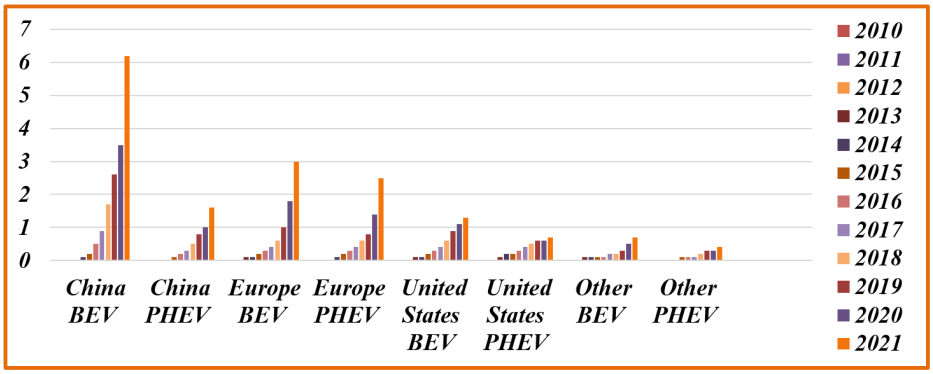

FIGURE 3. Global light-duty EVs sales in millions, 2010-2021.

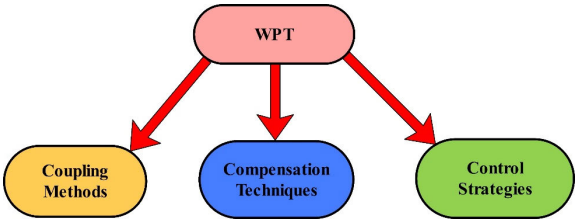

FIGURE 4. Taxonomy of WPT in various literatures.

and future hurdles and opportunities are presented in chapter VI, and the conclusion is presented in chapter VII.

II. STATE OF THE ART RESEARCH ON COUPLING METHODS FOR WPT SYSTEM

Fig. 5 shows the taxonomy of WPT in EVs. There are two main sections for static architecture: the transmitters (fitted under the roadway) and the receivers (in the vehicle). The process converts AC voltage from the main supply into DC when the vehicle reaches the fueling zone to recharge the battery. A wireless IPT facilitates this process. In traditional platforms, the power from the power supply would be transferred via an AC/DC converter, and a power-factor correction process would be utilized to boost efficiency by converting the input current near a sinusoidal signal in phase the grid voltage and thereby enhancing the power factor. An 80–120 kHz high-frequency AC voltage is generally produced by a DC/AC converter. A resonant capacitor is then employed to minimize significant loss while compensating systems increase the model's performance. The magnetic coupling is then strengthened and directed for wireless transmission using transmitter and receiver coils held in place by ferrite sheets. High-frequency AC is first transferred to maximum power, maximum DC voltage on the receiver side before being attached to the battery. Consequently, a BMS enables steady and safe operations by providing power reference, communications, and tasks like verifying the battery status.

When there is no physical connection between two coils, (i.e., they are just placed physically near to each other), magnetic coupling happens. This coupling might be an assisting coupling or an opposing coupling [4]. In WPT system for EV battery charging, there is only one side is supplied, so the coupling is always assisting because power is always transmitted from the supplied side to the other [29].

Various WPT coupling techniques are employed for EV charging and it is depicted in Fig. 6.

Inductive Coupling: The inductively coupled WPT system relies on the same basic principles of functioning as conventional transformers but it employs weak coupled coils named transmitting and receiving coils and are separated by an air gap. Fig. 7 depicts a simple inductively coupled WPT system. According to Ampere's law, an alternating current (AC) creates a magnetic field surrounding the conductor on the transmitting side coil. The receiving-side magnetic coupler is connected to the generated time-varying magnetic field. Through Faraday's law, an induced voltage is seen across the receiving coil when an associated induced emf is there. The alternating voltage induced is then transformed in to DC voltage using an AC/DC converter. It is possible to use this energy to recharge batteries. A magnetic core made of a ferromagnetic substance like iron or ferrite can improve coupling by boosting the flux within the coils. In 2015, [30] demonstrated a two-coil system with weak and strong magnetic coupling. Strong magnetic coupling allows for the achievement of an efficiency of 65%. In 2013, [31] developed a WPT technique with lower frequencies for medical applications. In the research, only the magnetic connection between the revolving magnets and the receiving coil affects how much power is sent to the loads. However, the power transfer efficiency is less effective or requires a considerably large receiving coil at the reduced working frequency. Enhance the efficiency by adjusting the secondary coil's frequency to match the working frequency [32], [33]. At radio frequencies, an air gap as large as 20 cm is possible, however it comes over the sacrifice of higher efficiency [34].

Capacitive Coupling: Capacitive coupling based WPT systems, which rely on the electrostatic field for transmitting power. As shown in Fig. 8, this type of system uses a pair of parallel metallic plates, one operating as a transmitter and the other as a receiver, to create an equivalent capacitor that transfers energy in the form of static electricity. In 2019, [35] developed a new method of designing capacitive WPT

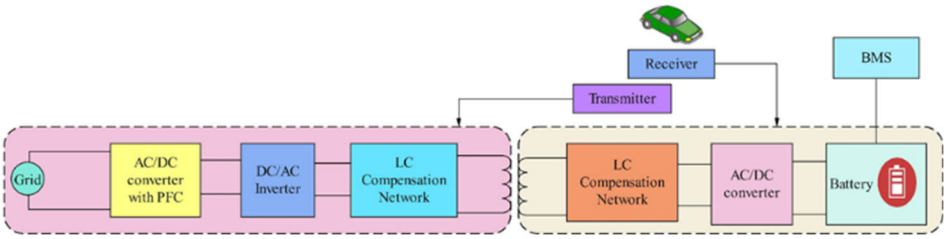

FIGURE 5. A typical layout of WPT system for EV charging.

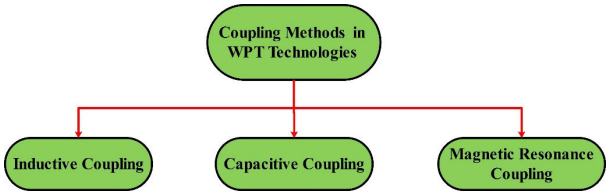

FIGURE 6. WPT classification based on coupling for EV charging.

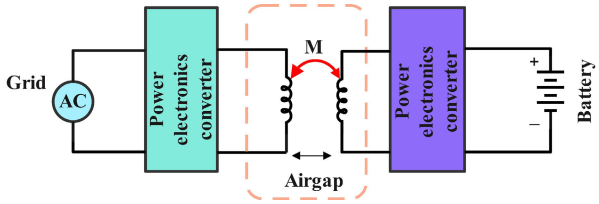

FIGURE 7. Inductive coupling method in WPT system.

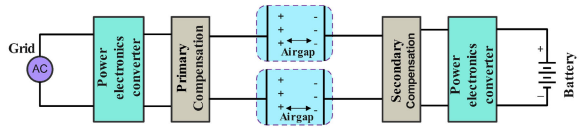

FIGURE 8. Capacitive coupling method in WPT system.

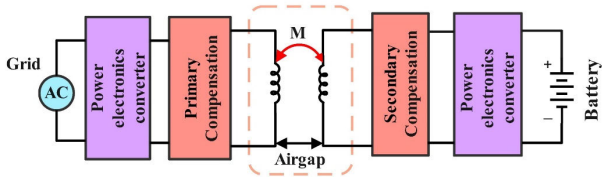

FIGURE 9. Inductive resonant coupling method in WPT system.

systems for EV charging that reduces the impact of parasitic capacitance. In this design, two capacitors are intended for the capacitive coupling process. The first device transmits 590 W with an efficiency of 88.4% and a power delivery density of 19.6 kW/m2 using squared connection plates 12.25 cm by 12.25 cm in size. The second process uses a circular coupling plate with a diameter of 12.25 cm and can transmit up to 1217 W with an efficiency of 74.7%, which is converted to a power transmission density of 51.6 kW/m2. In 2015, [9] developed a CPT system based on a Z-impedance compensation network. For the ability to compensate for the capacitive coupling interface, impedance is provided by an impedance circuit. The impedance networks have entirely corrected for the capacitive coupling interfaces when the input voltage of the networks is in phase also with current flowing into it. As contrary to inductive WPT system, this system can be operated for both small current and high voltage [20], [36], [37]. For reducing the impedances on both sides, extra inductors are connected in series to the plates of the capacitor. The above allows for soft switching behavior and boosts power transmission efficiency; it is also known as inductive compensation. Coupling capacitor size and plate separation determine the maximum possible power transfer [20].

Magnetic Resonance Coupling: When compared to conventional inductively coupled WPT system, the magnetic resonance coupling based WPT system offers significant enhancements in regards of its power transfer efficiency, design, and coupling coils. Fig. 9 displays fundamental architecture of the system for EVs batteries charging. To create a resonant state, compensation circuits (capacitors/inductors or both) are added to the transmitter and receiver sides of the coils in series or/and parallel configurations, unlike in an inductive WPT system. That boosts the efficiency of the system by minimizing unnecessary losses. In 2016, [9] implemented the WPT Waveform Layout for the transmitter. Greater DC power is gathered compared to different benchmark waveforms such as based on the linear model and non-adaptive model, while transfer power is constant.

Until now, there has developed various systematic tool for designing and improving waveform for WPT [38]. In [39], [40], and [41], researchers proposed the energy security strategy for WPT system. Compared to the non-resonant coupling condition, the magnetic flux line of the resonant coupling state is much more intense and uniformly distributed. By adjusting the resonant coupling phase, it is possible to purposefully alter the magnetic field in the resonant coil and, subsequently, the energy absorbed by the receiver coil [42]. In 2013, [43] demonstrated the design and analysis of a high-efficiency WPT system with an intermediary coil. Near the resonance frequency of the intermediate coil, the net self and magnetizing inductance of the transmitting side are enhanced by the intermediate coil, resulting in a boost in the actual coupling coefficient. It improves the system efficiency and creates the bifurcation phenomenon. Due to the

bifurcation phenomenon the system cannot operate at ZPA frequency. This reduces the transfer efficiency. As a result, the suggested design solution benefits from significant transfer efficiency and a reliable output voltage owing to the semi ZPA frequency function. In 2016, [44] produced a method for evaluating the U-coil WPT system's efficiency. This work introduced a fresh way to guarantee that a U-coil system is much more efficient than a two-coil counterpart, depending on the mutual inductance coupling concept. The U-coil system is advantageous in practice because it not only increases the efficiency of power transmission but also guarantees a clean environment along the energy transfer direction.

In 2016, [45] developed the superconducting WPT design for EVs with various added resonators. The resonator plays a key role in maintaining stronger resonance coupling between Tx and Rx coils and storing energy in the resonance coil, which improves transfer efficiency and delivery distance. Limited distance and efficiency of the WPT system have been major obstacles in commercialization services. In 2014, [46] developed a WPT for EV's resonant reactive shields evaluation and layout. The coupling coefficient between the load and shield coil affects the efficiency of the WPT. In 2017, [47] developed a study of rectangular and elliptical plane spiral coils used in EV WPT systems. When comparing the coupling coefficients of the two plane spiraling coils, it is interesting to observe that the coupling coefficient for square coils reduces while the coupling coefficient for round coils rises as the line spacing (distance between each turn of the coil) rises. Despite square coils have a greater coupling coefficient than round coils for line spacings less than 12 mm, this advantage fades as line spacings grow larger. The coupling coefficient of a square coil is greater than that of a round coil regardless of the presence or absence of a shielding material. As a result, the coupling condition of the square coil is greater than the round coils. The mutual coupling between two coils can also be improved by ferromagnetic materials installed in the coils.

In 2014, [48] developed a mathematical expression for a WPT-enabled electric transport bus network. While the bus is moving, it is charged. The energy needs of the full route's direction may be difficult to calculate in an open area. In 2014, [11] proposed three generalized architectural methods for eliminating the WEV EMF. If the canceling coils are positioned away from the magnetic coupling line, there shouldn't be any noticeable power loss. The WPTS, with a significant air gap between the primary and secondary sides and an extremely small magnetic coupling factor, cannot usually use this strategy. In 2013, [49], [50] developed a boost-buck converter with cascaded outputs for high-performance WPT systems. Due to the availability of innovative power electronics for energy production and conditioners, IPT often performs in kHz ranges, such as 20-150kHz.

Smaller, thinner, and more convenient resonators typically call for greater frequency. The ISM band's regulations limit the useful frequency level and the capabilities of

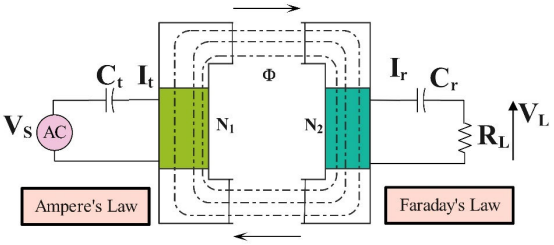

FIGURE 10. Basic concept employed in the WPT system.

power-switching equipment. In [51] and [52] researchers modeled the SN structure and used differential calculus to establish the mathematical formulae for the transmitter and receiver currents. To achieve a superior rate of the receiver making these changes and lower receiver-side losses, the compensation on the receiver side must be abolished. This creates an SN configuration. Reference [53] developed a bridgeless boost PFC rectifier in a single-level WPT system. The DC/DC WPT resonant converter stage, which employs resonant magnetic coupling to accomplish the intermediate level of WPT, uses the bridgeless boost PFC rectifier technique. The benefit of this approach is that it increases line input efficiency and power quality while lowering fabrication costs and complexities for large power WPT.

In [54], researchers developed an IM algorithm to see how well it helps an MRC WPT system keep its resonance. Improved efficiency and greater range are two key benefits of the proposed WPT system. Within 0.5–1.5 s, performance can improve to as high as 85%. As most commercial systems have a defined set of resonators that require adjusting to varying air gaps, regulating the coupling between the resonators, and varying its specifications is also impractical. In 2012, [55] developed a quantitative evaluation for the best WPT systems integration using the MRC technique. The MRC technique has drawn more focus on enhancing the WPT performance of the network. But there is a balancing problem with the mutual inductances of the coils for the best MRC-based WPT systems. In 2015, [56] developed a complex simulation approach that uses MRC and is rooted in coupled phases. All parts of a WPT system's characteristics, such as the inverter and rectifier, is modeled in this study. Modeling a second-order resonator holistically by using amplitudes and phases of coupled modes as state variables makes this approach stand out.

Table 1 shows the summaries report of different WPT technologies based on coupling methods describing operating frequency ranges, benefits and their shortcomings in EV applications.

Fig. 10 is a schematic representation of basic methodology of WPT system. By winding the conductors on the magnetic conductive material, the flux can be directed, and the coupling coefficient and efficiency can be increased. Primary and secondary turn numbers (N_1 and N_2), primary and secondary currents (I_t and I_r) and voltages (Vs and V_L), compensating resonant capacitors (C_t and C_r), load resistance (R_L), and

TABLE 1. Application and a brief discussion of developed compensation topologies of the WPT system.

Coupling methods	Frequency range	Benefits	Shortcomings
Inductive	10-50 kHz	The procedure for application is simple and clear. Unlike inductive resonant coupling method, secure functionality. Reverse mode power transmission can be feasible. Better performance in a reduced air gap. Galvanic isolation is possible	Power transfer efficiency decreases for greater coil distance (effective only for several mm airgap). Considerably large receiving coil at the reduced working frequency. Relatively low distance power transmission compared to inductive resonant coupling method. Balance between the coils should be there to obtain high efficiency. The transfer efficiency depends heavily on factors such as the coil's shapes, separation between the coils, and the materials surrounding them.
Inductive resonant coupling method	10-150 kHz	High power transfer is possible as compared to inductive and capacitive coupling ranging from several watts to MW level. Galvanic isolation is possible. Enhance WPT performance. Bidirectional power transmission can be feasible.	Higher cost. There should be EMI safety. More sensitive to the metallic obstacles in between the coupling pads. Power transfer range is small. Improving the quality factor to help make up for the weak coupling and thus higher power transfer range can be obtained.
Capacitive	100-600 kHz	Light weight and less costly than above coupling methods. Medium range of power transfer possible (up to kWs). Power transfer possible for air gap up to few cms. This can transfer power through metal. Improved misalignment problem as compared to magnetic WPT. No need of EMI shielding.	Unintentional outcome due to the impact of parasitic capacitance. Power transfer decreases compared to Inductive resonant coupling method capacitance of plates is small. A higher strong electric field is required.

magnetic flux (Φ) are the parameters of Fig. 10. When a high-frequency AC current is injected in the primary coil, the magnetic field formed changes over time (according to Ampere's law). The permeability of free space, the number of turns, and the current flowing through it all contribute to the magnetic flux that is produced. Magnetic flux that changes over time causes a current in the receiving coil (Faraday's Law), as depicted in the equation given below.

$$\oint \vec{B}.\vec{ds} = \mu_o I N_1 \tag{1}$$

$$E = -N_2 \frac{d\emptyset}{dt} \tag{2}$$

where B, μ_o, and E, denotes magnetic flux density, vacuum magnetic permeability and induced electromotive force (emf) respectively.

Fig. 10 shows that with WPT, there is a considerable air gap between the two coils. To enhance the interaction between coils and reduce contact losses, the coils are wrapped around a magnetic substance. Using Ampere's law, high-frequency ac current powers the transmitting coil to produce a magnetic field that varies over time. Faraday's law states that a voltage is induced in the receiving coil when a portion of the alternating magnetic field developed is coupled with it [57]. As a result of the significant air gap in the circuit, the induction phenomenon occurs. Therefore, in order to generate an effectively strong magnetic field for coupling receiving coils, an ample current (or magnetomotive force) has been essential. To minimize the power supply's apparent power rating, a capacitor is typically placed in series with the transmitting side coil to neutralize the inductive portion of the network for a realistic WPT arrangement. To eliminate secondary leakage inductance and improve power transfer efficiency, the secondary side is similarly adjusted to a similar resonant frequency. A high-frequency switching inverter is used to supply high-frequency ac current to excite the transmitting coil. The voltage generated in the coil is rectified by an ac-dc converter and delivered to a load on the receiving end [11], [58], [59].

A. MAGNETIC COUPLER

To boost the WPT system's efficiency, a well-designed coil is essential. Coil design, which depends on self-inductance, mutual inductance, and the ac resistance of the coupling coil depicted in Fig. 11, is typically performed to achieve a greater transmission efficiency and a high-power transmission capability.

In a WPT setup, the magnetic coupler plays a key role. The air gap detached the transmitting and receiving coils. The magnetic coupler which is also called the coupling pad should have large misalignment tolerances and a greater quality factor Q for the coupling coefficient [29], [61]. Numerous studies have proposed various coil topologies in an effort to boost the coupling coefficient and keep the quality factor higher [43], [62], [63], [64], [65], [66], [67], [68], [69], [70], [71], [72], [73], [74], [75], [76], [77], [78]. Ferrite bars or ferrite plates, with an insulating substance between the

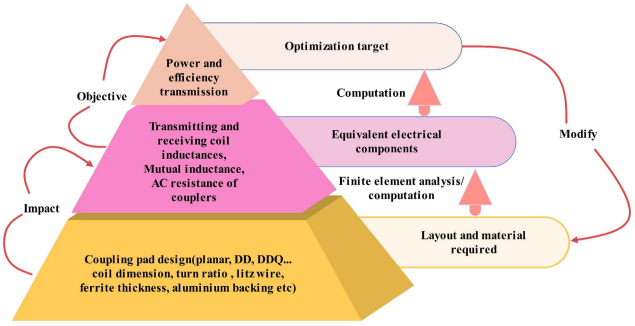

FIGURE 11. Basic methodology performed for coupler design [60].

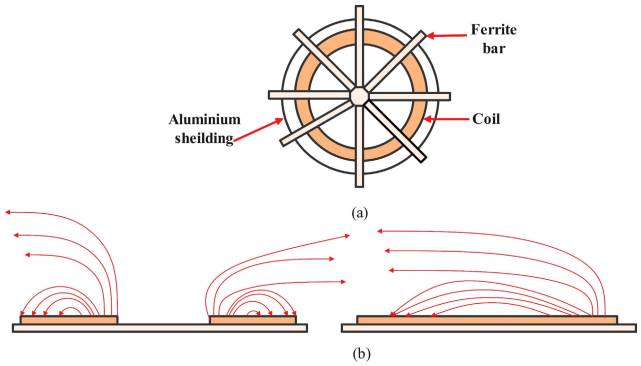

FIGURE 12. (a) Circular coupler. (b) Magnetic flux directions of circular coupler side view and facial view [67].

ferrite and the coil conductors, are used to boost the coupling coefficient. The self-inductance, quality factor, and mutual inductance of the coupling pad can all be enhanced by adding more ferrite bars. However, the core losses and the copper losses caused by electromagnetic field alteration in the coils both rise when the ferrite bar is included. [79].

The product kQ, the product of magnetic coefficients of coupling, and the quality factor of the inductors influence the efficiency of coupled coils in a WPT system [29], [61], [64], [65]. These characteristics depend on the inductors' cores' shape, composition, and separation. The inductor quality factor (Q), is calculated as the geometric mean of the transmitting and receiving side's quality factors, and it is written as,

$$Q = \sqrt{Q_t Q_r} \tag{3}$$

Higher Q is achieved by developing inductors with lower series resistance and higher self-inductance with a high working frequency. But taking SAE J2594/1 into consideration, which restricts the highest working frequency to about 85 ± 3.7 kHz [57], [61]. As a result, reducing the coil's resistance is essential for boosting Q. The self-inductance of a coil with cross-sectional area Aand average route length l can be written as,

$$L = \frac{\mu_O \mu_r N^2 A}{l} \tag{4}$$

where, μ_O and μ_r represent magnetic permeability of the free space and material of the flux route respectively and N denotes the number of turns in any coil.

When it comes to coils, the inductance increases with the square of the number of turns, but effective series resistance (ESR) increases according as turn ratio. As a result, raising the number of turns raises inductance more than the equivalent series resistance. At greater frequencies, it is also important to account for the relative distribution of current (i.e., the proximity phenomenon) inside nearby wires. Hence, the total quality factor of the inductor grows as the turn ratio rises [64], [65]. Therefore, the most effective self-inductance can be achieved by establishing a balance between the wire diameter and the number of turns. Raising the coil's self-inductance can also be achieved by placing ferrite bars on it. By directing the flux, ferrite bars help minimize leakage flux and make it possible to achieve a high coupling coefficient. The coil's equivalent series resistance (ESR) includes both dc and ac resistance.

Raising the conductor area of a coil lowers its dc resistance. Litz wire, which is used to minimize ac resistance, is well-suited to the working frequency region [29]. Various coupling pad structures have been detailed in published works. The coupler design for conventional lumped WPT relies on magnetic core geometries like Pot-type, U-type, and E-type cores [68], [69]. Bigger dimensions for greater power output and reduced performance under alignment condition [74] are two issues that plague the traditional coupler.

1) CIRCULAR COIL

The circular coil depicted in Fig. 12(a) is a commonly used coil configuration in a WPT system for electric vehicle battery charging. Numerous reports and improvements of circular coils can be found in [29], [64], [65], [72], and [73]. In [64] and [65], researchers provided the results of η-Pareto optimization and advice for developing a circular coil in terms of efficiency and area-related power density. Bosshard et al. [64], [65] used η-Pareto optimization to show the dc bus to battery load efficiency of 96.5 by using a 210-mm coil diameter and transfer distance of about 52 mm. When the separation between the coils is one-fourth the diameter, the coupling coefficient of a circular coil is a value of 0.2. For a coupling value of 0.15–0.2 at a spacing of 150–200 mm between coils, for instance, the coils' diameter should be 600–800 mm [69]. According to [29], for WPT coils to have appropriate thermal characteristics, the current density in the litz wire or equivalent cable should be under 3-5 A/mm2.

Due to the unidirectional nature of the EMF, which steps into and exits the coil from the facial view depicted in Fig. 12, circular coils and similar types (i.e., square and rectangular structures) are frequently utilized for the WPT system [68]. A fountain field imitating the shape of the coil rests over the ferrite, and the latter directs most of the flux underneath the coil and far from rebar and pipes in the ground's pavement. The leakage flux is decreased by the flux pattern's

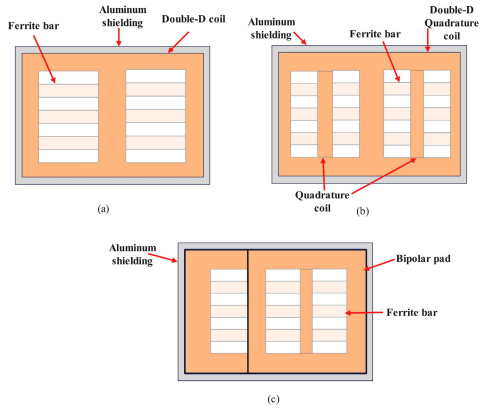

FIGURE 13. Examples of few magnetic coupler's layouts [71], [72]. (a) Double-D coil. (b) Double-D quadrature coil. (c) Bipolar coil.

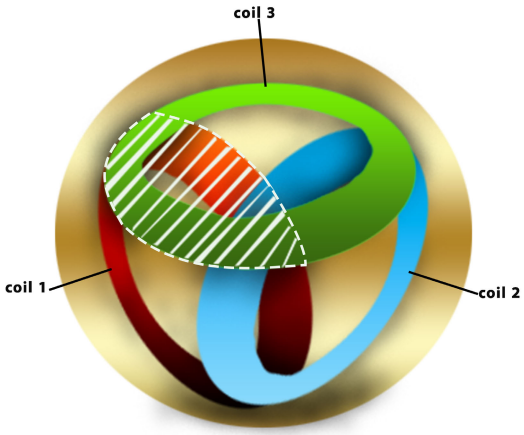

FIGURE 14. Tripolar pad [75], [76].

unidirectional nature. As an added bonus, aluminum shielding can reduce leakage flux without compromising system performance with appropriate engineering [68]. Researchers in [66] presented an outstanding approach to circular coupler design along with key results aspects for WPT system, and in [29] offered a very thorough review of WPT for applications in vehicles.

2) DOUBLE- D COIL

Budhia et al. [68] proposed double- d coil first time and suggested a polarized unidirectional flux coupler that takes the best features from both the flux pipe and circular pad configurations. The DD coil is made up of two single coils that are connected in series but in reverse order as depicted in Fig. 13(a). A rectangular spiral coil is the most common shape for a single coil. Due to their series magnetic connection, the center part of a double D (DD) coil is conceptually comparable to a flux pipe [68], [69]. Because the coils are mounted on top of the ferrite plate, aluminum shielding can be added underneath the ferrite without compromising performance.

Key characteristics of a DD coil include minimal leakage flux from the rear of the coil, decreased losses in the aluminum shielding, and unidirectional flux routes with a height corresponding to 50 % size of the coil. The quality factor under no load condition, has been improved as well [70], [71]. Improved coupling strength and lesser leakage flux have been seen in the DD coil compared with other coil topologies [67], [68], [69]. As a result, DD coils have found widespread use, particularly in EVs [70], [71], [72], [73], [74]. However, designing a coupling pad from scratch using finite element analysis (FEA) software is a lengthy process. There is a limitation of literature on the subject of DD coil modeling. In [75], researchers proposed a model of a DD coil with a ferrite core for use in determining the values of self-inductance, mutual inductance, and ac resistance. Different-sized transmitting and receiving coils are also considered. They suggested a genetic algorithm approach for the proposed coil mathematical model to optimize the coil structure.

3) MULTIPLE COIL COUPLERS

Different coils are used on the transmitting and receiving sides of multi-coil couplers, as detailed in [67], [68], [69], [70], [71], [72], [73], and [74].

The DD coil and the circular coil are used to design a multicoil polarized coupler. The sinusoidal flux component, and by extension the quadrature component, can be measured by using such coils [68]. The key benefits are misalignment tolerance and minimal air gap spacing fluctuation.

4) DOUBLE-D QUADRATURE (DDQ) COIL

As shown in Fig. 13(b), the DDQ coil is formed from the DD coil by incorporating the quadrature coil [68]. The coil is situated in the center of the DD coil. The coils are arranged so that the d-axis flux is collected by the DD coils and the q-axis flux is collected by the Q coil. Therefore, the coil architecture greatly ameliorates the misalignment. When compared to a circular coil or square coil, however, the size of the coils rises by a factor of about three [68].

5) BIPOLAR PAD

As shown in Fig. 13(c), the bipolar pad (BP) is a multi-coil coupler consisting of two overlapping coils structured on a ferrite bar [70], [71]. As can be seen in Fig. 13(c), BP comprises of two similar, partially overlapping, and mutually separated coils. The BP, like the DDQ pad, has improved coupling coefficients and can withstand large misalignment. Compared to DDQ pad, BP uses 25% to 30% less copper, which is a major benefit [71].

6) TRIPOLAR PAD

As illustrated in Fig. 14, a tripolar pad (TPP) comprises three-coil coupling pad whose coils have been designed to be mutually decoupled [75], [76]. A large rotational alignment sensitivity of a nonpolarized coil is made possible by this form of design [75], [76]. The maximum coupling coefficient can be obtained by operating the three coils separately. Researchers in [75] and [76] used a bipolar and circular

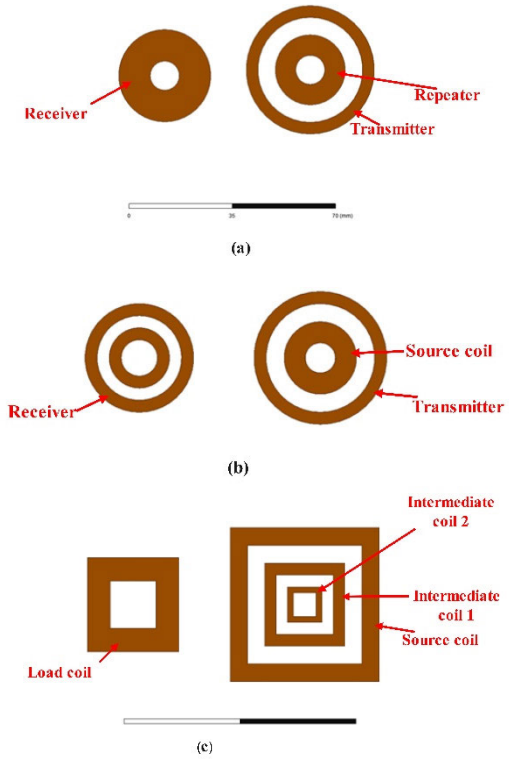

FIGURE 15. (a) WPT system included three coils [43], [78]. (b) Four coil WPT system [43]. (c) WPT asymmetric four coil system [79].

pad as the receiving coil, and they showed that the overall coupling coefficient is improved. To do this, the voltage and phase of the currents in the transmitting coils had to be modulated. With 150 mm of coil separation, the apparent power requirements are 45% lower than with the circular coil. Also, the measured leakage magnetic field is lower than the value recommended by ICNIRP [80]. Yet, the expense and complexity of control are heightened by the requirement of three independent inverters to drive three mutually decoupled coils [75], [76].

7) OTHER MAGNETIC COUPLERS

Many coil couplers have been documented in the literature to increase efficiency and load resistance fluctuation sensitivity [43], [77], [78], [79], [80], [81], [82], [83]. A third coil is merged to the transmitting or receiving side in the identical plane in the three-coil coupler depicted by Fig. 15(a). The inclusion of a third coil increases overall efficiency, makes the system more robust to fluctuations in load, and decreases EMF discharges caused by coil misalignments [77]. When the battery load deviates from the highest possible resistance, however, the system's efficiency declines more slowly if the source coil is located nearby to the transmitting coil. In addition, a coil on the receiving side known as an intermediate pad improves the coupling coefficients. The benefits include a boost in efficiency and the ability to transfer power over longer distances.

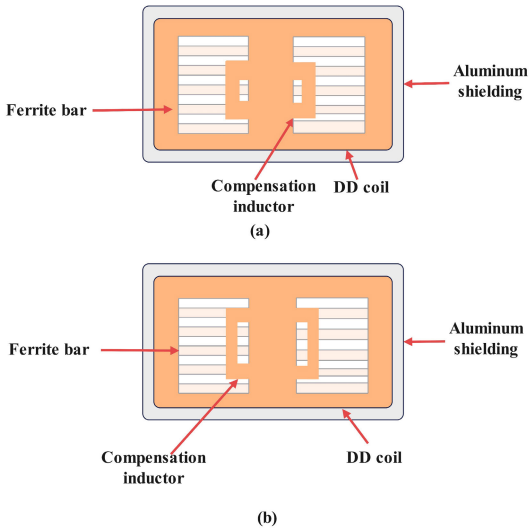

FIGURE 16. An inductor attached to the Double-D coil [80], [81], [82]. (a) transmitting coil. (b) receiving coil [79].

Incorporating a coil causes a bifurcation occurrence, hence it's important to follow a rigorous engineering method to prevent it. Furthermore, bifurcation might cause instability in the system for widely fluctuating load resistance [43]. The transmitter and receiver of [43], the four-coil system, each feature additional coils called source and load coils, as shown in Fig. 15(b). The coefficient of coupling is enhanced by using more than three coils. To improve performance even further above the standard four-coil technique, [79] adds two coils on the transmitting side coil, as illustrated in Fig. 15(c), to increase the coupling coefficient. In order to create a magnetic integrated compensating circuit, Zhang et al. [81] recommended including a magnetic inductor into the DD coil. The proposed structure is more space-efficient than alternatives since the inductor is built in. Fig. 16 also demonstrates that the transmitting side inductor is at an angle to the receiving side inductor. The secondary inductor and primary coil are set at a right angle, or 90 degrees. Some voltage can be induced by the secondary inductor to correct for misalignment [82].

In [84], a double DD is investigated. Incorporating double DD coils in a WPT system can boost power density by about 50% compared to a single DD coil system. An extra planar non-polar in-nature coil was added to both the transmitting and receiving sides to create a double DDQ coupling pad, which increased the power density and misalignment tolerance further [85].

Table 2 explores the comparisons of different magnetic couplers involving several parameters.

Fig. 17 and 18 provide a depiction of the convoluted pad arrangements and the magnetic flux flow in the couplers.

B. DESIGN OF TRANSMITTING TRACK AND PICK UP COIL FOR DWPT SYSTEM

Several terms (such as ''road-powered transmitter,'' ''segmented IPT tracks,'' and ''long power rail'') have been used

TABLE 2. Comparison of several magnetic couplers configurations [29], [64], [65], [66], [67], [68], [69], [70], [71], [72], [73], [74], [76], [77].

Coupler Configuration	Coupling Coefficient	Magnetic flux orientation	EMF Exposure	Performance with shielding on coupling coefficient	Misalignment tolerant
Circular	Low	One sided	High	good	poor
Flux pipe	Medium	Two sided	Low	poor	Medium
DD coil	High	Two sided	Low	poor	poor
DDQ coil	High	Two sided	Low	poor	High
BP	High	Two sided	Low	poor	Medium
TP	High	One sided	Low	good	High

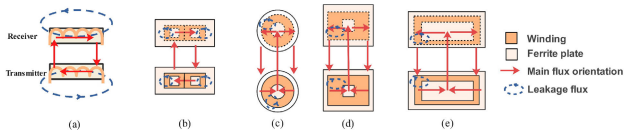

FIGURE 17. Example of magnetic flux nature in few couplers for WPT system EV charging: (a) Flux pipe, (b) bipolar, (c) circular, (d) square and (e) rectangular.

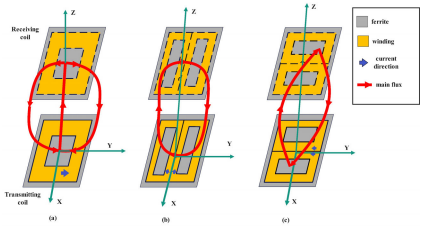

FIGURE 18. Different types of coupling pads in WPT EV charging. (a) Nonpolarized pads. (b) Polarized pads along X direction. (c) Polarized pads along Y direction.

to describe the various methods by which electric vehicles can be charged while in motion [58], [59]. The segmented WPT has a compact transmitting coil and separate power sources considering every coupler. In order for such couplers to function, an EV must be passing over them [58], [64]. The segmented IPT system [86] is being developed by researchers at Auckland University. The road is equipped with many floor pads spaced at regular intervals; each pad is activated as an EV drives over it. From a practical standpoint, this approach benefits from a small footprint, minimal electromagnetic interference (EMF), and light weight [86]. It is possible to use the same magnetic coupler for both static and dynamic charging. When incorporated into a road, however, the segmented construction presents challenges because to its control complexity, power supply architecture, and high maintenance expenditures.

ORNL started developing its segmented DWPT in 2011 [87]. This DWPT used multiple circular coils in a series rail with a pitch factor of 0.7 [88]. ORNL's WPT battery charger, having the highest load power of 6.6 kW and 85% efficiency at a 162-mm charging distance, was implemented in a variety of commercial electric vehicles, such as the Chevrolet Volt, Toyota Prius plug-in, Scion IQ, and Toyota RAV4 [87]. After a few modifications, the system's output was raised to 20 kW, maintaining the same 162 mm charging distance and ground clearance at an efficiency of 92%-93% [87]. KAIST also developed the installation of an extensive power source track laid along the roadside [58], [59]. The lack of magnetic components reduces the system's ability to tolerate lateral misalignment and so power rail's efficiency is improved by inserting magnetic material of various types, such as E-type, W-type, U-type, I-type, S-type, ultra slim S-type, and cross-segment (X) type shown in Fig. 19 [58], [59].

As shown in Fig. 19(f), it is suggested that the common power supply cable be replaced with a cross-segmented power supply rail. Each of the power rails is energized by a distinct power supply and is isolated from the others by a compensation switch box, which enables or disables each rail independently. As a result, half as much cable is required as with a scattered power supply rail [86]. Table 3 provides a comprehensive look at how the various power rails perform in contrast to one another and a brief overview of the most salient features of the analyzed power rail. Power rails of the cross-segmented (X) type are more effective and have lower leakage EMF and cabling requirements. More work needs to be done in this area to lower expenses and EMF leakage without sacrificing performance.

C. SHIELDING

The leakage EMF and its harmful effects on neighbouring objects and human interaction pose the greatest challenge to WPT. Standards for electromagnetic compatibility (EMC) and electromagnetic interference (EMI) must be met by the WPT system [80]. Extra losses and potential object heating can be caused by an alternating magnetic field inducing eddy currents inside a metal item resting on or near the transmitting coil [89]. Losses are incurred and the WPT system's effectiveness is diminished due to the shielding measures that reroute or take in those magnetic field. It has been demonstrated that adding aluminium shielding to the rear of the ferrite and coil is a viable approach. A variety of shielding techniques, such as conductive shielding [90], [91], magnetic shielding [92], and active shielding [11], [46], [93], have been investigated to lessen the leaking magnetic field.

Fig. 20 depicts a shielding layout comprising coils, ferrite and aluminum. The ferrite flux directions are not shown. Shielding decreases coil inductance and adds losses, necessitating additional capacitance compensation to attain a

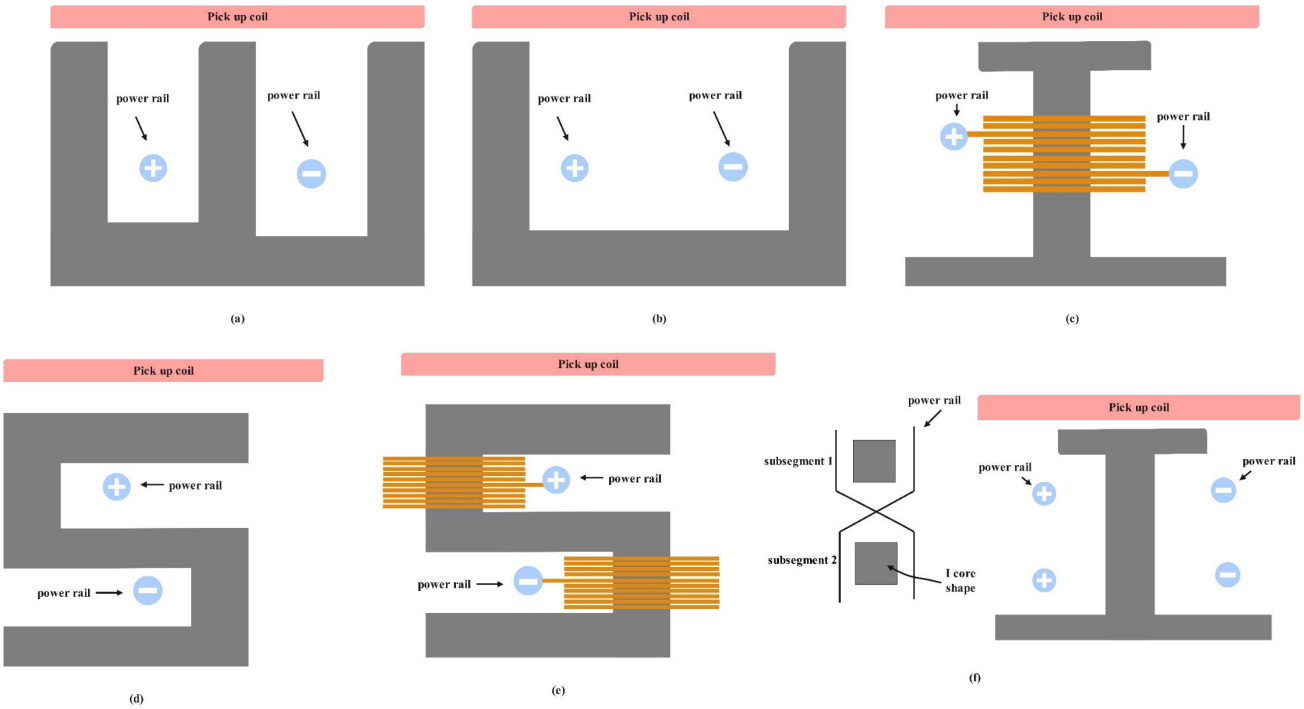

FIGURE 19. Several designs of power rail used in the DWPT system. (a) -type. (b) U-type. (c) I–type. (d) S-type. (e) Ultra slim S–type. (f) Cross-segmented (X-rail) [58], [59], [86], [87], [88].

resonant state [46], [89], [94]. One to two percent of a system's performance can be lost due to shielding [89]. Aluminum and copper are frequently used as shielding materials because they are highly conductive and create eddy currents that cancel out the incident flux but also cause losses in the shielding. By redirecting the magnetic flux into the coupler active region, guides with high permeability and high resistivity reduce flux entrance into the shielding ferrite [95], [96]. Utilizing the benefit of how straightforward, strong, and cost effective it is to put into place, passive shielding is required in all WPT EV battery chargers, involving static, quasi-dynamic, and dynamic WPT chargers. Resonant reactive shielding was reported by Kim et al. [46] and used no extra power. As can be seen in Fig. 21, it comprises of an extra coil coupled to an LC resonant circuit.

When compared to a conductive shield of the identical dimension, the leakage magnetic field is reduced by 64% thanks to the reactive shielding's induction of a nullifying magnetic flux lines. The leakage E-field close to the charging vehicle can also be reduced with passive shielding [46]. In comparison with previous cutting-edge WPT systems working at frequencies under 100 kHz, the gravimetric and volumetric power densities of shielding architectures are significantly greater [97], [98], [99]. In [100], the use of a resonant reactive coil to shield self-resonant (SR) coils in the MHz region is investigated; nevertheless, the impact of shielding is small.

Since the power output needs to be greater in a DWPT system, the corresponding leakage field may be significantly greater than in a similar static WPT application. Moreover,

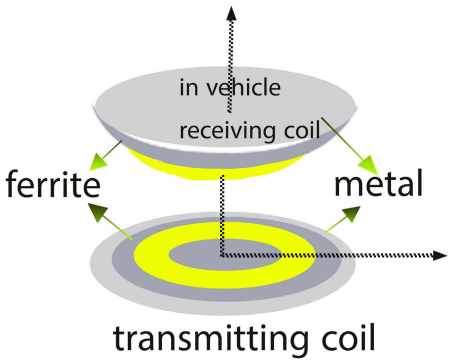

FIGURE 20. A shielding arrangement for WPT system with coils, ferrite and aluminium [101].

the receiver's mobility in relation to the transmitting coils causes a significant change in k [11], [89]. KAIST engineers looked into a passive shielding technique for DWPT [11], [96], [97], [98], [99], [100]. The KAIST group suggested placing a metal layer in the footwell of EVs to safeguard riders from greater EMF [96]. To prevent lateral leakage fields, the investigators positioned a vertical shielding sheet next to the power rails. Additionally, a number of the metallic brushes are mounted on EV in a fashion that allows for gentle contact with vertical metallic plates, thus reducing EMF. The EMF level is reduced from 144 mG to 35 mG when the number of metallic brushes is increased from 2 to 8 [11], [100]. Unfortunately, losses in a DWPT system can be in the kW order, therefore passive shielding has a negative impact

TABLE 3. Performance comparison of several power rail arrangements for DWPT system [58], [59], [86], [87], [88].

Power rail type and shape		Performance and Features
Type	Shape	
E	Fig. 19(a)	Rail width- 20cm, airgap-1cm, misalignment-0.3cm(lateral), efficiency-80%, power output-3kW/pick up, leakage EMF-10mG A simplified architecture that results in reduced production expenditures
U	Fig. 19(b)	Rail width- 140cm, airgap-17cm, misalignment-20cm(lateral), efficiency-72%, power output-5.2kW/pick up, leakage EMF-51mG Increased efficiency concerning the wider airgap, and reduced electromagnetic fields (EMF) as a result of the return path being located near the transmitting power rail
W	-	Rail width- 80cm, airgap-20cm, misalignment-15cm(lateral), efficiency-74%, power output-15kW/pick up, leakage EMF-50mG Improved coupling coefficient, magnetic resistance lowered by about a magnitude of three versus the U-type, and no need for aluminum shielding
I	Fig. 19(c)	Rail width- 10cm, airgap-20cm, misalignment-24cm(lateral), efficiency-80%, power output-25kW/pick up, leakage EMF-15mG Manufacturing time is lowered, and operating expenses are decreased by 20% compared to W-type
S	Fig. 19(d)	A decrease in expenditure in comparison to the I-type
Ultra slim S	Fig. 19(e)	Rail width- 4cm, airgap-20cm, misalignment-30cm(lateral), efficiency-71%, power output-22kW/pick up, leakage EMF<10mG Lower leakage EMF magnetic core width is reduced
Cross segment (X)	Fig. 19(f)	Higher efficiency lowered cable cost and leakage EMF

on system performance. Mechanical losses, touch potential, and an increased startup pricing is additional issues [11], [100], [101].

Fig. 22(a) depicts the overall approach of active shielding. There is an EMF cancellation coil, a capacitance-compensated transmitting, and receiver coils. One or two canceling coils may be used. The leaking EMF can be nullified by connecting a canceling coil with the transmitting coil in such a way that the current in both coils has to be in the opposite phase. Both Choi et al. [11], [58] and Park et al. [46] provided examples of how active shielding could be employed with DWPT. U-type, W-type, and I-type general design approaches are compared, and implementation challenges for each type are analyzed. The independent self EMF cancel (ISEC) method, the 3-dB dominant EMF cancel (3)-DEC) method, and the Linkage-free EMF cancel (LFEC) method are the three active EMF cancellation techniques presented by Park et al. [46].

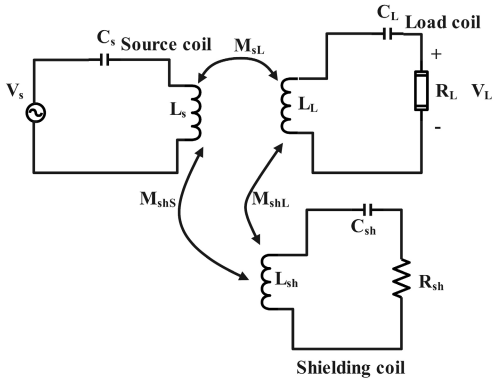

FIGURE 21. Design of resonant reactive shielding [46].

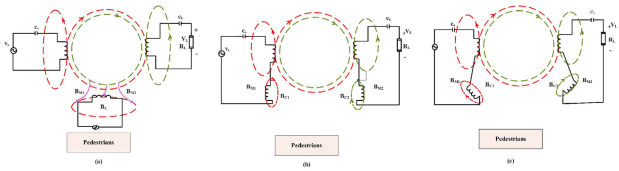

FIGURE 22. (a) Composition of active EMF cancel system. (b) ISEC technique for EMF cancel system using the primary coils to retrieve the cancelling currents. (c) LFEC technique for EMF cancel system [11], [97], [101].

ISEC works by canceling out the EMF with a counter magnetic field, first BC1 for the transmitting coil and then BC2 for the receiving coil as depicted in Fig. 22(b) [11], [101]. The transmitting and receiving coils supply the current for the canceling coils. This technique is easy to use, yields good results, and can be used with several primary and secondary coils. When the total magnetic flux, Bt, is smaller than the sum of the main magnetic flux and the cancellation field flux, Bm1 + BC1, as in the 3-DEC technique [101], the ISEC method is unable to cancel the electromagnetic field.

The LFEC technique for EMF cancel system is illustrated in Fig. 22(c). This technique combines the transmitting and receiving coils including the corresponding cancel coil. On the other hand, there is less interaction between the primary and secondary coils. Therefore, you should not use this approach [100]. For DWPT applications, Ahn et al. [96] demonstrated an active shielding approach that did not reduce performance. A wire is strung alongside the power rail in active shielding. The shield wire is active when it carries a current that is in phase with the primary coil current but at the same frequency. The KAIST group recorded an EMF of 62.5 milligauss with 60 kW at 80% efficiency [100]. Reference [100] summarizes this section by contrasting various shielding techniques described in the literature. Passive shielding is widely used to minimize leakage EMF for stationary WPT because it is simple, durable, and inexpensive to implement [95], [96]. Because this could actively nullify the leakage EMF and is appropriate for greater-power EVs, active

shielding is an encouraging approach to lowering DWPT's leakage EMF [97], [101].

In [101], an approach for a 6.6 kW wireless power transfer system for electric vehicles (EVs) using compact self-resonant coils is explored. Shielding design modification techniques are given after a thorough analysis of the high-frequency parasitic capacitance caused by magnetic and conductive shielding components. The prototype coils' dc-dc efficiency was 92.3%, and their volumetric power density was 7.1 kW/dm 3 [101]. Using the multilayer non-uniform SR coils described before at 3 MHz [99], [102], researchers provided a comprehensive shielding architecture solution, illustrated in Fig. 20.

III. COMPENSATION TECHNIQUES

The foundational idea of Ohm's law is used in the compensation theorems. Ohm's law states that a voltage drop happens over an impedance whenever a current flows through it. This voltage drop will oppose the input power. As a result, an additional supply voltage whose magnitude is equal to the voltage drop and whose polarity is reverse with respect to that voltage is applied. On this idea, the compensation theory operates. Another important effect of compensation is improving tolerance to coupling factor variation in the WPT system. Different compensation methods are used to improve the system voltage and power transfer capability.

A. NEED FOR COMPENSATION TECHNIQUES

1) REDUCED INPUT APPARENT POWER RATING AND ENHANCED POWER TRANSMISSION CAPACITY

When it comes to the resonant inductive power transfer system, compensation plays a crucial role. As the coupling coefficient drops below 0.3, the volt-ampere (VA) rating of the system can be minimized by employing compensation on both ends, provided that they are adaptable and have reasonably high operating features. The parasitic capacitance could not tend to resonate or makeup the WPT because of the way the system is crafted. To fine-tune the resonant frequency of process, extra reactive components (capacitors or inductors) are required. A compensation capacitor's most vital role is to provide the reactive power necessary for the inductances to produce a sufficient magnetic field by resonating with the transmitter and/or receiver coil. Consequently, the key function of compensation is to reduce the input apparent power or the VA rating of the primary converter for the loosely coupled transformer's transmitting coil [29], [103], [104], [105], [106].

Improper way of compensation technique, moreover, results in a surge in reactive current/power. A rise in reactive currents leads to greater losses in switches and conduction losses mainly on the primary converter end.

2) FIGURES MAXIMIZED POWER TRANSFER EFFICIENCY

The coupling coefficient and coils quality factors are the sole two variables that determine the highest possible efficiency

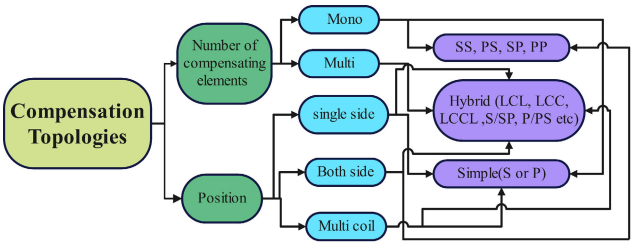

FIGURE 23. Compensation networks categorization.

of a WPT process, as reported in [107] and [108]. To achieve this efficiency, even so, proper compensation is vital. The use of soft switching also ensures a high level of efficiency. When working the system at above resonant frequency, where the transmitting current lags the voltage varied by the active switches, the converter can take advantage of turn-on zero-voltage switching using MOSFETs. The value of the compensation capacitors allows for modification of the input phase angle; therefore, soft switching should be considered when making compensation choices.

3) TO MAKE THE SYSTEM BIFURCATION AND MISALIGNMENT TOLERANT

Due to unexpected variations in some components of the WPT system, it is usual being compensating architectures to experience a splitting of the resonant frequency into multiple frequencies. In other words, when the ZPA frequency condition can be reached at two or more different frequency, a bifurcation or frequency splitting condition occurs [109], [110]. To ensure system stability, it is best to avoid the frequency splitting condition that occurs alongside numerous loading and variable frequency control. Also, risk of malfunctioning electronic parts can be increased. For specialized uses, it is also important to think about other characteristics, like being resistant to component variations and capable of handling power in both directions. Table 5 provides the necessary conditions to prevent the occurrence of the frequency splitting phenomenon in basic compensation topologies.

Constant voltage/current output, low cost, compact design, and minimizing reactive power are some of the other primary goals of the compensation techniques [111]. In addition, various energy storage characteristics necessitate a broad operational range from the charging system, that is extremely troublesome to achieve under varying loads and couplings [107], [112]. For this reason, the compensating system must decrease the sensitivity to load and coupling fluctuation and smooth out output fluctuations caused by a broad range of parameter deviation [113]. In Fig. 23, we can see an illustration of the presented compensation network categorization. It is introduced to categorize compensations based on their position on the transmitting or receiving side, both side compensation, or with multiple transmitting and receiving coils. This is possible for there to be one, two, or more compensating components on each side.

TABLE 4. Comprehensive comparison involving different parameters of four basic topologies [109].

Topology	Q_t	Q_r	Z_{ref} at resonance	Z_T	I_t at resonance	Output Characteristics
SS	$\frac{L_t R}{\omega M^2}$	$\frac{\omega L_r}{R}$	$\frac{\omega_o M^2}{R}$	$\frac{\omega^2 M^2}{Z_r + \frac{1}{j\omega C_r} + R_L} + Z_t + \frac{1}{j\omega C_t}$	$\frac{V_s R}{\omega_o M^2}$	Voltage source at the receiving side
SP	$\frac{\omega L_t L_r^2}{M^2 R}$	$\frac{R}{\omega L_r}$	$\frac{M^2 R}{{L_r}^2} - \frac{j\omega_o M^2}{L_r}$	$\frac{\omega^2 M^2}{Z_r + \frac{R_L}{1 + j\omega R_L C_r}} + Z_t + \frac{1}{j\omega C_t}$	$\frac{V_s {L_r}^2}{M^2 R}$	A current source at the receiving side
PS	$\frac{L_t R}{\omega M^2}$	$\frac{\omega L_r}{R}$	$\frac{\omega_o M^2}{R}$	$\frac{1}{\frac{\omega^2 M^2 (1 + j\omega R_L C_r)}{Z_r (1 + j\omega R_L C_r) + R_L} + Z_t + j\omega C_t}$	$\frac{V_s R}{\omega_o M^2}$	Voltage source at the receiving side
PP	$\frac{\omega L_t L_r^2}{M^2 R}$	$\frac{R}{\omega L_r}$	$\frac{M^2 R}{{L_r}^2} - \frac{j\omega_o M^2}{L_r}$	$\frac{1}{\frac{1}{\frac{\omega^2 M^2 (1 + j\omega R_L C_r)}{Z_r (1 + j\omega R_L C_r) + R_L} + Z_t} + j\omega C_t}$	$\frac{V_s {L_r}^2}{M^2 R}$	A current source at the receiving side

TABLE 5. Transmitting capacitance, frequency splitting condition and sensitivity to the coupling coefficient for major compensation topologies [109], [134].

Topology	Transmitting Capacitance (C_t)	(C_{tn})	Frequency Splitting Condition	Sensitivity to the coupling coefficient	Load reasonability
SS	$\frac{C_r L_r}{L_t}$	1	$Q_t > \frac{4{Q_r}^3}{{Q_r}^2 - 1}$	C_t and C_r do not depend on the coupling coefficient	$R_L < \sqrt{\frac{L_r}{C_r}}$
SP	$\frac{C_r {L_r}^2}{L_t L_r - M^2}$	$\frac{1}{1 - k^2}$	$Q_t > \frac{{Q_r}^2 + 1}{Q_r}$	C_r depends on the coupling coefficient	$R_L > \sqrt{\frac{L_r}{C_r}}$
PS	$\frac{C_r L_r}{\frac{M^4}{L_t L_r C_r R} + L_t}$	$\frac{1}{1 + Q_r^2 k^4}$	$Q_t > Q_r$	C_t depends on the coupling coefficient	$R_L < \sqrt{\frac{L_r}{C_r}}$
PP	$\frac{C_r {L_r}^2 (L_t L_r - M^2)}{(L_t L_r - M^2)^2 + \frac{M^4 C_r R}{L_r}}$	$\frac{(1 - k^2)}{(1 - k^2)^2 + Q_r^2 k^4}$	$Q_t > \frac{{Q_r}^2 + 1}{Q_r}$	C_r depends on the coupling coefficient	$R_L > \sqrt{\frac{L_r}{C_r}}$

The simplest compensation topologies are those with one compensating capacitor on either side of the WPT system. They are addressed in further depth in the following section. Various hybrid topologies have been built from these basic topologies, and these are discussed below. These hybrid topologies include one or more compensating capacitors, as well as an additional inductor. Because these topologies have distinct benefits, they can be employed in the specific application. The downsides of such systems are their increased complexity and cost, especially with the inclusion of extra inductors. All these questions are described in Tables.

B. ANALYSIS AND COMPREHENSIVE COMPARISON OF THE BASIC ONE-ELEMENT COMPENSATION TOPOLOGIES

A WPT system's compensation topology is crucial. Reactive power compensation is the primary focus of the compensation system, as described above. Meanwhile, soft-switching under varying operating scenarios is also dependent on slight portion of reactive power, which is essential for high-frequency converters to function efficiently. Hence, in order to maximize the WPT system's usefulness, it's important to consider a number of crucial design criteria, such as the source angular frequency and compensation capacitances. Accordingly, this section will analyze in depth to understand the features of basic one-element compensation topology. The analytical results of all the topologies are compared and summarized in Tables 4-6. The four basic compensation topologies, known as series-series (SS), SP, PS, and PP, are broadly employed in EV applications as shown in Fig. 24. Their names come from the arrangement of the transmitting and receiving side coil connected to the single compensation element on their transmitting and receiving sides. Capacitors connected in series or parallel with the transmitter coil are denoted by the first letter S or P, respectively [29], while capacitors connected in series or parallel with the receiver coil are denoted by the second letter S or P, respectively. In [109], [114], and [115], these basic topologies are examined in depth. By comparing these basic compensations, only SS topology has the property that its resonant frequency is not affected by variation in the coupling coefficient or load. EV and PHEV application necessitates this function of SS topology, and specifically for the quasi dynamic and dynamic wireless charging system. Irrespective of how efficient a driver is at parking or driving, the load varies as the battery charges along with the variation in the coupling coefficient with respect to the relative position between the transmitting and receiving coils [116].

TABLE 6. Load power and power transfer efficiency descriptions for four basic topologies.

Topology	Load Power	Power transfer efficiency	Maximum efficiency and its condition
SS	$P_{L-SS} = {A_{SS}}^2 {I_t}^2 R_L$ where, A_{SS} is current gain, $A_{SS} = \frac{I_t}{I_r} = \frac{j\omega M}{R_L}$	$\eta_{SS} = \frac{{A_{SS}}^2 R_L}{Z_T} = \frac{R_L}{(R_L + R_r)(1 + \frac{(R_L + R_r)R_t}{\omega^2 M^2}}$	$\eta_{SS-max} = \frac{R_L}{R_L + R_r}$ when, $\omega \gg \frac{\sqrt{(R_L + R_r)R_t}}{M}$
SP	$P_{L-SP} = \frac{{A_{SP}}^2 {I_t}^2 \omega^2 {L_r}^2}{R_L - j\omega L_r}$ where $A_{SP} = \frac{j\omega M(R_L - j\omega L_r)}{\omega^2 {L_r}^2}$	$\eta_{SP} = \frac{{A_{SP}}^2 \omega^2 {L_r}^2}{Z_T(R_L - j\omega L_r)}$ $= \frac{R_L}{R_L + R_r + \frac{{R_r}^2 R_t}{\omega^2 M^2} + \frac{R_t {L_r}^2}{M^2} + \frac{{R_L}^2 R_r}{\omega^2 {L_r}^2}}$	$\eta_{SP-max} = \frac{R_L}{R_L + R_r + \frac{R_t {L_r}^2}{M^2}}$ when, $\omega \gg \frac{\sqrt{{R_L}^2 M^2 R_r + {R_r}^2 {L_r}^2 R_t}}{L_r M}$
PS	$P_{L-PS} = {A_{PS}}^2 {I_t}^2 R_L$ where $A_{PS} = \frac{I_t}{I_r}$	$\eta_{PS} = \frac{{A_{SS}}^2 R_L}{Z_T}$ $= \frac{R_L}{(R_L + R_r)(1 + \frac{(R_L + R_r)R_t}{\omega^2 M^2}}$	$\eta_{PS-max} = \frac{R_L}{R_L + R_r}$ when, $\omega \gg \frac{\sqrt{(R_L + R_r)R_t}}{M}$
PP	$P_{L-PP} = {A_{PP}}^2 {I_t}^2 R_L$ where $A_{PP} = \frac{I_t}{I_r}$	$\eta_{PP} = \frac{{A_{PP}}^2 \omega^2 {L_r}^2}{Z_T(R_L - j\omega L_r)}$ $= \frac{R_L}{R_L + R_r + \frac{{R_r}^2 R_t}{\omega^2 M^2} + \frac{R_t {L_r}^2}{M^2} + \frac{{R_L}^2 R_r}{\omega^2 {L_r}^2}}$	$\eta_{SP-max} = \frac{R_L}{R_L + R_r + \frac{R_t {L_r}^2}{M^2}}$ when, $\omega \gg \frac{\sqrt{{R_L}^2 M^2 R_r + {R_r}^2 {L_r}^2 R_t}}{L_r M}$

Given the dual nature of series and parallel compensations on the output characteristics, Zhang et al. [117] recognized, transmitting and receiving sides could employ various compensation techniques to achieve the optimal load profile. For validating the above point, a constant output current supply regardless of the load variation is created by using the SS topology to compensate for self-inductance and a fixed output voltage source is generated by compensating the leakage inductance. When it comes to voltage and current gains, SS compensation typically has a number of ''particular'' working frequencies. In order to change the output profiles between a CC source and a voltage source, it is necessary to operate on varying ''particular'' frequencies [116]. Higher sensitivity with respect to coupling variation is highlighted by the fact that the voltage gain at the particular frequency of SS and SP compensations is observed to be proportional to the coupling coefficient [118]. In order to achieve a voltage gain that is not affected by the load, the impedance of a fixed-frequency SS-type topology is optimized in [116]. Keeping the frequency as close to the resonant frequency, helps to maintain the reactive power of the system low. This approach, however, necessitates a trade-off between reactive power and load voltage stability and does not address the underlying problem of how reactive power, load voltage gain, and a changing coupling coefficient interact with one another.

Power factor and the input-to-output voltage transfer function of the compensating network (compensation capacitors and two coils) are influenced by the transmitting-side capacitance in the SP topology [119]. Therefore, the inverter and resonant-circuit efficiencies are both impacted by the capacitance of the primary-side capacitor. When it comes to strong magnetic coupling, the SP topology is dependent on the coupling factor (2) and necessitates a larger value of the primary capacity [120], [121]. The primary capacity of an SP topology is found by solving for (2), where M is the mutual inductance that makes the value depend on the coupling coefficient. Choosing the primary capacity is heavily impacted by the selected topology. An important benefit of the SP topology is that it requires less secondary inductance than the SS topology [63], [112]. Concurrently, a higher primary capacity was required [29], [122]. Since the primary current is proportional to the primary input voltage, the output voltage of an IPT with an SP topology is proportional to the primary input voltage for a constant magnetic coupling system [123], [124]. When using an SP topology, increasing the system's mutual inductance improves its performance [125], [126].

In [127], the author explains how to determine the capacitance value to obtain the zero reactive power state for the compensation topology by considering the load scenario and the frequency-bifurcation behavior. A paralleled capacitor cannot be used for primary side compensation due to the voltage source being widely used to drive high power converters.

When the coupling factor and the receiving side quality factor is low, a higher transmitting side capacitance is needed in the PP topology, but this value can be reduced when the coupling is strengthened as well as the receiving side quality factor. Using a PS topology invariably requires a lower transmitting side capacitance, and this shift gets bigger to stronger coupling or a larger receiving side quality factor [29]. Because of the greater load voltage of the parallel receiving side and the higher current input demands of the parallel transmitting side, the PP topology has a low power factor

[128], [129], [130]. Greater efficiency and large power factor at weak coupling and a considerably higher range of load fluctuation as well as coupling factor are two of the major benefits of the PS and PP configurations [111], [127].

In the light load scenario, and with the no compensation at the receiving side, the corresponding impedance is zero at the main resonance frequency, curtailing the current just by the parasitic elements of the capacitor and inductor [125]. This is the big downside of the SS topology. The load dependency of the output to input voltage transfer function is another drawback of the SS compensation technique that can make the control more difficult and decrease the system's partial-load efficiency [63], [131]. The compensation action in response to a change in coil position is a crucial criterion. Basic topology misalignment is considered in [115], [127]. The total impedance (Table 4) of the system as seen by the power input is affected if the coils are not aligned properly. A lower total impedance occurs in the SS and SP topologies, leading to higher currents in both the load and the source. The total impedance rises with misalignment in the PS and PP topologies, leading to a sharp drop in the source and load currents.

The output current could not vary with the load at the resonance frequency [63], and it has been established that SS compensation does not depend on the coupling coefficient. This means the system is relatively insensitive to coil imbalance, and the resonant frequency of the resonator should remain stable in the absence of element tolerance levels. The average absolute value of the phase of the primary input impedance is significantly lower when the secondary side employs series compensation (SS or PS) as opposed to parallel compensation (SP or PP) [132], [133].

By maintaining the inductive input impedance of the converter, zero-voltage switching is guaranteed in the primary side switches of the SS topology while the output diodes are turned on and off at zero current. In fact, very high frequency execution is feasible if all switches support soft-switching [121]. The output voltage of an IPT with an SP topology is proportional to the transmitting current, which is in turn regulated by the transmitting side voltage source for a constant magnetic coupling system [123]. A rise in mutual inductance in an SP topology enhances system efficiency [125], [130].

According to the study carried out in [134] and [135], the effectiveness of a parallel topology is superior to that of a series topology when dealing with a high load on the secondary side.

The SS topology excels, if somewhat within a limited load range, once the separating value of the load resistance is less than the impedance of the resonant capacitor on the receiving end. In [134], you can see a drastic reduction in these features. At greater load resistance, however, the SP compensation is preferred as the impedance of the receiving side resonant capacitor dominates the equivalent impedance of the parallel branch containing load resistance and compensating capacitor [134].

An additional favorable aspect of utilizing series topology on the receiving side is that, at the resonance frequency, the reflected reactance of a series compensated receiver is zero, while the reflected reactance of a parallel compensated receiver system is negative (Table 4) [109]. The reflected reactance appears in the context of parallel compensation on the receiving side, but its value is not load dependent, so it can be changed as needed. Once the load is zero, this could be proved that the reflected resistance and the power transfer capability both increase to infinity under the assumption of a uniform transmitting current with the series topology [109]. When the amount of load grows infinitely large, an identical scenario occurs with parallel-compensated WPT networks [109]. This can be considered a key distinction between series-compensated and parallel-compensated receivers. When the transmitting side has a series topology, the reflected resistance equals the load resistance. But the transmitting side capacitance and inductance, as well as the reflected reactance, determine the load reactance. The transmitting side inductance, reflected resistance, and reactance all affect the load conductance, while the transmitting side capacitance and inductance all affect the load susceptance for a parallel compensated transmitting side [109]. In addition, [136] looked into receiver-side compensation configurations, and found relationships between the values of transmitted-side parameters that corroborated the aforementioned conditions.

The coupling factor having either no impact or a little impact on the voltage and current stress is a further consideration [125], [135]. If there is an alignment error between the transmitting and receiving coil, coupling of magnetic fields reduces drastically. Under such a circumstance, the compensation system must ensure the WPT system operates reliably. The total impedance of the system seen from the source side must be infinity for the source driven by a current supply and zero for voltage driven source to enable zero or a poor coupling circumstance [137]. However, the SS topology is restricted from having zero coupling. The bifurcation could not take place if the transmitting side quality factor is higher than the receiving side quality factor. It is important to determine the transmitting side capacitors for operating at the resonant frequency in order to examine the relation of the compensation configurations on the coupling coefficient and they are shown in Table 5. Systems that have long primary tracks are good fits for a series compensation, as this type of compensation involves placing the capacitive element in series with the transmitting track. Because of this, the track voltages can be controlled such that they remain within the utmost permissible levels. When analyzing the sizing for the capacitors, the series compensation provides better voltages and smaller currents as compared to parallel compensation [138]. Because of the greater efficiency, the SS compensation

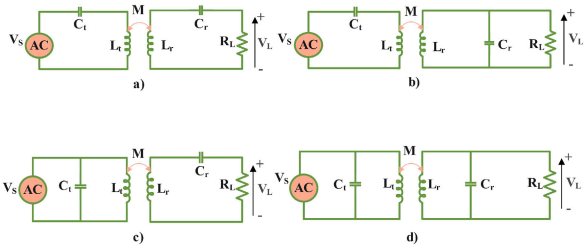

FIGURE 24. Basic one element compensation topologies (a) SS (b) SP (c) PS (d) PP.

finds the most widespread usage in practical applications and operation [136], [139].

In 2018, Duc Hung Tran et al. [140] presented an FHA approach and the Thevenin theorem for a four-coil WPT model in series-series compensation. The suggested technique can fulfil the zero phase angle criteria in dual CC, and CV modes and operates at a set frequency at every charge mode and allows for full soft switching of fundamental switching components. Given that it is not intended to reach the ZPA condition throughout the entire charge cycle, this system cannot achieve full soft switching. In 2019, Jason Pries et al. [141] considered wye-connected three-phase resonance systems with series compensation. It offers a series-compensated three-phase resonance circuit adjusting approach based on the Clarke transformation. Different control schemes were used to adapt the framework to voltage, current, load, and packaging requirements for specific applications. In 2015, [142] presented high-frequency DC-AC and AC-DC WPT stages with a current-fed configuration for the inverter stage. Inverter switching strain is reduced by half compared to the traditional LC parallel resonance tank networks using resonance tank networks. In 2015, Changbyung Park et al. [143] adopted a series-series resonant compensation scheme for constant power I-type IPT systems in OLEVs with DQ-power supply rails. This work introduced a dq power supply rail powered by two high-frequency AC currents of the d and q phases. This technology maintains narrow width, greater air gap, better power output, and reduced building costs. This study's parameters are stationary phasors, which are complex numbers. In 2019, Ali Zakerian et al. [144] modeled a typical WPT system with an EV charging series-series correction circuits. It lowers the device's startup and ongoing running costs.

C. MULTIELEMENT HYBRID COMPENSATION TOPOLOGIES

In order to circumvent the aforementioned challenges of basic one-element compensation topologies, employing SP compensation with one or more elements forming a hybrid topology is a useful technique. Multiple capacitors can be added in series or parallel on transmitting or receiving side (as shown in Fig. 25f–h), or extra inductances can be added in series or parallel. (Fig. 25a-e). Capacitance (C) and inductance (L) can also be connected in tandem to form different circuit configurations. Due to the isolation of the output voltage from the load, the LCL compensation is widely used in specific contexts. In addition, the resonant network's input port can have a power factor of unity independent of load or coupling [145]. Incorporating a capacitor into the coil branch creates a second, enhanced LCC compensation that keeps all of the benefits of the original. Also, since the additional capacitor partially cancels the leakage inductance of the coil, the achievable voltage gain is enhanced [110]. It's worth noting that the T-type compensation output also reveals a duality relationship with the secondary-side compensation technique. Secondary parallel compensation will alter the output source characteristics similarly to how secondary series compensation does [128]. Cascaded LCL-P compensation using a boost converter has been widely used for charging electric vehicles, according to a prior study [146]. To link the boost inductor, the LCL-P compensation is used as a current source. Besides SS compensation topologies, many other novel compensation topologies have been proposed. However, not all of them share the same qualities. When applied to WPT, the inductor/capacitor/inductor (LCL) resonant circuit described in [105] provides a primary side resonant circuit. Nonetheless, it did not demonstrate the approach to design such three components, and the resonant frequency varies with the coupling coefficient and load. Primary and secondary sides of the circuits in [147] and [148] use LCL and capacitor/inductor/capacitor/inductor (CLCL) systems. The coupling coefficient and load have no effect on the resonant frequency. The inductances of the extra inductors are the same to or higher than the inductances of the main coils in such configurations, but such two studies only addressed designing and control. In [1], the study investigated a double-sided LCC compensation configuration where the introduced inductors have lower inductances than the main coils. Double-sided LCL or CLCL architectures are equivalent in many ways to this one. As described within this article, ZVS condition was achieved, and all relevant features were discussed.

Furthermore, work in [149] proposed a hybrid compensation scheme that could power multiple electric bicycles (EBs) with one DC/AC converter by transitioning between SS and series-inductor-capacitor-capacitor (S-LCC) topology. Even so, accurate and consistent placing of magnetic couplers had been essential for the aforementioned compensation configurations. Otherwise, the system deteriorates significantly due to coil misalignment.

Using the qualities of compensation topology, studies also have been able to decrease the impact of variations in the coupling factor, simplifying the system configuration and cutting down on extra components. In order to transmit the nominal power at a coil misalignment of 25%, a CCL-type compensation configuration has been suggested in [115]; however, the paper does not specify the coupling coefficient variation range. A four-coil design was used in the literature [150]. To maximize the efficient load scenarios, the researchers enhance the compensating capacitance within each coil to reduce the power curve's variation to the coupling

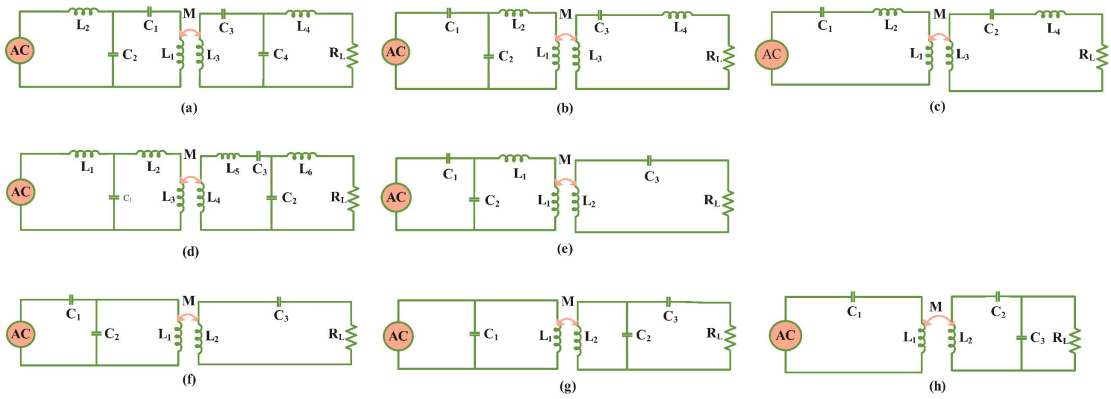

FIGURE 25. Multiple element hybrid compensation topologies: (a) LCC-LCC (b) CCL-LC (c) LC-LC (d) LCL-LCCL (e) LCC-S (f) SP-S (g) P-PS (h) S-SP.

factor. A constant power transmission was accomplished over varying distances in [151]. The authors did this by using a changing capacitor array to monitor the highest possible output. On the other hand, the tunable resonant system requires the addition of numerous passive elements and switches. Because there are now more points at which a system could possibly perform poorly, the stability of that kind of a scheme suffers as a direct consequence.

High efficiency is retained across a large variety of magnetic coupling and loading in hybrid topologies (e.g., LCL-LCL, LCC-LCC) [144]. Nevertheless, in the event of a greater power transfer, the additional inductances and capacitances in the hybrid topologies, as well as their parasitic resistances, may cause much copper loss than the SS topology for the same power output. Hybrid topologies are more expensive and challenging to regulate than SS topologies. Nonetheless, when used in conjunction with a voltage source inverter on the transmitting side, the current source characteristics of LCL-LCL and LCC-LCC topologies on the secondary side make them promising hopefuls for the rechargeable batteries uses [26], [152]. Capacitor and inductor equivalent impedances have 180° opposite phases. For the CC/CV method through hybrid circuit design for bulk charging of electric bikes, either the LCL or CLC topology can be utilized [148], [152].

As mentioned in [152] and [153] once the input voltage is held constant, the RMS output current of the double-sided LCC compensation topology remains unchanged. Zero Current Switching (ZCS) can be attained by fine-tuning the LCC compensation. The reactive power on the secondary side can also be balanced out by the LCC pickup, resulting in a pickup with a power factor of unity. The above compensation operates regardless of the coupling coefficient and the applied load [1], [154]. Because of its low inverter current stress, high efficiency, greater misalignment sensitivity, and load independence features, double-sided LCC compensation has gained widespread adoption [83], [152], [154], [155], [156].

The transmitting side series resonant circuit has benefits such as a reliable power supply and the elimination of dc component in the input signal thanks to a capacitor connected in series. When a sizable amount of high-frequency current flows through a series capacitor, however, a large capacitor voltage is produced [157]. There is no dc component suppression in the parallel compensated transmitter circuit, but it does provide no-load regulation and a reliable current supply. On the receiver side, the stable voltage is produced by a receiving side series resonant circuit that reflects only the resistive part to the transmitting side. The stable current required for battery chargers is provided by the parallel receiving side resonant circuit. Both real and imaginary components of the impedance can be reflected to the transmitting side using this circuit [157].

The study in [158], which contrasts double-sided SS compensation with LCC compensation, is used to evaluate the superiority of one classical compensation topology over the other. As can be seen in the study, under optimal conditions, the double-sided LCC compensation topology is more resilient to changes in the coupling coefficient. Dual LCC compensation topology reduces voltage and current stresses on series capacitors and main coils [158].

In order to achieve the fixed gain intersection, point at zero phase angle of the input impedance, a novel S/SP type compensation contactless resonant converter is proposed in [159]. While the constant gain value does not depend on either the load or the coupling coefficient, it does remain constant over time. The output voltage gain is also insensitive to parameter changes near the gain intersection point, which is a nice feature. Under the influence of large variations in the parameters, the S/SP type of compensation is able to achieve a stable output with minimal circulating losses [160], [161].

At full resonant frequency, the S/S compensated converter's gain in output voltage is proportional to the load, leading to a large output voltage swing. Therefore, the S/S compensation is unable to realize a constant voltage gain at the input phase angle of zero. When compared to an SP compensated converter, a S/SP compensated converter's output voltage gain is less sensitive to changes in the transformer's parameters. Constant gain and high efficiency are

thus possible for the full resonant frequency with the S/SP compensated and SP compensated converters. As a result, the S/SP compensation can be used for a variety of specifications and in high scenarios [160].

When it comes to reactive power, the S/SP compensation does quite well because it achieves proper compensation of both the leakage reactance and the magnetizing inductance. As can be seen in literature [160], the input to output voltage transfer ratio is also constant over a limited range of load and coupling factor. The major downside is that as the coupling factor is reduced, the reactive power rises sharply, implying only partial decoupling. The output reliability and reduction of reactive power need to be kept across a broad working condition, but due to the loosely coupled nature of transformers, neither compensation configuration could really ensure this. As a result, it is necessary to find a balance between the design parameters. Table 7 [161] summarizes the concepts of load independent output type, load impedance matching requirements, and compensation element design for mostly adopted basic and hybrid compensation topologies, and a similar table can be formed for the remaining compensations.

In the available literatures of DWPT systems, basic compensations like second order LC circuit and higher order geometries are examples of compensation geometries used by the researchers. Table 8 highlights different systems transfer characteristics used for key control strategy, zero-voltage switching (ZVS), and interconnectivity of one compensation to others in WPT system, which govern their functions in both WPT and DWPT controls. The CCC-T configuration [114] works like a series-series (SS) compensation, the LSP-S topology [123] works like an LCCL-series (LCCL-S) compensation, and the LCC-LCC topology [26] performs analogously to a series-parallel (SP) compensation.

A WPT system with basic compensation topologies is shown in Fig. 24. In this model, V_s is the high-frequency supply voltage, which is produced from a high frequency inverter. The transmitting and receiving side coils have self-inductances of L_t & L_r and internal resistances of R_t & R_r respectively. M is the mutual inductance and R_L is the equivalent load resistance. The capacitors C_t and C_r are used in series with the inductances to eliminate reactive power and improve power transmission efficiency.

Fig. 26 depicts the T-equivalent circuit of WPT system comprising four basic compensation techniques. Using Fig. 26, a comprehensive summary of four basic topologies involving receiving side Quality Factor (Q_r), reflected resonant impedance at the transmitting side (Z_{ref}), total impedance is seen from the transmitting side (Z_T), resonant transmitter current (I_t) and output characteristics are given in Table 4. Z_t and Z_r are the transmitting and receiving side inductive impedance MRC-WPT system and is defined by ignoring parasitic capacitances of both coils,

$$Z_t = R_t + j\omega L_t \tag{5}$$
$$Z_r = R_r + j\omega L_r \tag{6}$$

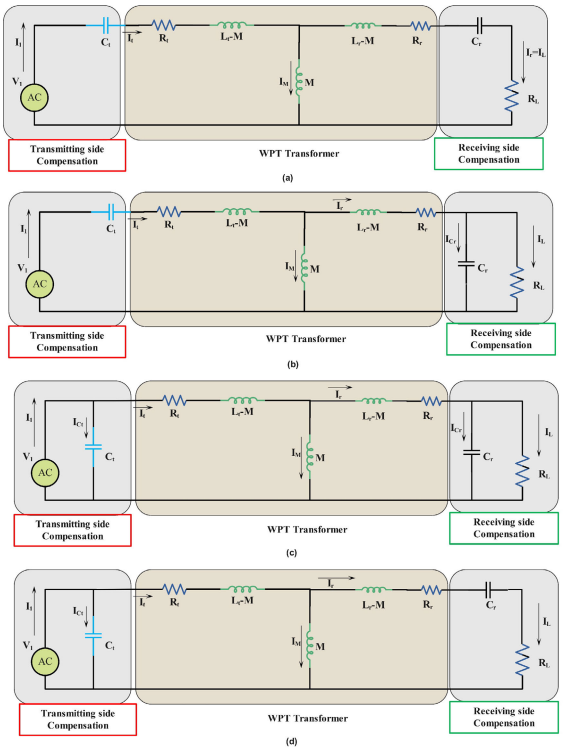

FIGURE 26. T-equivalent circuit of WPT system comprising (a) SS, (b) SP, (c) PP and (d) PS compensation topologies.

where, R_t, R_r, L_t and L_r are the internal resistances and self-inductances of the transmitting and receiving coils respectively. Normally, the transmitting and receiving side resonant frequencies are equal and given by

$$\omega_o = \frac{1}{\sqrt{L_r C_r}} = \frac{1}{\sqrt{L_t C_t}} \tag{7}$$

Mutual inductance (M) is defined as

$$M = k\sqrt{L_t L_r} \tag{8}$$

where k is the coupling coefficient.

In Table 5, transmitting capacitance (C_t) expression, conditions to avoid frequency splitting phenomenon and sensitivity to the coupling coefficient for basic compensation topologies are shown [109], [134]. Here Q_t, C_r and R_L denote the transmitting side quality factor, receiving side capacitance and load resistance respectively. The receiving side quality factor (Q_r), that has to be measured in order to obtain transmitting side compensation. The expression for Q_r in series and parallel compensated receiving side is described in Table 4, with ω_o depicting the resonant frequency. The quality factor is a measure of the performance of a coil in a circuit., defined as the reactive power divided by the active power. When there is more than one ZPA frequency in a WPT system, frequency splitting phenomena develops. This phenomenon is proven to be strongly dependent on coil quality factors [29], [109]. To prevent the WPT system from experiencing the frequency splitting phenomenon, Q_t must be higher than Q_r at all times.

TABLE 7. Comparison of performance among basic and hybrid Compensations.

Topology/Attribute	SS	SP	LCL/LCC-S	LCC-LCC
Load independent output type	current	voltage	voltage	current
load impedance matching criteria	$\frac{R_L}{\omega_o L_r} \approx k$	$\frac{R_L}{\omega_o L_r} \approx \frac{\sqrt{k^2+1}}{k}$	$\frac{R_L}{\omega_o L_r} \approx k$	$\frac{R_L}{\omega_o L_r} \approx k$
Compensation element design	$C_t = \frac{1}{\omega_o{}^2 L_t}$ $C_r = \frac{1}{\omega_o{}^2 L_r}$	$C_t = \frac{1}{\omega_o{}^2 L_t(1-k^2)}$ $C_r = \frac{1}{\omega_o{}^2 L_r}$	$C_t = \frac{1}{\omega_o{}^2 L_p}$ $C_r = \frac{1}{\omega_o{}^2 L_r}$	$C_t = \frac{1}{\omega_o{}^2 L_p}$ $C_{t1} = \frac{1}{\omega_o{}^2 L_t}$ $C_r = \frac{1}{\omega_o{}^2 L_r}$ $C_{r1} = \frac{1}{\omega_o{}^2 L_{r1}}$
Capability to lower the reactive power	Superior under the wider range of load and coupling. Poorly linked with the load once away from ZVS	Superior under the rated scenario. decrease ones moves away from the rated operating point.	Superior under the wider range of load and coupling. Poorly linked with the load once away from ZVS	Superior under the wider variety of load and coupling.

TABLE 8. Comparison of major compensations in DWPT system, their transfer characteristics and useful aspects for developing key control strategy.

Compensation Topology	System transfer characteristics	pros and cons	Connection with another topology
S/S [143]	At resonant frequency, load current is constant.	ZVS operation is easy. weak magnetic coupling and greater current when load is smaller.	Can be linked with another topology easily.
S/P [61], [132]	Makes possible with some adjustments to the network's topology in the dynamic wireless power transfer, for power outlets to turn on and off by themselves [26].	Higher current in power with respect to coupling coefficient. As reflected impedance contains capacitive part also, ZVS operation is difficult.	Can be linked with another topology easily.
P/S [166]	Ideal for circuits with minimal inductance. Significant voltage stress throughout switching devices and wide power swings in relation to the coupling coefficient.	ZVS operation is difficult as it contains current source inverter.	Can be linked with another topology easily.
LCCL/S [167]	At resonant frequency, transmitting current is constant	Filtering of transmitter current can be done effectively, power variations are lower [22, 41]. Compensation circuit size and volume increases. ZVS operation is easy.	Can be linked with another topology easily.
LCCL/P [168]	At resonant frequency, transmitting current is constant.	Greater power variations in comparison to LCCL/S. As reflected impedance contains capacitive part also, ZVS operation is difficult.	Can be integrated with another topology easily.
LCCL/LCCL [169]	Good control over transmitter current.	ZVS operation is easy. power variations are lower. Effective filtering of both transmitter and receiver currents. Greater size and volume of the compensators in comparison to the topologies mentioned earlier.	Can be integrated with another topology easily.
Hybrid series topology [170]		power variations are lower with respect to coupling coefficient. ZVS operation is easy. It involves combine advantages of S/S and LCCL/LCCL. Compensation circuits designs are more complex.	Can be integrated with particular coupler coils on both sides only.

As can be seen in Fig. 5, a normal WPT system consists of multiple levels of conversion. The input power and output or load power is calculated as

$$P_{in} = I_1^2 Z_T \tag{9}$$

$$P_L = I_L^2 R_L \tag{10}$$

Using equation (5) and (6), power transfer efficiency of the WPT system is given by Eq. (7).

$$(\%) = \frac{P_L}{P_{in}} \times 100 \tag{11}$$

To mitigate the issues such as large frequency or phase shift associated with varying load, we need to operate the transmitting side ZPA at or close to the receiver side resonant frequency [109], [162], [163]. With this methodology, we can balance out not only the transmitting inductance (L_t) but also the reflected impedance (Z_{ref}) that is already connected in series with the transmitting coil. The normalized transmitting capacitance (C_{tn}) can be defined as the ratio of transmitting side capacitance from Table 5 to the transmitting capacitance obtained from (5) and Fig. 27 depicts C_{tn} with respect to coupling coefficient for $Q_r = 10$. This is done so that the

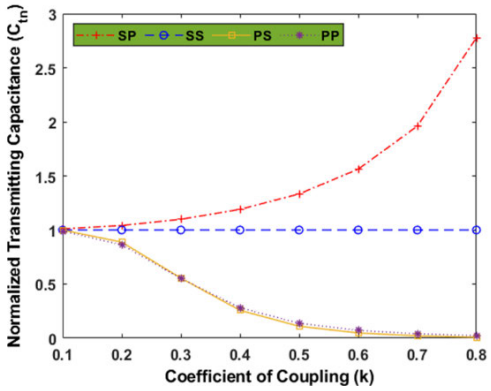

FIGURE 27. Normalized transmitting capacitance with respect to coupling coefficient.

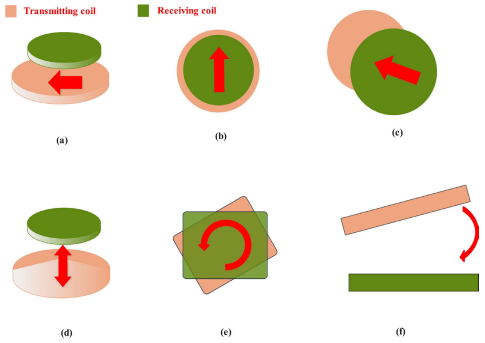

FIGURE 28. Examples of Misalignment forms of few coils: (a) longitudinal. (b) lateral. (c) xy plane (d) vertical. (e) rotational. (f) angular.

effects of the coupling coefficient and Q_r on the proposed transmitting side compensation design can be obtained.

Fig. 27 demonstrates that the SS topology does not necessitate any modifications.

A higher C_t with enhanced coupling is essential for the SP topology. When the coupling is weak as well as Q_r is low, a higher C_t is needed for the PP topology, but this value can be reduced when the coupling is strengthened or Q_r is high. With better coupling or a higher Q_r, C_t needed for a PS topology circuit will always be lower. Table 6 describes the load power and power transfer efficiency expressions for four basic topologies [162], [164], [165].

In both the SS and SP architectures, the input side impedance is quite small at the resonant frequency, enabling a significant portion of input current to flow via the transmitter coil to produce the greatest magnetic field across the coil and, consequently, a suitable induced emf and current to be generated in the receiver coil to power the EV battery.

However, the input impedance of the PS and PP architectures is greater at the resonant frequency and so a lower current flow in the transmitter coil, resulting in a poor induced emf and current at the receiving side. And thus, the SS and SP architectures are much more effective at transmitting power than the PS and PP.

Table 9 represents a brief discussion of developed compensation topologies of the WPT system involving different compensation topologies and their industrial applications.

IV. MISALIGNMENT TOLERANCE

In most installations, WPT transmitting coils are buried or mounted flush with the ground, however in some cases, surface mounting may be allowed as long as a stringent height limit is followed [57]. Aligning the transmitting and receiving coils properly is essential for achieving maximum power transfer efficiency to charge an EV. It can be challenging to correctly place the transmitter and receiver during either the static or dynamic charging of an EV, as this is highly dependent on the driver, EV, along with surrounding neighborhood. For misalignment, SAE J2594/1 recommends a system performance of 80% or higher [57]. SAE J2594/1 specifies that a WPT system requires to be capable to tolerate longitudinal and lateral misalignments, as well as z-axis variability because of automobile ground clearance and loading. Acceptance limits for both angular and rotational misalignment (yaw) are further outlined, with specifications provided in Tables 10 and 11. Many experts have weighed in on the issues mentioned above and offered their own suggested methods [61], [171], [172], [173], [174], [175], [176], [177], [178], [179]. While a few approaches emphasize control strategies such as adjusting the resonance frequency to boost system performance [182], others target optimizing the coil structure to increase alignment sensitivity [63], [64], [67], [69]. The LCC and LCL resonant compensation systems are two examples of higher levels compensating methods that have received attention from researchers [61].

The different misalignment forms, in addition to the fluctuation in coupling coefficient and angular form of misalignment, are depicted in Figs. 28 and 29. When the air gaps are half the diameter of the transmitting coil, the main coil diameter needs to be the same as, or just a little larger than, the receiving coils for a favorable coupling coefficient. As a result, several investigators have turned to the modular technique, because following this recommendation results in very large coils [178], [179]. In [67], it was reported that a polarized flux pipe may tolerate ore misalignment than a circular pad. In [73], a DDQ coupler was investigated to increase the system's alignment sensitivity. It has three coils, two of them were installed in the direction of d-axis and one installed along the q-axis for quadrature. The quadrature axis coils pick up the flux in the direction of q-axis, which helps to adjust for misalignment. As can be seen in [73], the d-axis receives the sum of the q-axis's output. In [73], it was reported that a BP might function with less copper. Similar to the DDQ coil, it exhibits identical misalignment behaviors.

The misalignment behavior of basic or one element compensation topologies were compared and looked at in [61], and the results were described in Section IV. Misalignment has minimal impact on S-S and P-S circuit compensating methods. Misalignment in a network has been shown to significantly reduce its performance. Adding a capacitor in

TABLE 9. Application and a brief discussion of developed compensation topologies of the WPT system.

References	Compensation topology involved	Application and discussion
[180]–[183]	SS SP, PS and PP	The SS design shines with low and high frequencies, whereas the SP topology provides a more satisfactory response at medium and intermediate frequencies. With a small load and higher working frequency, the SS compensation could have better results as compared to SP one, and both are superior to the PS and PP topologies in terms of power transfer abilities. How well a topology operates in a particular application depends on relation between operating frequency (f) and the crossover frequency (f_c) [132]. For SS design, $f > f_c$ For SP design, $f < f_c$ Possible uses include biomedical implant powering and battery recharge for automobiles.
[184]	SS and SP	SS topologies work better than SP with identical primary and receiving coil sizes. However, the SP design is more effective when $L_t > L_r$
[185]	SS, SP, PS, and PP	In particular, the SP design is well-suited for recharging batteries as they offer fixed load voltage, which is not the case with others. SS and SP designs perform better compared to other hybrid designs.
[186]	SS, SP, LCC-S, LCC-P, LCC-LCC	After considering the on-resistance of the primary converter semiconductors and Z_{ref}, an observation was made for resonance in PS and PP at the primary side, and it was more efficient than SP and SS. Also, for the receiving end, resonance in SP and PP was more effective as compared to SS and PS.
[186], [187]	SS, SP, PS and PP	SP architecture excels with low operating frequencies, while SS excels at higher frequencies and is preferable for EV applications. Both designs involve a voltage source, while the PP and PS topologies have used current sources. Therefore, SS and SP forms are more appropriate for real-world applications. Regarding response time, SP topology is preferable to SS topology when the load on the system is greater. Contrarily, the SS-type system can continue to function well despite considerable frequency fluctuations.
[188]	LCC-C	A particular LCC-C compensation circuit topology's resonant impedance matching property are identified. Using a wireless charging device for implanted cardiac pacemakers has been proven to benefit from the compensating network. The WPT approach can operate at optimum efficiency and stable resonance thanks to the compensating circuit.
[189], [190]	SS, SN	When both coupling factors and the quality factors of the coils are high, the SN topology becomes as efficient like SS design. Like LLC converter, SN one shares a common topology. Given the reduced number of receiver-side components required by the Series-None (SN) topology, this architecture finds utility in biomedical implant and portable electronics applications. The resonance in the receiver winding, that might lead to more power losses in the transmitting side converter is disregarded by S-N. As a result, it is anticipated that this architecture will only function in strong coupling. However, a parasitic capacitor parallel to the receiver winding makes SN design seem like SP one, resulting in the same resonance frequency, even without a capacitor compensation on the receiving end. To simplify the receiver, a dc-dc converter is often left out, although the SN topology's constant voltage output makes it hard to regulate the charging current. Because of the CV output, the SN topology is also vulnerable to short-circuit failure.
[191]–[193]	LCL-T and LCL-LCL	Research on LCL topology for EV dynamic battery chargers was conducted. The behavior of the topology seems like a current supply at the resonance to prevent a overcurrent fault on the receiving end and on the transmitting end as well. To rephrase, the LCL design circuit would achieve a steady current and power factor equal to one.
[194]	LCL-N	Stronger coupling allows for the removal of the receiver-side compensating network. When the LCL compensation is applied to the primary side, it creates the inductor-capacitor-inductor-none (LCL-N) topology. Here, the magnetic flux in the ferrites is cancelled out because the phase shift between the transmitter and receiver currents is more than 90 degrees. Therefore, the LCL-N topology requires less ferrite depth as completely compensated architectures. Since there is no CC or CV output characteristic, the LCL-N architecture is capable of zero-voltage switching under all load situations, can tolerate open-circuit and short-circuit faults, and may be used for both constant-current and constant-voltage charging. This architecture is anticipated to only function in strong coupling and for high-power applications.
[154], [83], [168], [1]	LCC-LCC and LCC-C	The recommended dual LCC design circuit not only achieves the ZVS condition in the primary side inverter but also guarantees constant variation for ω_o regardless of the magnetic coupling factor and the load. This is one of the most common technical issues with EV dynamic battery chargers, it was suggested to develop a powerful responsiveness to the change of coupling effect.
[195], [196]	N-S	For a non-series (N-S) architecture, a small transmitter is favoured if the transmitter is positioned on a moving platform with permanently installed receivers. The N-S topology is expected to handle only low transfer powers, resulting in its ineffectiveness for greater power applications.
[173], [197]–[199]	SS, SP, PS, PP	Other fundamental topologies are presented in contrast to the S-S topology, which can keep its feature of distinct resonant frequency over fluctuations in the magnetic coupling factor. These topologies include the SP, PP, and PS described in this research. However, they are less competitive.

TABLE 10. J2954 guidelines of the misalignment tolerance for WPT sytem [57].

Offset direction	Misalignment distance (mm)
ΔX	± 75
ΔY	± 100
ΔZ	*Given by manufacturer*
Pitch, roll, and yaw	Testing at 2, 2 and 3 degrees

TABLE 11. SAE J2954 guidelines for Z- classes [57].

Z- Class	Ground clearance range to transfer power from ground surface to pick up coil surface
Z1	100 to 150
Z2	140 to 210
Z3	170 to 250

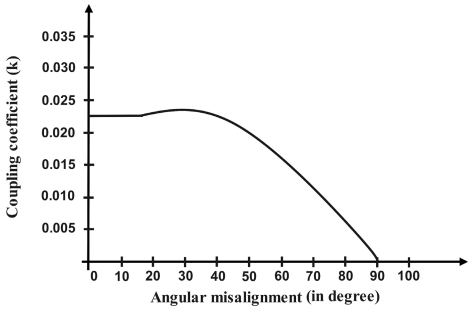

FIGURE 29. Angular misalignment with respect to the coupling coefficient behaviour in a WPT system [95].

series to the receiving side parallel arrangement was suggested by researchers in [179] to increase misalignment efficiency. In [175], researchers claimed a 15% improvement in power transmission performance over a P-P network with a horizontal misalignment of 100 mm. In addition, the power factor value went up from PF = 0.3 to 0.4. In order to achieve the lowest possible frequency and phase shift, the developed method incorporates varying coefficients of coupling. Optimizing the compensating capacitor is an alternative method for enhancing efficiency in misalignment. Four coil WPT systems have been shown to increase efficiency by 38.3 percent [150]. At a coefficient of coupling of 0.18 researchers in [1] and [150] provide a considerable misalignment sensitivity ranging as large as 310 mm and only a 1% reduction in performance. By fine-tuning the variables of the compensation system, misalignment performance is improved and zero voltage switching of the full bridge inverter has been achieved. It was stated in [182] that a control technique may be used to increase the WPT EV charger's efficiency by 5-7% by finding the optimum value of switching frequency and phase shift. Double-sided LCC compensation networks are stated to exhibit tolerance to misalignment, making them ideal for high-power applications. Moreover, it doesn't call for any extra power electronics or supplementary coils [1], [150]. Adjusting the frequency and phase shift to make up for misalignment is a powerful solution that needs no extra elements for applications that use less power [182].

As the front-rear direction for misalignment can be more easily handled by the drivers, current solutions for door-to-door misalignment involve magnetic coupler design, compensation networks, power electronics converters, and the control. It has been demonstrated that decreasing the winding width of a magnetic coupler increases its tolerance for misalignment [200]. Misalignment tolerance was improved in bipolar coils [201] and solenoid coils [202]. Also, it was decided to use anti-parallel windings [203], [204]. Multi-element compensating networks [205], [206], [207], which incorporate compensations like series and LCC (inductor-capacitor-capacitor) compensations, could increase misalignment sensitivity in compensating systems. In addition, the control and power electronics implementation have been designed with this goal in mind [208], [209], [210].

Researchers in [211] suggested a misalignment-tolerant, two transmitting coils, WPT system for EVs with an adjustable architecture to address the issue of door-to-door misalignment as depicted in Fig. 30. In the middle of the system, the S-S topology can be implemented by connecting the two transmitting coils in series to supply power to the load. To improve power transfer capabilities and withstand poor couplings, the two transmitting coils create the LCCC-S (inductor-capacitor-capacitor-series) topology near separation points. With the proposed approach, reliable performance and greater efficiency may be achieved despite a total door-to-door misalignment of 500 mm and 100 mm between the front and back of the vehicle. There are more elements involved in the above topology since it has two transfer power-coupling coefficient profiles and switches can be utilized to transition between the two topologies. In addition, it has been suggested that using four-coil couplers will enhance alignment sensitivity [205], [212]. Using the features of SS and LCL-S compensations with the two distinct frequency channels researchers in [213] developed a dual-frequency adjusting approach to keep the power output stable throughout a wide range of coupling coefficients (0.5 to 0.72). But all these systems have either complicated resonant geometries or limited tolerance for coupling. Against coupling coefficient fluctuations from 0.35 to 0.74, the authors in [214] suggested a system as depicted in Fig. 31 in which the fundamental and third frequency channels become to be the primary power transfer channel in powerful and poor coupling scenarios, respectively, to achieve lower power variations.

For WPT with a wide air gap variation, a reconfigurable resonant design with two switches and four operation modes is suggested [215]. The suggested scheme can be switched between four distinct operational modes by adjusting the switch connections. When the air gap is changed from 95 mm to 215 mm, the suggested changeable resonant design maintains a high transfer efficiency of 92–95 percent while maintaining increased power output. To combat the efficiency loss that occurs due to misalignment, a novel coil WPT

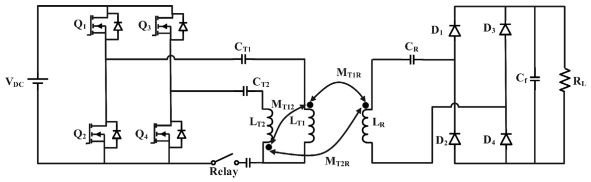

FIGURE 30. Reconfigurable dual transmitting coil-based arrangement for higher misalignment tolerant WPT system [211].

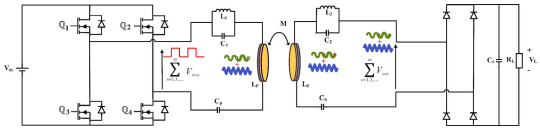

FIGURE 31. Misalignment tolerant dual-frequency-detuning WPT system [214].

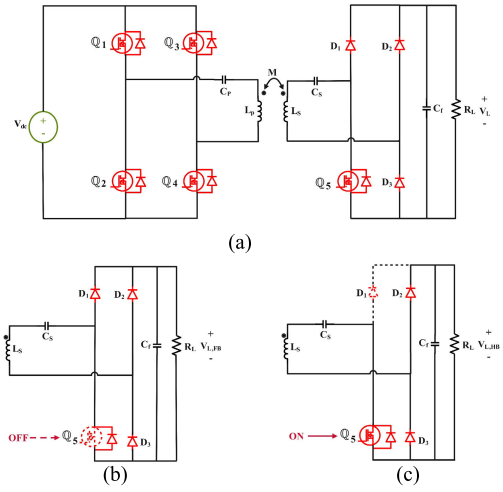

FIGURE 32. (a) The reconfigurable rectifier-based SS compensated WPT system. (b) full bridge diode rectifier on receiving side, and (c) asymmetrical half bridge rectifier on receiving side [218].

method is presented in [216] that uses double transmitters and double receivers which have decoupled coils built right in. Additionally, in [217], we have a novel S-S-LCLCC modified three-coil WPT system proposed to increase performance flexibility over fluctuating loads and alignment. In [218], a detuned SS-compensated WPT system based on a customizable rectifier is presented to jointly increase the system performance and withstand a wide coupling variation as shown in Fig. 32. The corresponding ac load is changed from one value to the other using a reconfigurable rectifier that can switch between full-bridge and half-bridge operation to increase the predicted coupling range of the detuned SS topology. By changing the coupling coefficient from 0.1 to 0.4, the proposed approach improved efficiency from 68.6% to 87.5%.

Tolerance for both nonpolarized and polarized transmitting coils is proposed in [219], along with a unique decoupling technique and quadrupole Rx coil featuring diode rectifiers connected in series. With the nonpolarized coil and the

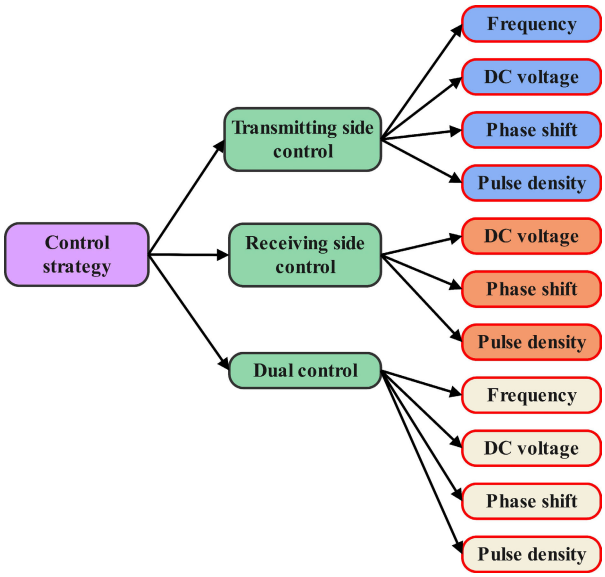

FIGURE 33. Categorization of control strategies for WPT systems.

polarized coil arranged at two orthogonal directions, the suggested method showed that considerable coupling with high transmission of power could be realized through high alignment sensitivity.

V. CONTROL METHODS

The needs of the battery management system can only be fulfilled with the help of proper control. In addition, working with increased efficiency is highly important for WPT systems because just a slight decrease in efficiency in such a system would result in a sizable power loss. Therefore, regulating the voltage and current at the output and maximizing efficiency are main control objectives. As a result, two degrees of freedom are typically required to achieve such objectives: one to regulate the output so that it tracks the reference, and another to fine-tune the system voltage gain (or rather, impedance matching) for maximum efficiency. Both primary and secondary sides are equipped with power electronics converters. Therefore, as illustrated in Fig. 33, the control strategies can be subdivided into transmitting-side control, receiving-side control, and dual-side control.

A. TRANSMITTING SIDE CONTROL

The transmitting side DC/AC converter is used to regulate the transmitter current in this approach. In some situations, PFC is also controlled. Information from the receiving side, like SOC, battery voltage, and SOH, is necessary in primary side control for regulating the primary side in relation to the load. In this strategy, communication with the other side is kept to a minimum. Therefore, the vehicle's weight and price can be decreased by minimizing the number of on-board electrical components [59], [162]. The working frequency of receiving side should follow with primary side frequency. As a result, only the primary side is responsible for regulating

the frequency. Primary side inverters allow for regulation of both working frequency and output by varying the number of switching cycles per second [220], [221]. To accomplish zero voltage switching (ZVS), the operating frequency must be higher than the inductive impedance's resonance frequency. Keep in mind that frequency splitting can occur and that there could be more than one peak [240].

B. RECEIVING SIDE CONTROL

A control on the receiving side is preferred to streamline grounded infrastructures. With receiving-side control, an active AC/DC converter and a DC/DC regulator are used to control the charging of the battery, which adds to the vehicle's overall weight and price, as the pick-up electrical components increases. In 2016, [222] proposed a model for maximizing efficiency and power management on the receiving side. The suggested approach uses the DC-DC converter to control the battery charging current directly. The proposed system maximizes transferring efficiency by calculating the DC terminal voltage's set point and stabilizing the DC link voltage using the HAR since this DC terminal voltage became unsteady. Reference [223] developed simultaneous wireless data and power transmission for charging EVs. The controller design can observe the receiving (vehicle) side's operational state and regulate the charging current under battery health. However, it is inappropriate for high-frequency carrier communications in limited-power IPT systems. A control on the receiving side is preferred to streamline grounded infrastructures. With receiving-side control, an active AC/DC converter and a DC/DC regulator are used to control the charging of the battery, which adds to the vehicle's overall weight and price, as the pick-up electrical components increases.

In 2016, [28] developed a 3 kW WPT device for supercapacitor recharging in electric vehicles. On the receiving side, a Buck converter with a PI controller is used to regulate the charging current for the varying loads. However, during the charging cycle, the equivalent resistance of various power sources fluctuates, impacting the current charging and device performance. In 2014, [224] stated that the mismatched coils in WPT systems can be electronically tuned. The saturable reactor comprises a transformer wound on an electromagnetic core. By applying a DC current to the secondary side of the transformer, a DC magnetic flux could be introduced into the core to change the inductance of the primary side. It may be used in various WPT applications, such as charging inductance for EV and cellular applications, which result in an incorrect and coil-distorted alignment, and it can be effectively performed based on electronics decoupled controlling systems are suggested in the research [225], wherein only the DC-to-DC converter on the receiver side controls the output voltage and the receiving side AC/DC converter handles impedance matching. Effectiveness comparisons between the PI-controlled and Fuzzy-controlled DWPT DC-DC buck-boost converter is presented in [226]. Despite having smooth voltage, current, and power outputs, the settling time for a PI controller is higher. When using a Fuzzy control strategy, however, the parameters will quickly stabilize at the target values.

C. DUAL CONTROL

Controlling the WPT system from both the transmitting and the receiving sides is essential to this approach. The Link between the two sides is important for this strategy. Though the required result can be attained with only one side of control in play, highly efficient performance cannot be assured. To accomplish these goals, dual-side control is proposed [26], [227]. For instance, in order to improve efficiency [228], Rx-side control is to accomplish the target output while Tx-side control is to decrease the inverter's output power. It is important to remember that the output can be regulated in phase-shift control by adjusting not just the phase differences of individual side converters, but also the phase difference between primary and secondary side converters. By controlling the three phase differences in this way, the WPT system operates similarly to a dual-active-bridge (DAB) system [229]. As a means of reducing reactive power on the receiver side and maximizing efficiency, phase-shift control incorporates frequency control [230], [231], [232], [233]. When it comes to dynamic wireless charging implementations, it is best if both sides can be controlled individually. Yet, when employing two separate controllers, stability concerns must be thoroughly addressed [125]. Voltage control, which covers dc voltage regulation, phase-shift control, and pulse density modulation, may be applied on any side. Adjusting primary side inverter input voltage or secondary side rectifier output voltage with dc-dc converters is known as dc voltage regulation. For phase shift control, we need to vary phase differences of individual side converters. Although it is speedier than dc voltage regulation, ZVS condition may not be possible. The goal of pulse density modulation is to change the equivalent rms voltages by reducing or increasing the number of pulses [234]. The parameters transmitting side inverter and receiving side rectifier node voltages are adjustable by all three of such approaches.

Significant misalignment results in a drastic decrease of k, making misalignment a frequent issue in WPT systems. Power and current output in the well-known S-S design is inversely related to k. The converters' VA rating should take into account the worst scenario, when k is the lowest, leading to a big VA rating and a wide working range, if the nominal output is to be maintained across the whole coupling range. The problem can be fixed by employing frequency control [235], wherein the coils are intentionally built to be slightly out of tune with one another, hence reducing the resonant frequency. With global ZVS characteristics, it has been demonstrated that power rating operation is possible throughout a broad array of coupling (with fluctuation as much as 275%) [236].

There has been a large shift toward using lithium-ion batteries in portable electronic devices and vehicles. In order to

increase battery life and recycling efficiency, battery profiles typically begin in constant-current (CC) mode and transition to constant-voltage (CV) mode later on. The battery's equivalent resistance, $R_b = V_b/I_b$ (where V_b and I_b are the charging voltage and current, respectively) changes by tens to hundreds of ohms over the course of a complete charging of EV. For WPT setups using either CC or CV outputs in conjunction with variable loads, there are primarily two types of control schemes to choose from. There are primarily two types of high-frequency inverter (HFI) control schemes: Phase shift control schemes for the HFI allow the IPT systems to adapt the charging current or voltage to the load conditions [226]. Additionally, systems with load-independent currents/voltages against variable loads can operate at split frequencies which can lead to a stability issue due to the occurrence of frequency bifurcation phenomenon [109], [221], [222]. It is possible to modulate the dc-dc converters' duty cycle to generate the desired output currents or voltages with the appropriate control schemes [236], [237].

The aforementioned control schemes allow IPT systems to maintain constant output currents or voltages across a wide range of input modulation indices and/or complex control circuitry, but at the expense of robustness [226], [233].

While a DWPT system's steady-state functionality is ascertained by the coupler, converter, and compensation architectures, control systems are required to keep the system operating as intended when the load, coupling, and other parameters change. Segmentation, zero voltage switching, and compensation mode control mechanisms are all secondary goals in DWPT systems that aid in the system's primary goal of power flow control and other crucial functions. According to Fig. 34, there are four different levels of energy conversion involved in a traditional WPT system and it is done with the help of different types of power electronics converters. On the transmitting side, which involve front-end converters and high-frequency inverters, and on the receiving side, rectifiers and back-end dc-dc converters. Table 12 lists the steps of the primary control goal of any DWPT system is to maintain power flow control in spite of coupler imbalance and vehicular speed. Controlling power transfer with an open-loop system requires circuit-based methods, which can lead to complex peripherals. While closed-loop controls improve reliability with less complicated power circuitries, they also increase control design difficulty. The impacts of communication also need to be cautiously tackled in the design of primary and dual-side based closed-loop control functionalities.

Segmentation control, which is employed to activate the correct pads depending on the vehicle place to keep the optimal power transfer, provides the most essential and crucial control goal in a DWPT system. Turning off the sections of the system that aren't in need enables with leakage field management and increases system power transfer efficiency. As can be seen in Table 13, power flow and segmentation controls can be implemented in either an open or closed loop, but ZVS and mode switching controls are more commonly implemented in the open loop. Due to the better consistency of vehicle responses over transmitting side projected measurements, communications are an integral portion of the DWPT control cycle for systems with transmitting- and dual-side closed-loop controls [162], [244], [253], [254]. Moreover, the communication lag could constrain the control bandwidth in such system applications, making their reliance on interactions a likely field of consideration. The communications chosen for a DWPT system must meet stringent requirements for stability, bandwidth, and confidentiality. Despite the potential advantages of not relying on wirelessly transmitted feedback information, just systems governed from the receiving side can be said to have this luxury. The phase shift method is employed in the Fig. 35 for both the transmitting and receiving side controllers. Varying the phase shift angle between the leg voltages of a single converter and the two converter voltages allows for control of the WPT system currents and power. The transmitting side controller is responsible for creating the phase difference (α) between the two legs of the transmitting side inverter. Tuning the inverter's output voltage to the rated current (reference signal) that the transmitter circuit can handle is done with this parameter (α) [Fig. 35] [148], [207], [241]. Phase difference (β) between receiving side converter legs and between both converters' output voltages (δ) are both generated by the receiving side controller.

By changing the receiving side control variables (β, δ), the desired amplitude and phase of the transfer power can be attained [Fig. 35] [148], [241]. The pulse-phase modulation (PPM) method illustrated in Fig. 35 is then used to convert the phase shift variables from both controllers (α, β and δ) into switching commands. The direction and amplitude of the converter voltages are changed using these governing variables to obtain the needed transfer power in the WPT system. This control technique can be employed in the bidirectional wireless power transfer system.

A summary of recent high-power wireless chargers available for real world applications as well as those developed in research labs can be found in Table 14.

VI. ANALYSIS AND DISCUSSION

This section presents the analysis and discussion of the different performances of research papers and the study of the results that indicates the importance of various implementation technologies of WPT systems for EV charging.

A. ANALYSIS BASED ON TRANSFER POWER AND EFFICIENCY

The basic compensation topologies are depicted in Fig. 24, and transfer power and efficiency have been explored for the 2 kW WPT system with coupling variation and coil misalignment behavior with mutual inductance and input impedance seen by the power source is illustrated in Fig. 36 [32], [128]. As depicted in Fig. 36, when the input impedance is reduced, as it is in the SS and SP topologies, this results in an increase not only in the current that is delivered to the load but also

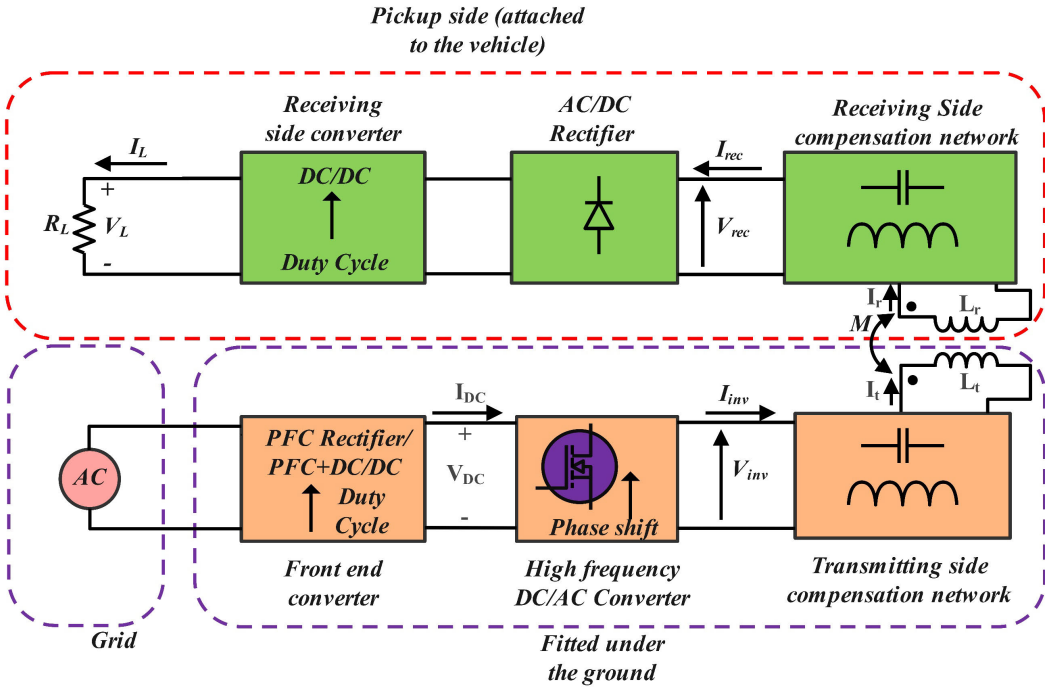

FIGURE 34. Different stages of energy conversion involved in a typical WPT system.

TABLE 12. The control parameters linked to the different converter positions in DWPT.

Position of Converters		Topologies	Control parameters
Transmitting side	AC/DC or DC/DC converter	Power factor correction (PFC) AC/DC converter [10] PFC (AC/DC) + buck or boost (DC/DC) converter [142], [238]	PFC duty cycle Buck or boost converter duty cycle
	High frequency DC/AC converter	Single phase inverter [162] Multi-phase inverter [239] Class EF inverter [240]	Phase shift angle between two legs of inverter Switching frequency of the inverter Duty cycle of switches
Receiving side	AC/DC converter	Full bridge diode converter [241], [242] Full bridge active rectifier [238], [241]-[243]	No controls
	DC/DC converter	Buck converter [244] Boost converter [245] Buck-boost converter [246]	Duty cycle of DC/DC converter

in the current that is supplied by the source. The overall impedance rises when there is a misalignment in the PS and PP topologies, which results in a precipitous drop in the currents that are fed and absorbed respectively [127].

With low coupling coefficient or mutual inductances, PS and PP compensations provide good PF and efficiency throughout a broad range of mutual inductance and load [129], [283]. Parallel secondary requires high voltage loads, and parallel primary requires a large current source, all of which work against the PP topology's low PF [284]. If the receiving side is compensated in series (SS or PS), the average transmitting input impedance is reduced more than if the receiving side is compensated in parallel (SP or PP) [285]. The Table 6 described earlier in the paper is the comparison of the most fundamental topologies involving load characteristics and power transfer efficiency as a function of mutual inductances.

It has been pointed out that the output current does not depend on the load at the resonance frequency nor does the SS compensation rely on the coupling coefficient. As a result, the system's tolerance to coil misalignment is higher, and the resonant frequency of the resonator is stable, provided there are no flaws in the elements.

The copper consumption of the four most common types of basic compensation for 200kW is listed as follows in [284]: SS > SP > PP > PS. Copper usage is minimized for SS compensation and somewhat increased for SP. More copper is needed for PP and PS compensation than for SS. With

TABLE 13. Comparison of different open and closed loop controls and segmentations used in DWPT system.

Control Objective	Proposed control type	Control methods	Pros and cons
Power flow	Open loop	Greater receiver pads and LCCL/LCCL topology [169]. Crossed DD transmitter [247]. Hybrid compensations on either side with DD coupling pads [170], [207].	System stability is poor. Compensation circuits designs are more complex. Communication are normally not needed.
	Closed loop	Transmitting side control [10], [88] [248], [249] Receiver side control [239], [250], [146], [251], [244] Dual control [250], [146], [244], [252], [253], [254]	Better system reliability. Dual control systems require more complicated designs for the control mechanisms. Control on both the receiving and transmitting ends could be lowered. Normally receiving-side control cases don't necessitate communication. Communication is essential for transmission and dual control.
Segmentation	Open loop	Constant current driven through paralleled LCCL compensator [255] Circuit based autotuning [256]	system stability is poor. System control designs are more complex. Communication is normally not needed.
	Closed loop	Primary side detection [168], [257]–[260] Receiving side control [246], [261], [262]	System stability is good. System control designs are more complex. Communication is needed.

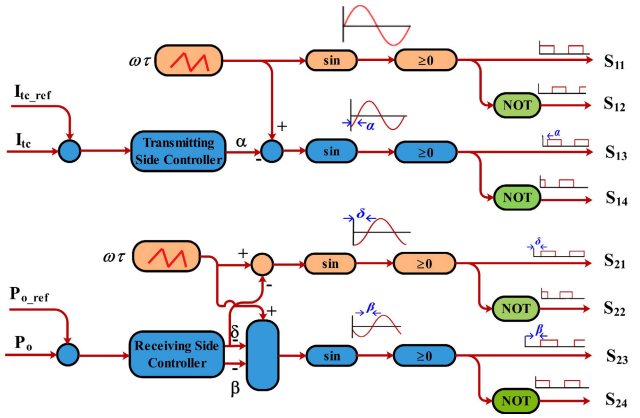

FIGURE 35. Example of phase shift control technique of transmitting and receiving side converters in WPT system.

a higher necessary current and lower operating frequency, PS compensation still only needs a relatively low frequency to function. Therefore, SS and SP topologies are cost-effective and suitable for high-power applications. In [32], the 200-kW system was analyzed in detail. The SS compensation is found to be the one that utilizes the least amount of copper. The requirement of copper increases by 4.6% in SP topology, 30% extra copper needed for PS and 24% more for PP. While the SS topology uses less copper overall, the PS topology operates at a significantly lower frequency of just 11 kHz. The reason for this is that the operating frequency increases as the current (and hence the wires) decreases. As a result, series primary compensation topologies require higher switching frequencies, despite the fact that series secondary (SS) and series primary (SP) compensations offer greater cost benefits for high-power transmissions [115], [125].

B. ANALYSIS BASED ON IMPLEMENTATION TOOLS, COMPENSATION AND OPERATING FREQUENCY

Most of the research papers use MATLAB as the tool for the implementation of WPT in the EV charging. This article investigated the correlation between load power, transmission efficiency, and coupling coefficient under different load conditions at resonance to effectively compare and contrast the transfer characteristics of SS and SP compensation circuits. When the coupling coefficient, k is 0.15, we also examine the way in which the frequency splitting varies with load. Fig. 37 and Fig. 38 depict the findings of the simulation analysis. Fig. 37 shows that with a load resistance of 160 ohms, the SP topology has a higher output power and efficiency than the other topologies. Under the same conditions of output power and transmission efficiency, the SS topology has a greater transmission distance when the load R_L=40. Accordingly, a small load system would benefit more from the SS compensation topology, while a large load system would benefit more from the SP compensation topology.

With a fixed coupling coefficient k, as depicted in Fig. 38, both SS and SP can operate at their suitable loads to deliver their highest power output. As the SP's load continued to increase, a new condition known as frequency splitting exhibited itself. The SS topology also has the same condition when loads are lower.

To examine the impact of dynamic response of different parameters such as load resistances, compensation capacitors and coupling coefficients on the phase angle of total impedance seen from power supply in the SS compensated WPT system, every parameter is varied with respect to other variable in [286] and [287]. Using a 400-V power supply, Fig. 39 displays the phase of the total impedance of the WPT system as a function of working frequency with selective parameter variation. The load resistance varies from 40Ω to 800Ω, and the coupling coefficient is set to 0.25 in Fig. 39(a); load resistance kept at 40Ω in Fig. 39(b) and 39(c). Because the battery voltage and charging current are not constants throughout the charging process, R_L varies depending on the stage of the charge. The phase of total impedance curve shows that the circulating energy loss is high for light load conditions when operating at 400 V output voltage, as the phase angle increases with increasing load resistance. In addition,

TABLE 14. Recent developed static and dynamic WPT system for EV charging.

WPT system Name/Country/Year	EVs Application type	Power Transfer Efficiency	Frequency/Compensation topology used	Power level	Power transfer distance	Availability
Turin Project/Italy/2013 [263], [264]	Static/Bus	90%	15-20 kHz	60 kW	40 mm	Commercially available
Bombardier/Germany, Belgium/2010 [265], [58]	Static/Bus	>90%	20 kHz	40-200 kW	-	Commercially available
WiTricity/United States/2010, 2019 [266], [267]	Static/Car, SUV	91-93 %	85 kHz	7.7, 11 kW	90-250 mm	Commercially available
KAIST/South Korea/2014, 2015 [10], [268]	Dynamic/Bus	>80%	20 kHz, 60 kHz/S-S	100 & 180kW	70-200 mm	Commercially available
UOS/South Korea/2016 [269]	Dynamic/Train	90.4%	60 kHz/S-S	150 Kw	70 mm	Commercially available
CARTA/ United States/2011 [270], [10]	Static/Bus	90% (ac-dc)	15-20 kHz	60 kW	40 mm	Commercially available
ETH Zurich/Switzerland/2016 [271], [272]	Static/LDEV	95.8%(dc-dc)	85 kHz/S-S	50 kW	100-200 mm	laboratory prototype
NUT/Japan/2019 [273]	Static/EV	91.1% (dc-dc)	85 kHz/S-S	22 kW	90 mm	-
WHU/CHINA/2019 [274]	Static/LDEV	94% (dc-dc)	85 kHz/S-S	35.1 kW	200 mm	-
Qualcomm Halo/2010, 2017 [240]	Static/Car	90%	85 kHz	3.6 kW, 7 kW & 20 kW	160-220 mm	Commercially available
Toshiba/Japan/2014, 2017 [275], [276]	Static/Car, Bus	>85 %(ac-dc)	85 kHz/S-S	44 kW	100-130 mm	Commercially available
INTIS/Germany/2019 [277]	Static/LDEV	>90%	30 kHz	100 kW	200 mm	Commercially available
ORNL/2018 [141]	Static/LDEV	95%(dc-dc)	85 kHz/S-S	50 kW	150 mm	laboratory prototype
ORNL/2018 [237], [278]	Static/LDEV	96.9%(dc-dc)	22 kHz/S-S	120 kW	152 mm	laboratory prototype
Wave/United States/2019 [267]	Static/Bus	-	-	500 kW	-	Commercially available

TABLE 14. *(Continued.)* **Recent developed static and dynamic WPT system for EV charging.**

ZTE projects/China/2014 [279]	Static/Bus	90% (ac-ac)	45 kHz	30 & 60 kW	200 mm	Commercially available
Momentum/United States/2018 [280]	Static/Bus	94% (ac-dc)	20 kHz/S-S	200 kW	178 mm	Commercially available
USU/United States [250]	Dynamic/Bus	86% (dc-dc)	20 kHz/LCC-LCC	25 kW	-	Commercially available
IPT technology/Germany	Static /Bus [281] Dynamic/Bus & Truck [282]	92% 90%	20 & 85 kHz -	50 kW & 100 kW 180 kW	130 mm -	Commercially available

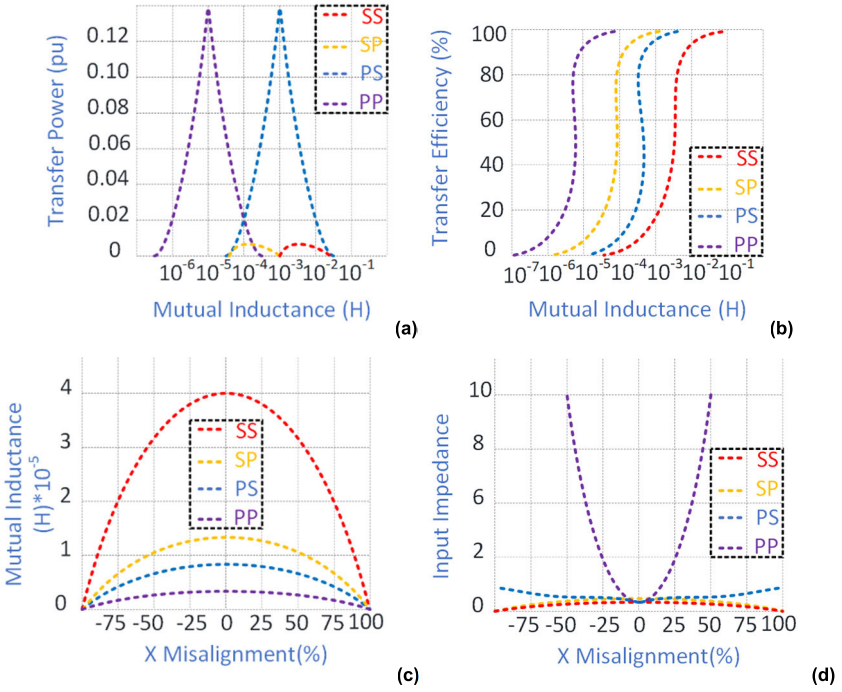

FIGURE 36. **Comparison of different basic compensation topologies: (a) transfer power and (b) efficiency with mutual inductance variation; (c) mutual inductance and (d) input impedance with coil misalignment [32], [128].**

the efficiency plot verifies that a decrease in power leads to a decrease in efficiency for a given output [286].

The transfer efficiency at 85kHz, coupling separation of 160mm, and coil misalignment of 90mm are analysed and compared among the compensations of LCC-LCC, LCC-S, and LCC-P in [287] and [288]. In Fig. 40, we can see how the three different compensations function in terms of transfer efficiency across a range of coupling separations. As the load resistance increases, the efficiency of the LCC-S rapidly decreases, particularly at poor coupling conditions ($k = 0.2$); the efficiency of the LCC-P is low at reduced load resistance but surpasses the efficiency of other topologies at high loads ($R_L > 60$); the efficiency of the LCC-LCC configuration could be constant over a large range of loads if the compensation factor chosen wisely. If the coupling coefficient is poor ($k = 0.2$), then the compensation factor should also be large ($p = 0.4$, for example). The power dissipation on wireless coils can be minimized by choosing a suitable compensation factor on the secondary of the LCC-LCC system. This would be crucial while developing an LCC-LCC network for applications requiring decreased mutual inductance and greater load resistance. Also, a low primary compensation factor

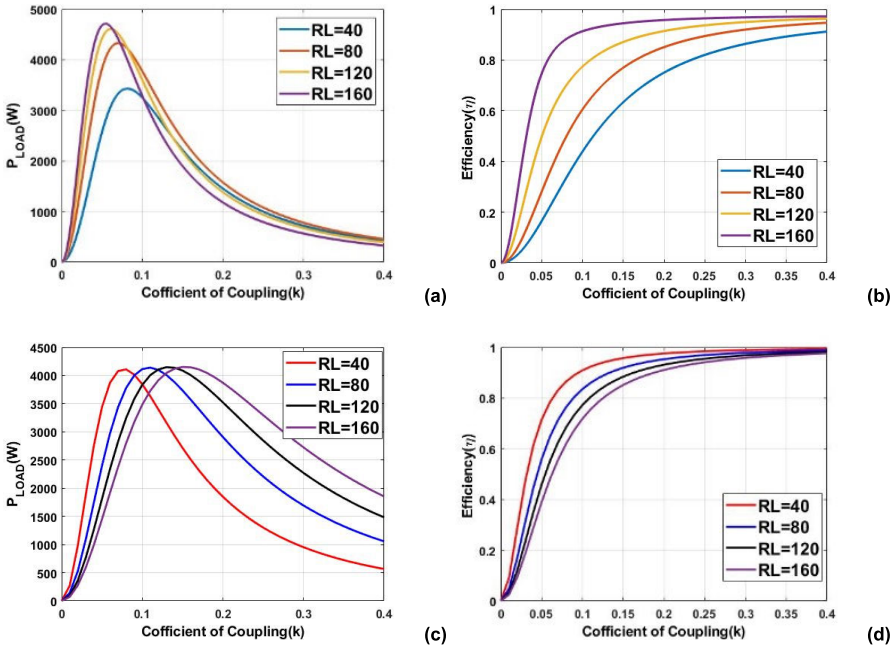

FIGURE 37. SS and SP compensated WPT system behavior for different loads (a) load power with coefficient of coupling and (b) efficiency with coefficient of coupling.

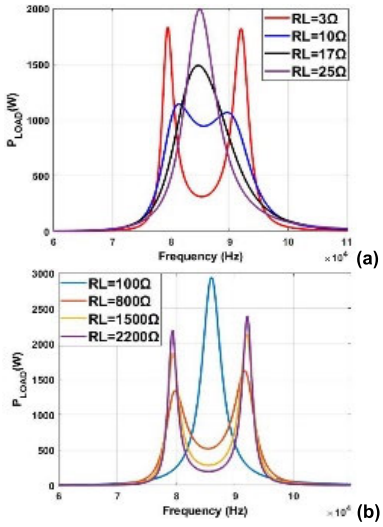

FIGURE 38. Comparison of load power and frequency bifurcation in (a) SS and (b) SP compensated WPT system.

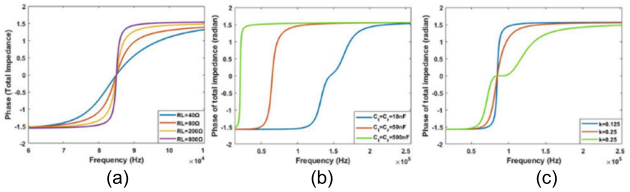

FIGURE 39. Phase of total impedance seen from power supply in SS-compensated WPT system with respect to frequency: (a) varying load resistances (b) varying compensation capacitances (c) varying coupling coefficients.

TABLE 15. Parameters required for MATLAB/SIMULINK implementation.

Components	Values	Components	Values
f_0	85KHz	R_L	6.34 Ω
L_t	120μH	L_r	120μH
C_t	29.28nF	C_r	29.28nF
R_t	0.5Ω	R_r	0.5Ω
k	0.01-0.3		

reduces transmitting side converter losses but necessitates a larger source voltage.

A test model for a 0.5 kW WPT system operating at a resonant frequency of 85 kHz has been simulated in MATLAB using the parameters available in Table 15 to determine the SS and SP compensation input and output characteristics. The simulated model's circuit diagram is depicted in Fig. 41. DC source is employed for the high frequency inverter in the MATLAB/SIMULINK model rather than a PFC converter. Fig. 42 displays the voltage and current waveforms for the various stages in the WPT system using MATLAB/SIMULINK.

Basic compensation geometries are compared with respect to the key factors including shortcomings and EV applications are outlined in Table 16.

C. METRICS FOR RELIABLE AND SAFE OPERATION

For wireless EV battery chargers to enter the commercial market, automakers will need to ensure the devices are compatible with all vehicles, can be used in any location, are safe,

TABLE 16. Summary of WPT technologies based on coupling methods.

Analysis	SS	SP	PS	PP
Load resistance dependency	C_t & C_r does not dependent on load resistance	C_r depends on the load resistance	C_t depends on the load resistance	C_r depends on the load resistance
Coupling coefficient variation	C_t & C_r does not dependent on coupling coefficient	C_r depends on the coupling coefficient	C_t depends on the coupling coefficient	C_r depends on the coupling coefficient
Apparent power rating	High at the input side	High at the input side	Small at the input side	Small at the input side
Acceptance of zero coupling	not allowable	allowable	allowable	allowable
Transmitting side converter voltage rating	Requires lower DC link voltage but greater than SP	Requires lower DC link voltage than SS	DC link voltage requirement is higher as compared to SS and SP	DC link voltage requirement is higher as compared to SS and SP
Transmitting side converter current rating	Transmitting coil current	Transmitting coil current	Real part of transmitting coil current	Real part of transmitting coil current
Input impedance	Reduces with coil unbalancing	Reduces with coil unbalancing	Rises with coil unbalancing	Rises with coil unbalancing
Effectiveness for low power WPT system	Less useful than parallel compensated receiver	Better than series compensated receiver	Less useful than parallel compensated receiver	Better than series compensated receiver
Shortcomings	At partial loading, load varies with input to output voltage transfer ratio. High frequency current flowing through the series capacitor and thus develops high voltage across capacitor.	There is less DC component blocking.	Requires greater voltage to transmit more power. For avoiding any sudden change in voltage, it needs current input.	Power factor is poor. Greater output voltage of the receiver. Requires a higher current input for the parallel transmitter. Input resistance is higher.
EV applications	Static and dynamic wireless charging for EV. Segmented dynamic wireless charging for EV. Bidirectional power transmission for EV.	Low and medium power level EV applications in which a stable voltage gain is required, even though feedback control is not needed.	High power WPT system	High power WPT system

and don't harm the environment. To do so, they must follow the standards set forth by relevant international bodies. For the auto industry specifically, standardized practices facilitate the marketing, production, comprehension, and comparison of products.

One of the primary organizations that establishes guidelines for contactless high power EVs battery chargers is the Society of Automotive Engineers (SAE). The 2016 publication of SAE j2954 proposed norms involving contactless power transfer marked the debut of this document [289]. The 2022 release of SAE j2954 version 4.0 represents the latest and most widely recommended iteration [57].

The coupled inductance of a magnetic coupler must also be maintained despite being subjected to misalignment in multiple directions. Similarly, a Yaw of up to 6%, a Roll of up to 2%, and a Pitch of up to 2% can all happen at the same time. Coupler designs, how well they work together, and the highest levels of stray magnetic fields were also suggested. Research performed by academic and automotive partners have shown that circular and double-D pads can transfer power to one another effectively and efficiently [290]. For medium as well as heavy-duty vehicles, SAE suggested a different set of WPT directives known as J2954/2. Fig. 43 depicts a WPT power level based on the global standards and frequencies [291], [292].

The International Electro-Technical Commission (IEC) has also been instrumental in developing guidelines for wireless charging stations, most notably as IEC 61980. Despite their differences, SAE J2954 and IEC-61980-1, 2, and 3 all cover the same ground. It has an air gap constraint of 24cm and can handle power scales up to 22kVA. In addition, it fulfils necessities for power flow in both directions. These are the rules for the future of the massive diffusion of the EV. ISO-19363 is an international standard that is in lockstep with SAE J2954 and IEC 61980 [293]. The working frequency and frequency band established by such groups are 85 kHz and 81.38–90 kHz, respectively; the latter was subsequently expanded to cover 79–90 kHz for light-duty automobiles. China Communication Standard Association is China's own national norm (CCSA) [284]. For transmissions with a power level of up to 7.7 kW in Japan, the Broadband Wireless Forum (BWF) is the go-to organization. The ARIB allows for transmissions with a maximum power of 100W in the CPT between 425 kHz and 524 kHz [293], [294].

Concerns such as electromagnetic interference (EMI) and leakage magnetic fields, which induce thermal problems and

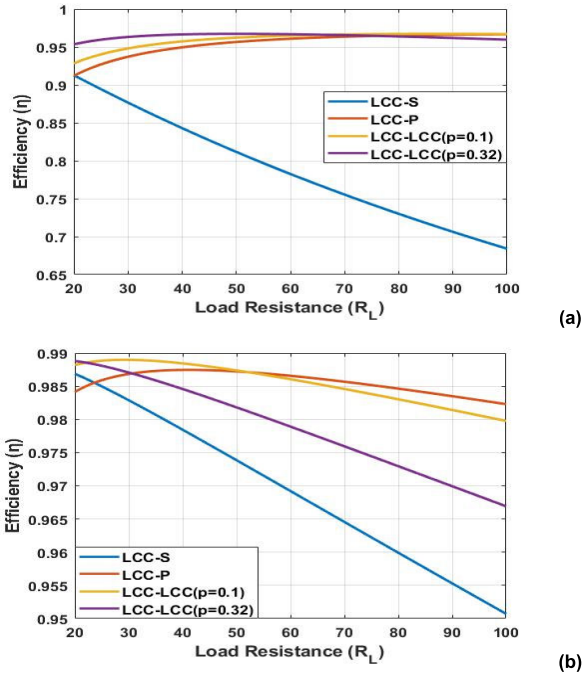

FIGURE 40. Comparison of transfer efficiencies of three hybrid compensations at two different coupling coefficients (k) : (a) k = 0.2; (b) k = 0.6 [288].

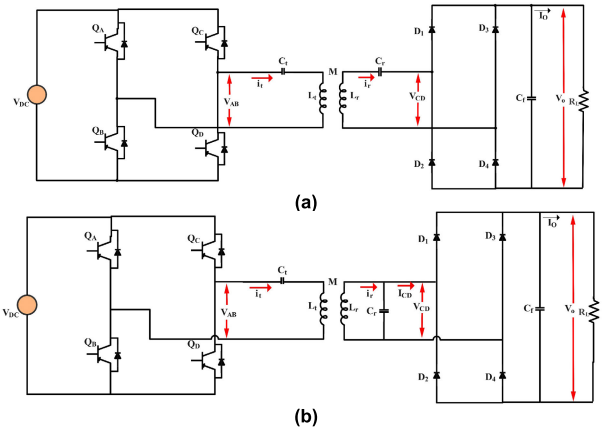

FIGURE 41. Example of (a) SS and (b) SP compensated WPT model for EV charging developed in MATLAB/SIMULINK.

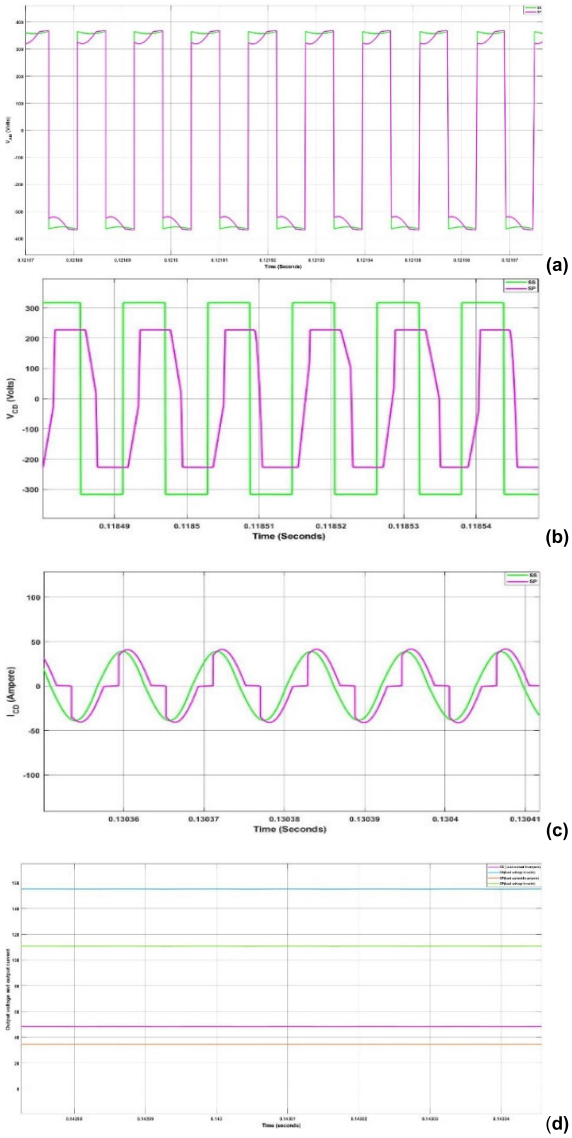

FIGURE 42. Voltage and current waveforms for SS and SP compensated WPT model using MATLAB/SIMULINK.

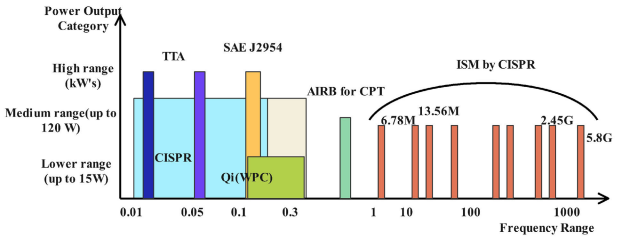

FIGURE 43. WPT power output range based on the global standards and frequencies.

are harmful to living organism exposure, are due to a rise in power thresholds and air gap. Several groups have established safe levels of exposure to EMFs, and following those guidelines necessitates employing safety measures like shielding and foreign object detection (FOD) techniques. The International Commission on Non-Ionizing Radiation Protection (ICNIRP) has announced its recommendations for limiting human exposure to field radiations and EMI. The frequency ranges covered by the ICNIRP's 2010 recommendations for standards are well suited for use in wireless EV charging systems, spanning from 1 Hz to 100 kHz [293]. The frequency range covered by the updated ICNIRP 2020 recommendations is 100 kHz to 300 GHz [295]. Typically, the maximum allowable electric field strength is 83 V/m, but ICNIRP guidelines have a limit of 1.35 × 10-4f, where f is the electric field frequency. Leakage electromagnetic fields should therefore meet the quite stringent IEEE C95.1-2345 Standard, that further provides additional details on neurological implications

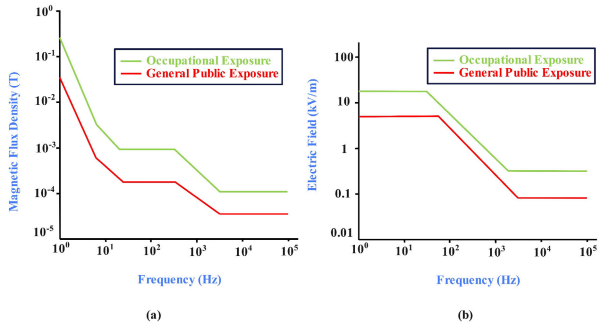

FIGURE 44. Standard exposure level for (a) magnetic and (b) electric fields in the workplace and in public life.

TABLE 17. General Public EMF exposure standard levels [57].

Quantity	General public EMF exposure referenced (rms Field Strength for 79-90 kHz)	Maximum limits for non-sinusoidal quantity (1.414*rms value)
Magnetic Field	27 μT or 21.5 A/m	38.18 μT or 30.40 A/m
Electric Field	83 V/m basic restriction levels = $1.35 \times 10^{-4} * f(Hz)$ = 11.475 V/m at 85 kHz	117.36 V/m 16.23 V/m at 85 kHz
Touch Current	0.2 * f(kHz) = 17mA at 85 kHz	0.2828 * f(kHz) = 24.038 mA at 85 kHz

TABLE 18. Combined EMF exposure levels for laboratory testing [57].

Quantity	Laboratory EMF exposure (rms value)	Maximum limits for non-sinusoidal quantity (1.414*rms value)
Magnetic Field	15 μT or 11.9 A/m	21.21 μT or 11.9 A/m
Electric Field	83 V/m	16.8266 V/m
Touch Current	15.8 mA	22.3412 mA

like brain stimulation below 100 kHz and tissue heating at more than 100 kHz [295]. EV could also be equipped with metal shielded displays for the safety of the driver and riders [125], [296].

The workplace and the general public's exposure standard level for magnetic and electric fields are depicted, in Fig. 44. The standard range takes into account both the CNS (the fundamental limit for CNS at 50 Hz is 33 $Vm^{-1}T^{-1}$) and the PNS (60 $Vm^{-1}T^{-1}$) effects, and is determined under the assumption of highest linkage of the field to the susceptible body. The range between 25 Hz and 10 MHz is used as the fundamental standard range for electric field exposure in the workplace.

Table 17 and 18 summarizes the EMF exposure references for general public and for laboratory testing respectively, according to ICNIRP 2010 [80].

D. DESIGNING A DYNAMIC WIRELESS CHARGING INFRASTRUCTURE

Because of benefits, WPT technology can be used on a large scale to make charging easy and safe, like in the charging infrastructure for electric and electrified transportation. As the power supply and the charged unit have been associated via the magnetic field, WPT enable significant functional mobility by permitting the unit to be powered at any moment, in whatsoever location, including when the automobile is in motion. As a result, this is simply a realistic solution to the challenge of concern linked with the limited range of EVs and other electronics and thus increasing the battery capacities of EVs [56], [250], [297]. Depending on these considerations, the concept of dynamic wireless charging (DWC) was introduced, and it has since been a hotspot for EV inductive charging study [143], [253]. As depicted in Fig. 45, DWC proposes installing inductive charging plates in a narrow stretch of road to allow electric vehicles to recharge while on the move. Theoretically, the DWC approach can address the issue of limited travelling range. In practice, putting this idea into action is hard when vehicles are moving fast and requires a lot of money up front. Furthermore, the quasi-dynamic charging idea suggests that completely automated dispersed charging would substitute long waiting physical recharging at bus stations, shopping buildings, and eventually red lights on the way, as these are the places where EVs assemble or come to a halt [41], [265], [266]. Range stress is eliminated, and the battery's useful life is extended, all thanks to DWC's narrow discharge cycles, which are a result of opportunity recharging. Because of that, the price of an EV drops. Long-term advantages of installing DWC infrastructure can outweigh the early network expenses, as well as the overall cost won't go up by much, allowing DWC a commercially sustainable alternative [41], [298], [299].

Designing a DWC's infrastructure requires thoughtful analysis. The length of the transmitter coils and the vehicle speed are key factors in the power transfer technique. It also focuses on the exploration of the inability of altering people's mentalities and norms if it relates to driving fast. The track's length is also a considerable factor. The transmitter path besides the road would be quite enough for proper functioning, and it can be split into portions for better efficiency. However, its effectiveness relies on factors like working frequency, how fast the driver is heading, and how congested the roadways are. Additionally, the network is comprised of coils at each portion [56].

The power transmission in DWC is dependent on speed of the vehicle's movement. When the pickup coil attached to the vehicle moves, the flux linkage varies accordingly. Power is transmitted at maximum efficiency when the transmitting coil and pickup are in perfect alignment. The efficiency drops to half when the moving pickup coil is halfway between two stationary coils on the track. Fig. 46 illustrates how the variation in the location of the track coils affects the amount of power that gets transmitted [300]. Power delivered to the EV is represented by the red line. Pickup coil orientations

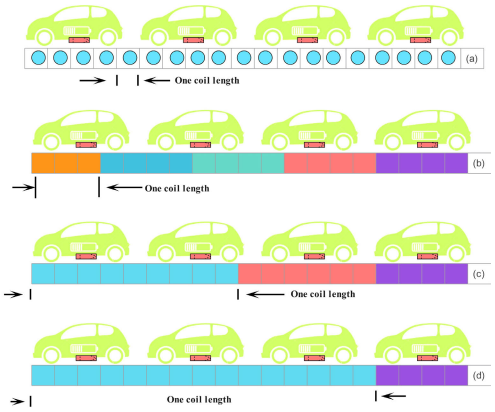

FIGURE 45. Arrangement of coils in different track lengths segmentation.

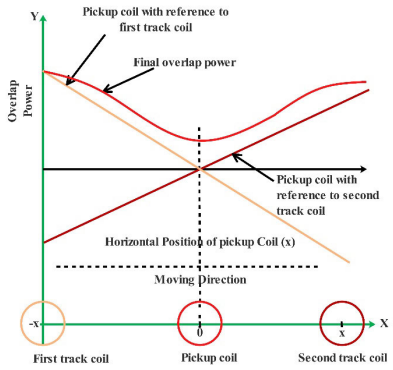

FIGURE 46. Transmitted power from transmitting to pick up coils.

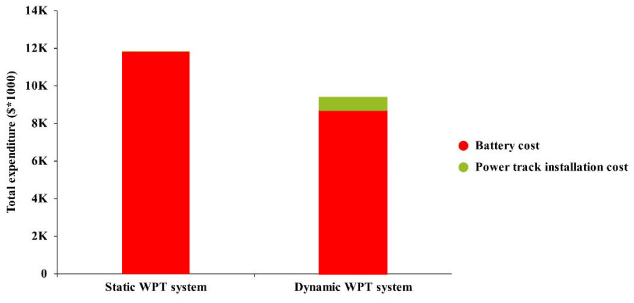

FIGURE 47. Cost benefit analysis of SWC and DWC over a 10-year period of setup and operation [298].

relative to track coils 1 and 2 are depicted by orange and maroon lines. The pickup coil's location relative to the first and second primary coils is shown along the x-plane. When the track coil and the pickup coils are correctly positioned, a significant amount of power will be transmitted to the pickup, but as the gap between them progresses; less power will be transmitted. All primary coils are linked in series and phase, which results in the aforementioned power transmission fluctuation. As a result, the coils are both energized at the same time. As illustrated in [128], a stream of magnetic field lines emerges, which travel back through the air.

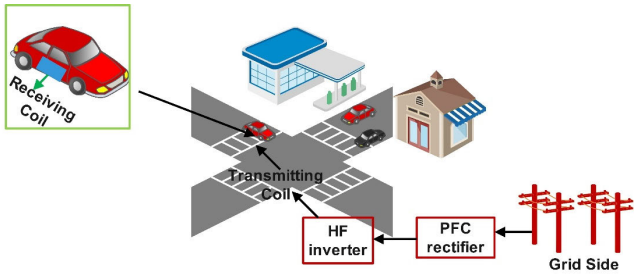

FIGURE 48. Real world application road view of wireless power transfer for EV charging.

Using an analytical algorithm optimization approach, researchers in [298] and [299] examined the overall expenditure of static and dynamic WPT system, as depicted in Fig. 47. These stats were computed on the 10 years operation of 18 buses powered by both static and dynamic WPT system. When comparing the overall operating costs of static and dynamic WPT system, a savings of $2 462 268 (or 20.8%) is realized through the adoption of DWC. DWC's high-track building expenses can be traced back to the pricey batteries needed for static WPT system.

E. COMING GENERATIONS BARRIERS AND OPPORTUNITIES

•Improvement in transfer distance range and misalignment:

The transmission range is the primary issue for researchers and consumers. Real WPT systems shown in Fig. 48, as opposed to the wired charging method, should take advantage of the energy transfer over a large range. However, for electromagnetic WPT systems, a large separation results in a very weak coupling effect. Also, misalignment of resonant coils occurs commonly in magnetic couplers; increasing the degree of spatial freedom for WPT systems might improve the system's practical value. However, when the WPT system coils become misaligned, their mutual coupling weakens, leading to a precipitous drop in power transfer efficiency. Soon, researchers will concentrate on overcoming this technological barrier.

•Bidirectional wireless charging technique and effects of WPT charging stations on the reliability and health of the electrical grid:

EVs are becoming increasingly popular and will eventually replace traditional internal combustion engine cars. Therefore, the importance of energy intake for EVs will escalate. Along with what has already been described, a major area of interest in smart grid and electric vehicle research is the vehicle-to-grid (V2G) concept, which investigates the relationship between a large number of EVs charging at once and the electrical grid. The V2G method can turn EVs into portable energy banks that can regulate power supply and demand. It is widely acknowledged that there would be many benefits for the grid if the EV charging process could be optimized. Using valley filling and peak shaving, the EV could help equalize the loads. Because the batteries in EVs function

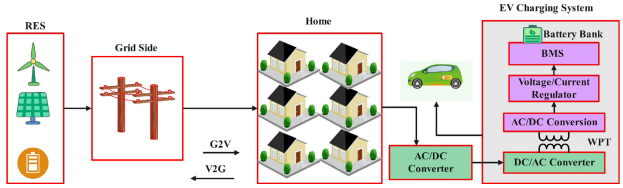

FIGURE 49. Bidirectional power transfer applications for wireless charging systems.

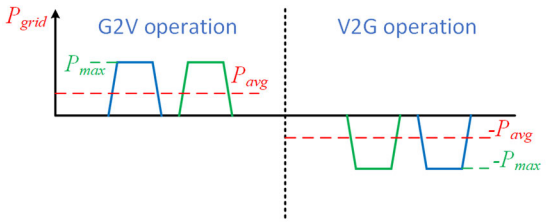

FIGURE 50. Grid-side power profile using segmented DWPT systems. [247].

like portable energy banks, it would be simpler to integrate wind power and other forms of intermittent renewable energy into the grid as depicted in Fig. 49.

A reversible WPT operation is achieved by changing the receiver side uncontrolled diode rectifier with active rectifier [266], [300], [301]. There is potential for the bidirectional WPT to deliver superior performance in V2G contexts. WPT system has been shown in investigations to increase EV operators' intention to interact their vehicles to the transmission network [298], [301]. As a result, after the roadway power transfer technique cools down, the bidirectional EV wireless charging will be a key area of focus.

In [291], researchers looked into the best way to set up public charging sites for EVs. The system demand characteristics should be used to make a wise choice about how many wireless charging stations should be placed in each metro region. In an equivalent manner, Chen et al. [134] looked into which tracks of a regional roadway system needed equipment for dynamic charging. Their model figures out the best trip time and speed for an EV so that the vehicle could get to their arrival point without depletion of battery. But in the model, neither the power network load profile nor the high hours of load are taken into account. For upcoming investigation, an optimization technique could assist EVs opt for dynamic charging lanes which improve demand characteristics. In [302], three distinct scenarios are looked at to show that the use of DWPT technologies makes the grid voltages change a lot. In order to keep the grid healthy, the above paper suggests using an integration of intelligent monitoring and battery storage or dc distribution systems.

A segmented DWPT system's grid-side power distribution is shown in Fig. 50. The highest power Pmax is clearly much higher than the average transmission of power Pavg. Grid-side power health is likely to be severely impacted by power fluctuations. As transmitting pad length decreases, this issue typically becomes extra critical. In order to reduce the severity, Ruddell et al. [303] suggested integrating a WPT system with a SC power bank. At the vehicle end, this technology is employed to dampen the impact of high-power surges on the battery [303].

•Electromagnetic (EM) safety and energy security:

In terms of energy sustainability, electromagnetic (EM) safety will be a key technological hurdle before full commercial usage. It is exciting that electromagnetic metamaterials can also subtly resolve EM leakage. Also, all relevant channels such as communication networks can access the transmitted energy from the electromagnetic field. Hence, studies on electromagnetic metamaterials and how to safeguard the power being transferred wirelessly will be required.

•Tailored design based on different applications:

Underwater charging [304], [305], recharging drones [306], powering driverless cars [305], urgent situation battery packs, and alternate power supply units in medium-voltage power transmission [307] are just a few of the specific uses where wireless charging technology has attracted considerable interest recent times. Therefore, the layout of magnetic couplers, compensation networks, and control method in such applications must be tailored to meet specific requirements. One possible limitation of magnetic coupling-based wireless charging is its ability to function in all environments. Correspondingly, an alternative to magnetic-field-based wireless chargers is the high-power wireless power transfer system using capacitive coupling, supersonic vibration, laser beams, or any other medium [308], [309], [310].

•Problems with Building And implementing the Charging Infrastructure:

Especially for static and DWPT structures installed in highways, incorporating a WPT system into the operating transportation system is a challenging job. Multiple features portray this difficulty: coil magnetic features may be affected by the mechanical configuration, construction stuff may lead to losses, and coil integration must not compromise the mechanical integrity of the roadway. At the same time, the physical resilience of the coil needs to be sufficient to bear the weight being applied to the route. Concrete magnetic characteristics are specified in [311] and [312], and the impact on coil electrical performances is explained, providing directives for customizing the coil geometric features in order to assess construction component losses. However, ferrite and aluminium shielding integration has not been addressed. In [313], the author examines dielectric losses induced in pavement surfacing materials. According to the findings, surfacing material losses are negligible when compared to those from other causes. Additionally, the losses' extreme sensitivity to moisture necessitates a waterproof mechanical structure's design. Making magnetizable concrete by combining magnetic material with cement is described as a solution to the brittleness of ferrite in [314]. With this method, the price of building should go down and the mechanical strength of coils will go up.

In [315] and [316], researchers examine the long-term effects of incorporating cordless charging stations into Belgium's road surface by looking at the country's specific situation in light of the overall connectivity survey. The inductive charging system deployment proved that non-standard road materials could be successfully integrated into existing roadway. However, a related research examined the durability of the WPT embedded roads based on information gathered from an Italian testing site [317]. The findings of the study sounded a note of caution about the installation of charging infrastructure along highways. The researchers argued that although installed coils contribute hardly 1% to entire road surface load, however, they are responsible for further of about 30% reduction in the lifecycle of the road.

Further study is required to understand and estimate the impact of coils incorporated in roadways on physical integrity and loss formation within the road stuff, as suggested by the existing literature. It is important to consider the coupler's electromagnetic as well as practical effectiveness once it has been incorporated into an asphalt- or concrete-based path. Subsequently, it's important to evaluate shielding, labelling, material choice, and coil incorporation during the initial stages of design.

•Financial Analysis as well as Emerging Techniques of Incorporation:

Encouraging DWPT charging is driven by the beneficial economic factors it has been found to have. Setting a wireless battery charger has the potential to greatly alleviate the battery storage requirement of vehicles and lower their expenditures. Battery expense, route infrastructure, distribution system converter, and power reliability and grid impact overheads are additional factors to think about. Then, an in-depth analysis can be carried out using a variety of metaheuristic objective features. The financial and ecological effects of DWPT systems were investigated by Limb et al. [317]. Their success is conditional on spending funds up front and embracing emerging innovations. Nonetheless, they show that DWPT systems may be more cost-effective and environmentally sustainable than vehicles powered by internal combustion engines. The financial impact of the OLEV was investigated by Mi et al. in Seoul, South Korea, assuming a yearly mileage of 20,000 kilometres for each vehicle and the installation of DWPT systems on all main highways [56]. By 2024, they demonstrated, the mass production of OLEVs will have a positive benefit-to-cost fraction [56].

WPT technologies may enhance the adoption of renewable energy when they are incorporated into a sub - district distribution grid. One can set up an implementation method where the DWPT structure acts as a nearby, adjustable load on a distribution grid, based on the varying energy consumption of the system. In addition, DWPT systems that are incorporated with power storage and renewable sources could lessen or even nullify their effect on the power network. As the WPT routes could be energized by renewable energy sources with a shield from static storage systems for energy, this may additionally reduce or minimize the requirement to install additional power networks along the roads and highways.

•Improvement in WPT Specification guidelines:

One more difficulty comes from the need for adapting different power sources and magnetic couplers from several companies. If the primary side has a unique flux trend, then the secondary sides must be adjusted to properly link to the primary. In addition, the coil shape must be aligned with compensation criteria and power converters to meet the recommended wattage over a broad working area. Therefore, it is essential to establish the integration among power electronic devices, compensation geometry variables, different kinds of coils (i.e., circular, DD, etc.), and configurations [316].

Standards for high-power contactless charging technologies designed greater than 22 kVA (as compared to the source end) are yet to be specified in terms of permissible stray field scale, working frequency, power circuitry components and converters, compensation geometry, as well as coil shape, despite SAE J2954 proposed conduct is already applicable to WPT1 to WPT3 transportation contactless battery charging systems [317], [318]. As a result, further progress in interoperability is required to encourage the use of high-power contactless battery charging systems. Researchers in the field of dynamic charging systems can expect to expend similar effort due to the lack of technical guidance in that area, forcing them to define their own boundaries and compatibility requirements. There is still a wide variety of DWPT operation frequencies in use, some of which fall outside the J2954-recommended frequency range for stationary EV charging [166], [249]. For the sake of lowering infrastructure and installation costs, it is preferable for vehicles to be able to communicate with one another regardless of whether they are classified as light, medium, or heavy duty. As a result, the pick-up and power electronics on the driver's side could be standardized, as a solitary system might serve both purposes.

•Considerations in terms of energy and sustainability:

There are two points involved when considering the role that wireless charging of electric vehicles serves in the preservation of nature. If we take not of all of the different systems that are capable of being powered by electricity, the use of electric energy rather than petrol or diesel engines comes out on top. The fact that electrical machines do not immediately pollute the environment is the most significant advantage that they offer. Nonetheless, there is a problem with the electrical components to store energy. As a result, the equipment will be operated either wirelessly by WPT or, if a battery is used to power the machine, by readily rechargeable WPT. WPT powers the equipment wirelessly, so it uses less battery and makes the device lighter. In order to evaluate the differences and similarities between wired and WPT systems, Brown [319] carried out a study at the University of Michigan in the form of a 12-year outline investigation. Two different inferences emerged.

1) By lowering the need for battery packs, WPT technologies can contribute to mitigate the effects of

greenhouse gas emissions and the extra power demands of a widespread wireless power network.
2) Additional expenses associated with setting up a wireless network could be repaid by the smaller and lighter batteries used in EVs.

Plug-in charging referred to as wired power transfer, and WPT both have perks as well as drawbacks in terms of technological advancements. However, WPT is clearly superior in terms of ease of use, safety, and environment and sustainability. The transfer of power over distances of meters is suggested to improve environmentally friendly transport in the future by reducing the need for cords and batteries [236].

VII. CONCLUSION

One of the primaries aims of WPT charging systems is to achieve higher efficiency in comparison to plug-in charger. As a result of their reliability, convenience, and efficiency in charging EVs with minimal human intervention, wireless battery charging technologies are becoming increasingly popular in the research area in both academics and industry. This paper gives a comprehensive and extensive overview of the state-of-the-art for a WPT system for EVs battery charging. This paper's major goal is to examine and investigate the numerous techniques for WPT in EVs, such as compensation topologies and their derivations, power electronics circuits and architecture, control strategies, standards, and communication networks in stationary and dynamic wireless charging based on the analysis and review of the current major literatures. The factors used for the study include the various coupling, compensation and control schemes, implementation tools, and performance metrics. Some of the most significant technological research gaps uncovered are below:

1) To determine how to maximize power transmission while keeping coil dimensions at a lower level.
2) Since electromagnetic fields and radio waves interact with one another, high-frequency EM fields have an effect on radio transmissions.
3) Due to even minor misalignment lowering the efficiency of a high-power transfer system, the question appears on how to swiftly the transmission and receiver coils will be in a perfectly aligned position.
4) How electromagnetic fields affect the electronic devices used in autonomous vehicles.
5) Misalignment can be tolerated to a certain extent due to resonance.
6) The system's temperature will get affected if an external item enters the WPT system.
7) For high-power transmission networks, resonance causes the WPT system to become cumbersome.
8) The requirement of a small resonant WPT system necessitates a more effective compensation topology.

There are also some areas in which more research is needed in relation to sustainable viewpoints: Guidelines and limitations on electromagnetic fields that might lessen the impact on living beings, electricity distribution system management that regulates the requirements and availability of electricity for WPT charging stations, the incorporation of battery health in the optimization of the broad implementation of WPT networks, regulations promoting the expansion and advancement of WPT and EV innovation. Increasing the resonant link frequency of compensators has been a primary focus of research and development. New high-frequency magnetics and semiconductors with enhanced features will receive a lot of focus in the coming years of study. Employing mixed and standard compensation designs in multilevel/multi-pulse converters with a multicoil topology is another intriguing path to go. If these issues can be resolved, WPT system for EVs battery chargers will likely undergo a dramatic shift in their commercial adoption. Integration in both directions with the grid makes it possible for vehicles to act as portable energy storage systems that help control the grid by storing extra energy from renewable sources. The importance of WPT system developments over the coming years toward promoting electrical vehicles and strengthening the long-term viability of transport electrification will largely depend on how much advancement is made in those domains.

REFERENCES

[1] S. Li, W. Li, J. Deng, T. D. Nguyen, and C. C. Mi, "A double-sided LCC compensation network and its tuning method for wireless power transfer," *IEEE Trans. Veh. Technol.*, vol. 64, no. 6, pp. 2261–2273, Jun. 2015, doi: 10.1109/TVT.2014.2347006.

[2] A. Kurs, A. Karalis, R. Moffatt, J. D. Joannopoulos, P. Fisher, and M. Soljačić, "Wireless power transfer via strongly coupled magnetic resonances," *Science*, vol. 317, no. 5834, pp. 83–86, Jul. 2007, doi: 10.1126/science.1143254.

[3] X. Mou, O. Groling, and H. Sun, "Energy-efficient and adaptive design for wireless power transfer in electric vehicles," *IEEE Trans. Ind. Electron.*, vol. 64, no. 9, pp. 7250–7260, Sep. 2017, doi: 10.1109/TIE.2017.2686299.

[4] A. P. Sample, D. A. Meyer, and J. R. Smith, "Analysis, experimental results, and range adaptation of magnetically coupled resonators for wireless power transfer," *IEEE Trans. Ind. Electron.*, vol. 58, no. 2, pp. 544–554, Feb. 2011, doi: 10.1109/TIE.2010.2046002.

[5] B. L. Cannon, J. F. Hoburg, D. D. Stancil, and S. C. Goldstein, "Magnetic resonant coupling as a potential means for wireless power transfer to multiple small receivers," *IEEE Trans. Power Electron.*, vol. 24, no. 7, pp. 1819–1825, Jul. 2009, doi: 10.1109/TPEL.2009.2017195.

[6] A. Kurs, R. Moffatt, and M. Soljačić, "Simultaneous mid-range power transfer to multiple devices," *Appl. Phys. Lett.*, vol. 96, no. 4, Jan. 2010, doi: 10.1063/1.3284651.

[7] S. Aldhaher, D. C. Yates, and P. D. Mitcheson, "Design and development of a class EF_2 inverter and rectifier for multimegahertz wireless power transfer systems," *IEEE Trans. Power Electron.*, vol. 31, no. 12, pp. 8138–8150, Dec. 2016, doi: 10.1109/TPEL.2016.2521060.

[8] S. Cheon, Y.-H. Kim, S.-Y. Kang, M. L. Lee, J.-M. Lee, and T. Zyung, "Circuit-Model-Based analysis of a wireless energy-transfer system via coupled magnetic resonances," *IEEE Trans. Ind. Electron.*, vol. 58, no. 7, pp. 2906–2914, Jul. 2011, doi: 10.1109/TIE.2010.2072893.

[9] L. Huang, A. P. Hu, A. K. Swain, and Y. Su, "Z-impedance compensation for wireless power transfer based on electric field," *IEEE Trans. Power Electron.*, vol. 31, no. 11, pp. 7556–7563, Nov. 2016, doi: 10.1109/TPEL.2016.2557461.

[10] J. Shin, S. Shin, Y. Kim, S. Ahn, S. Lee, G. Jung, S.-J. Jeon, and D.-H. Cho, "Design and implementation of shaped magnetic-resonance-based wireless power transfer system for roadway-powered moving electric vehicles," *IEEE Trans. Ind. Electron.*, vol. 61, no. 3, pp. 1179–1192, Mar. 2014, doi: 10.1109/TIE.2013.2258294.

[11] S. Y. Choi, B. W. Gu, S. W. Lee, W. Y. Lee, J. Huh, and C. T. Rim, "Generalized active EMF cancel methods for wireless electric vehicles," *IEEE Trans. Power Electron.*, vol. 29, no. 11, pp. 5770–5783, Nov. 2014, doi: 10.1109/TPEL.2013.2295094.

[12] *Trends in Electric Light-Duty Vehicles—Global EV Outlook 2022—Analysis—IEA*. Accessed: Mar. 10, 2023. [Online]. Available: https://www.iea.org/reports/global-ev-outlook-2022/trends-in-electric-light-duty-vehicles
[13] *Global EV Sales by Scenario, 2020–2030—Charts—Data & Statistics—IEA*. Accessed: Mar. 10, 2023. [Online]. Available: https://www.iea.org/data-and-statistics/charts/global-ev-sales-by-scenario-2020-2030
[14] A. Tsakalidis, J. Krause, A. Julea, E. Peduzzi, E. Pisoni, and C. Thiel, "Electric light commercial vehicles: Are they the sleeping giant of electromobility?" *Transp. Res. D, Transp. Environ.*, vol. 86, Sep. 2020, Art. no. 102421, doi: 10.1016/j.trd.2020.102421.
[15] J. Dai and D. C. Ludois, "Biologically inspired coupling pixilation for position independence in capacitive power transfer surfaces," in *Proc. IEEE Appl. Power Electron. Conf. Expo. (APEC)*, Mar. 2015, pp. 3276–3282, doi: 10.1109/APEC.2015.7104822.
[16] C. Liu, A. P. Hu, B. Wang, and N. C. Nair, "A capacitively coupled contactless matrix charging platform with soft switched transformer control," *IEEE Trans. Ind. Electron.*, vol. 60, no. 1, pp. 249–260, Jan. 2013, doi: 10.1109/TIE.2011.2172174.
[17] J. Dai and D. C. Ludois, "Single active switch power electronics for kilowatt scale capacitive power transfer," *IEEE J. Emerg. Sel. Topics Power Electron.*, vol. 3, no. 1, pp. 315–323, Mar. 2015, doi: 10.1109/JESTPE.2014.2334621.
[18] D. C. Ludois, M. J. Erickson, and J. K. Reed, "Aerodynamic fluid bearings for translational and rotating capacitors in noncontact capacitive power transfer systems," *IEEE Trans. Ind. Appl.*, vol. 50, no. 2, pp. 1025–1033, Mar. 2014, doi: 10.1109/TIA.2013.2273484.
[19] M. P. Theodoridis, "Effective capacitive power transfer," *IEEE Trans. Power Electron.*, vol. 27, no. 12, pp. 4906–4913, Dec. 2012, doi: 10.1109/TPEL.2012.2192502.
[20] F. Lu, H. Zhang, and C. Mi, "A review on the recent development of capacitive wireless power transfer technology," *Energies*, vol. 10, no. 11, p. 1752, Nov. 2017, doi: 10.3390/en10111752.
[21] J. Kim and F. Bien, "Electric field coupling technique of wireless power transfer for electric vehicles," in *Proc. IEEE Tencon Spring*, Apr. 2013, pp. 267–271, doi: 10.1109/TENCONSpring.2013.6584453.
[22] F. Lu, H. Zhang, H. Hofmann, and C. Mi, "A double-sided LCLC-compensated capacitive power transfer system for electric vehicle charging," *IEEE Trans. Power Electron.*, vol. 30, no. 11, pp. 6011–6014, Nov. 2015, doi: 10.1109/TPEL.2015.2446891.
[23] J. Wang, M. Leach, E. G. Lim, Z. Wang, and Y. Huang, "Investigation of magnetic resonance coupling circuit topologies for wireless power transmission," *Microw. Opt. Technol. Lett.*, vol. 61, no. 7, pp. 1755–1763, 2019. Accessed: Mar. 10, 2023. [Online]. Available: https://onlinelibrary.wiley.com/doi/pdf/10.1002/mop.31803
[24] S. Li, Z. Liu, H. Zhao, L. Zhu, C. Shuai, and Z. Chen, "Wireless power transfer by electric field resonance and its application in dynamic charging," *IEEE Trans. Ind. Electron.*, vol. 63, no. 10, pp. 6602–6612, Oct. 2016, doi: 10.1109/TIE.2016.2577625.
[25] A. Berger, M. Agostinelli, S. Vesti, J. A. Oliver, J. A. Cobos, and M. Huemer, "A wireless charging system applying phase-shift and amplitude control to maximize efficiency and extractable power," *IEEE Trans. Power Electron.*, vol. 30, no. 11, pp. 6338–6348, Nov. 2015, doi: 10.1109/TPEL.2015.2410216.
[26] T. Diekhans and R. W. De Doncker, "A dual-side controlled inductive power transfer system optimized for large coupling factor variations and partial load," *IEEE Trans. Power Electron.*, vol. 30, no. 11, pp. 6320–6328, Nov. 2015, doi: 10.1109/TPEL.2015.2393912.
[27] T. Essandoh, R. Johnson, and E. Watson, "ChargeSpot: Wireless power transfer through high resonant frequency," Univ. Central Florida, FL, USA, Tech. Rep., 2013. [Online]. Available: https://www.ece.ucf.edu/seniordesign/fa2013sp2014/g20/docs/g20documentation1.pdf
[28] Z. Li, C. Zhu, J. Jiang, K. Song, and G. Wei, "A 3-kW wireless power transfer system for sightseeing car supercapacitor charge," *IEEE Trans. Power Electron.*, vol. 32, no. 5, pp. 3301–3316, May 2017, doi: 10.1109/TPEL.2016.2584701.
[29] C.-S. Wang, O. H. Stielau, and G. A. Covic, "Design considerations for a contactless electric vehicle battery charger," *IEEE Trans. Ind. Electron.*, vol. 52, no. 5, pp. 1308–1314, Oct. 2005, doi: 10.1109/TIE.2005.855672.
[30] W. X. Zhong and S. Y. R. Hui, "Maximum energy efficiency tracking for wireless power transfer systems," *IEEE Trans. Power Electron.*, vol. 30, no. 7, pp. 4025–4034, Jul. 2015, doi: 10.1109/TPEL.2014.2351496.
[31] H. Jiang, J. Zhang, D. Lan, K. K. Chao, S. Liou, H. Shahnasser, R. Fechter, S. Hirose, M. Harrison, and S. Roy, "A low-frequency versatile wireless power transfer technology for biomedical implants," *IEEE Trans. Biomed. Circuits Syst.*, vol. 7, no. 4, pp. 526–535, Aug. 2013, doi: 10.1109/TBCAS.2012.2220763.
[32] S. Chopra and P. Bauer, "Analysis and design considerations for a contactless power transfer system," in *Proc. IEEE 33rd Int. Telecommun. Energy Conf. (INTELEC)*, Oct. 2011, pp. 1–6, doi: 10.1109/INTLEC.2011.6099774.
[33] X. Wei, Z. Wang, and H. Dai, "A critical review of wireless power transfer via strongly coupled magnetic resonances," *Energies*, vol. 7, no. 7, pp. 4316–4341, 2014, doi: 10.3390/en7074316.
[34] A. P. Sample, D. J. Yeager, P. S. Powledge, A. V. Mamishev, and J. R. Smith, "Design of an RFID-based battery-free programmable sensing platform," *IEEE Trans. Instrum. Meas.*, vol. 57, no. 11, pp. 2608–2615, Nov. 2008, doi: 10.1109/TIM.2008.925019.
[35] S. Sinha, A. Kumar, B. Regensburger, and K. K. Afridi, "A new design approach to mitigating the effect of parasitics in capacitive wireless power transfer systems for electric vehicle charging," *IEEE Trans. Transport. Electrific.*, vol. 5, no. 4, pp. 1040–1059, Dec. 2019, doi: 10.1109/TTE.2019.2931869.
[36] T. Imura, K. Suzuki, K. Hata, and Y. Hori, "Comparison of four resonant topologies based on unified design procedure for capacitive power transfer," *IEEJ J. Ind. Appl.*, vol. 10, no. 3, pp. 339–347, 2021, doi: 10.1541/IEEJJIA.20008612.
[37] E. Abramov and M. M. Peretz, "Multi-loop control for power transfer regulation in capacitive wireless systems by means of variable matching networks," *IEEE J. Emerg. Sel. Topics Power Electron.*, vol. 8, no. 3, pp. 2095–2110, Sep. 2020, doi: 10.1109/JESTPE.2019.2935631.
[38] K.-W. Kim, H.-S. Lee, and J.-W. Lee, "Waveform design for fair wireless power transfer with multiple energy harvesting devices," *IEEE J. Sel. Areas Commun.*, vol. 37, no. 1, pp. 34–47, Jan. 2019, doi: 10.1109/JSAC.2018.2872311.
[39] Z. Zhang, K. T. Chau, C. Qiu, and C. Liu, "Energy encryption for wireless power transfer," *IEEE Trans. Power Electron.*, vol. 30, no. 9, pp. 5237–5246, Sep. 2015, doi: 10.1109/TPEL.2014.2363686.
[40] E. Ahene, M. Ofori-Oduro, and B. Agyemang, "Secure energy encryption for wireless power transfer," in *Proc. IEEE 7th Int. Adv. Comput. Conf. (IACC)*, Jan. 2017, pp. 199–204, doi: 10.1109/IACC.2017.0053.
[41] N. H. Hussin, M. M. Azizan, A. Ali, and M. A. M. Albreem, "Comparison of performance based on power of energy encryption in medium field for wireless power transfer system," *Int. J. Adv. Sci., Eng. Inf. Technol.*, vol. 7, no. 5, p. 1805, Oct. 2017, doi: 10.18517/ijaseit.7.5.2283.
[42] A. Ahmad, M. S. Alam, and R. Chabaan, "A comprehensive review of wireless charging technologies for electric vehicles," *IEEE Trans. Transport. Electrific.*, vol. 4, no. 1, pp. 38–63, Mar. 2018, doi: 10.1109/TTE.2017.2771619.
[43] S. Moon and G.-W. Moon, "Wireless power transfer system with an asymmetric four-coil resonator for electric vehicle battery chargers," *IEEE Trans. Power Electron.*, vol. 31, no. 10, pp. 6844–6854, Oct. 2016, doi: 10.1109/TPEL.2015.2506779.
[44] Z.-H. Ye, Y. Sun, X. Dai, C.-S. Tang, Z.-H. Wang, and Y.-G. Su, "Energy efficiency analysis of U-coil wireless power transfer system," *IEEE Trans. Power Electron.*, vol. 31, no. 7, pp. 4809–4817, Jul. 2016, doi: 10.1109/TPEL.2015.2483839.
[45] Y. D. Chung, C. Y. Lee, H. Kang, and Y. G. Park, "Design considerations of superconducting wireless power transfer for electric vehicle at different inserted resonators," *IEEE Trans. Appl. Supercond.*, vol. 26, no. 4, pp. 1–5, Jun. 2016, doi: 10.1109/TASC.2016.2532904.
[46] S. Kim, H.-H. Park, J. Kim, J. Kim, and S. Ahn, "Design and analysis of a resonant reactive shield for a wireless power electric vehicle," *IEEE Trans. Microw. Theory Techn.*, vol. 62, no. 4, pp. 1057–1066, Apr. 2014, doi: 10.1109/TMTT.2014.2305404.
[47] Z. Luo and X. Wei, "Analysis of square and circular planar spiral coils in wireless power transfer system for electric vehicles," *IEEE Trans. Ind. Electron.*, vol. 65, no. 1, pp. 331–341, Jan. 2018, doi: 10.1109/TIE.2017.2723867.
[48] Y. J. Jang, E. S. Suh, and J. W. Kim, "System architecture and mathematical models of electric transit bus system utilizing wireless power transfer technology," *IEEE Syst. J.*, vol. 10, no. 2, pp. 495–506, Jun. 2016, doi: 10.1109/JSYST.2014.2369485.

[49] M. Fu, H. Yin, X. Zhu, and C. Ma, "Analysis and tracking of optimal load in wireless power transfer systems," *IEEE Trans. Power Electron.*, vol. 30, no. 7, pp. 3952–3963, Jul. 2015, doi: 10.1109/TPEL.2014.2347071.

[50] M. Fu, C. Ma, and X. Zhu, "A cascaded boost–buck converter for high-efficiency wireless power transfer systems," *IEEE Trans. Ind. Informat.*, vol. 10, no. 3, pp. 1972–1980, Aug. 2014, doi: 10.1109/TII.2013.2291682.

[51] C. Xiao, D. Cheng, and K. Wei, "An LCC-C compensated wireless charging system for implantable cardiac pacemakers: Theory, experiment, and safety evaluation," *IEEE Trans. Power Electron.*, vol. 33, no. 6, pp. 4894–4905, Jun. 2018, doi: 10.1109/TPEL.2017.2735441.

[52] Y. Zhang, T. Kan, Z. Yan, Y. Mao, Z. Wu, and C. C. Mi, "Modeling and analysis of series-none compensation for wireless power transfer systems with a strong coupling," *IEEE Trans. Power Electron.*, vol. 34, no. 2, pp. 1209–1215, Feb. 2019, doi: 10.1109/TPEL.2018.2835307.

[53] J. Liu, K. W. Chan, C. Y. Chung, N. H. L. Chan, M. Liu, and W. Xu, "Single-stage wireless-power-transfer resonant converter with boost bridgeless power-factor-correction rectifier," *IEEE Trans. Ind. Electron.*, vol. 65, no. 3, pp. 2145–2155, Mar. 2018, doi: 10.1109/TIE.2017.2745471.

[54] K. E. Koh, T. C. Beh, T. Imura, and Y. Hori, "Impedance matching and power division using impedance inverter for wireless power transfer via magnetic resonant coupling," *IEEE Trans. Ind. Appl.*, vol. 50, no. 3, pp. 2061–2070, May 2014, doi: 10.1109/TIA.2013.2287310.

[55] X. Zhang, S. L. Ho, and W. N. Fu, "Quantitative design and analysis of relay resonators in wireless power transfer system," *IEEE Trans. Magn.*, vol. 48, no. 11, pp. 4026–4029, Nov. 2012, doi: 10.1109/TMAG.2012.2202883.

[56] H. Li, K. Wang, L. Huang, W. Chen, and X. Yang, "Dynamic modeling based on coupled modes for wireless power transfer systems," *IEEE Trans. Power Electron.*, vol. 30, no. 11, pp. 6245–6253, Nov. 2015, doi: 10.1109/TPEL.2014.2376474.

[57] *Wireless Power Transfer for Light-Duty Plug-In/Electric Vehicles and Alignment Methodology*, Standard SAEJ2954, Aug. 2022. [Online]. Available: http://standards.sae.org/j2954_202208/

[58] S. Y. Choi, B. W. Gu, S. Y. Jeong, and C. T. Rim, "Advances in wireless power transfer systems for roadway-powered electric vehicles," *IEEE J. Emerg. Sel. Topics Power Electron.*, vol. 3, no. 1, pp. 18–36, Mar. 2015, doi: 10.1109/JESTPE.2014.2343674.

[59] C. C. Mi, G. Buja, S. Y. Choi, and C. T. Rim, "Modern advances in wireless power transfer systems for roadway powered electric vehicles," *IEEE Trans. Ind. Electron.*, vol. 63, no. 10, pp. 6533–6545, Oct. 2016, doi: 10.1109/TIE.2016.2574993.

[60] M. Wu, X. Yang, H. Cui, W. Chen, L. Wang, L. Zhu, X. Yu, and Z. Yan, "Modeling of Litz-wire DD coil with ferrite core for wireless power transfer system," *IEEE Trans. Power Electron.*, vol. 38, no. 5, pp. 6653–6669, May 2023, doi: 10.1109/TPEL.2022.3222228.

[61] J. M. Miller, O. C. Onar, and M. Chinthavali, "Primary-side power flow control of wireless power transfer for electric vehicle charging," *IEEE J. Emerg. Sel. Topics Power Electron.*, vol. 3, no. 1, pp. 147–162, Mar. 2015.

[62] J. M. Miller and A. Daga, "Elements of wireless power transfer essential to high power charging of heavy duty vehicles," *IEEE Trans. Transport. Electrific.*, vol. 1, no. 1, pp. 26–39, Jun. 2015.

[63] R. Bosshard, J. W. Kolar, J. Mühlethaler, I. Stevanović, B. Wunsch, and F. Canales, "Modeling and η-α-Pareto optimization of inductive power transfer coils for electric vehicles," *IEEE J. Emerg. Sel. Topics Power Electron.*, vol. 3, no. 1, pp. 50–64, Mar. 2015.

[64] G. A. Covic and J. T. Boys, "Modern trends in inductive power transfer for transportation applications," *IEEE J. Emerg. Sel. Topics Power Electron.*, vol. 1, no. 1, pp. 28–41, Mar. 2013.

[65] R. Bosshard and J. W. Kolar, "Inductive power transfer for electric vehicle charging: Technical challenges and tradeoffs," *IEEE Power Electron. Mag.*, vol. 3, no. 3, pp. 22–30, Sep. 2016.

[66] B. R. Long, J. M. Miller, A. Daga, P. C. Schrafel, and J. Wolgemuth, "Which way for wireless power: High Q or high k?" in *Proc. IEEE PELS*, Oct. 2016, pp. 6–10.

[67] M. Budhia, G. A. Covic, and J. T. Boys, "Design and optimization of circular magnetic structures for lumped inductive power transfer systems," *IEEE Trans. Power Electron.*, vol. 26, no. 11, pp. 3096–3108, Nov. 2011.

[68] M. Budhia, J. T. Boys, G. A. Covic, and C.-Y. Huang, "Development of a single-sided flux magnetic coupler for electric vehicle IPT charging systems," *IEEE Trans. Ind. Electron.*, vol. 60, no. 1, pp. 318–328, Jan. 2013.

[69] M. Budhia, G. Covic, and J. Boys, "A new IPT magnetic coupler for electric vehicle charging systems," in *Proc. 36th Annu. Conf. IEEE Ind. Electron. Soc.*, Glendale, AZ, USA, Nov. 2010, pp. 2487–2492.

[70] A. Zaheer, G. A. Covic, and D. Kacprzak, "A bipolar pad in a 10-kHz 300-W distributed IPT system for AGV applications," *IEEE Trans. Ind. Electron.*, vol. 61, no. 7, pp. 3288–3301, Jul. 2014.

[71] G. A. Covic, M. L. G. Kissin, D. Kacprzak, N. Clausen, and H. Hao, "A bipolar primary pad topology for EV stationary charging and highway power by inductive coupling," in *Proc. IEEE Energy Convers. Congr. Expo.*, Phoenix, AZ, USA, Sep. 2011, pp. 1832–1838.

[72] G. Elliott, S. Raabe, G. A. Covic, and J. T. Boys, "Multiphase pickups for large lateral tolerance contactless power-transfer systems," *IEEE Trans. Ind. Electron.*, vol. 57, no. 5, pp. 1590–1598, May 2010.

[73] D. Patil, M. Ditsworth, J. Pacheco, and W. Cai, "A magnetically enhanced wireless power transfer system for compensation of misalignment in mobile charging platforms," in *Proc. IEEE Energy Convers. Congr. Expo. (ECCE)*, Montreal, QC, Canada, Sep. 2015, pp. 1286–1293.

[74] J. T. Boys and G. A. Covic, "IPT fact sheet series: No. 2 magnetic circuits for powering electric vehicles," Dept. Elect. Comput. Eng., Univ. Auckland, Auckland, New Zealand, Tech. Rep., 2014, p. 2. [Online]. Available: https://www.qualcomm.com/content/dam/qcomm-martech/dm-assets/documents/ipt_fact_sheet_2_-_uoa_2014.pdf

[75] S. Kim, G. A. Covic, and J. T. Boys, "Tripolar pad for inductive power transfer systems for EV charging," *IEEE Trans. Power Electron.*, vol. 32, no. 7, pp. 5045–5057, Jul. 2017.

[76] S. Kim, A. Zaheer, G. Covic, and J. Boys, "Tripolar pad for inductive power transfer systems," in *Proc. 40th Annu. Conf. IEEE Ind. Electron. Soc. (IECON)*, Dallas, TX, USA, Oct./Nov. 2014, pp. 3066–3072.

[77] M. Kiani, U.-M. Jow, and M. Ghovanloo, "Design and optimization of a 3-coil inductive link for efficient wireless power transmission," *IEEE Trans. Biomed. Circuits Syst.*, vol. 5, no. 6, pp. 579–591, Dec. 2011.

[78] S. Moon, B.-C. Kim, S.-Y. Cho, C.-H. Ahn, and G.-W. Moon, "Analysis and design of a wireless power transfer system with an intermediate coil for high efficiency," *IEEE Trans. Ind. Electron.*, vol. 61, no. 11, pp. 5861–5870, Nov. 2014.

[79] R. Bosshard, "Multi-objective optimization of inductive power transfer systems for EV charging," Ph.D. dissertation, Dept. Inf. Technol. Elect. Eng., ETH Zürich, Zürich, Switzerland, 2015.

[80] International Commission on Non-Ionizing Radiation Protection, "Guidelines for limiting exposure to time-varying electric and magnetic fields (1 Hz to 100 kHz)," *Health Phys.*, vol. 99, no. 6, pp. 818–836, 2010.

[81] J. Zhang, X. Yuan, C. Wang, and Y. He, "Comparative analysis of two-coil and three-coil structures for wireless power transfer," *IEEE Trans. Power Electron.*, vol. 32, no. 1, pp. 341–352, Jan. 2017.

[82] J. Deng, J. Deng, W. Li, S. Li, and C. Mi, "Magnetic integration of LCC compensated resonant converter for inductive power transfer applications," in *Proc. IEEE Energy Convers. Congr. Expo. (ECCE)*, Pittsburgh, PA, USA, Sep. 2014, pp. 660–667.

[83] W. Li, H. Zhao, S. Li, J. Deng, T. Kan, and C. C. Mi, "Integrated *LCC* compensation topology for wireless charger in electric and plug-in electric vehicles," *IEEE Trans. Ind. Electron.*, vol. 62, no. 7, pp. 4215–4225, Jul. 2015.

[84] N. Prosen, J. Domajnko, and M. Milanovič, "Wireless power transfer using double DD coils," *Electronics*, vol. 10, no. 20, p. 2528, Oct. 2021, doi: 10.3390/electronics10202528.

[85] J. Domajnko and N. Prosen, "A wireless power transfer system using a double DD quadrature coil structure," *Electronics*, vol. 12, no. 4, p. 890, Feb. 2023, doi: 10.3390/electronics12040890.

[86] A. Gil and J. Taiber, "A literature review in dynamic wireless power transfer for electric vehicles: Technology and infrastructure integration challenges," in *Sustainable Automotive Technologies 2013*. Ingolstadt, Germany: Springer, 2013, pp. 289–298.

[87] S. Choi, J. Huh, W. Y. Lee, S. W. Lee, and C. T. Rim, "New cross-segmented power supply rails for roadway-powered electric vehicles," *IEEE Trans. Power Electron.*, vol. 28, no. 12, pp. 5832–5841, Dec. 2013.

[88] J. Huh, S. W. Lee, W. Y. Lee, G. H. Cho, and C. T. Rim, "Narrow-width inductive power transfer system for online electrical vehicles," *IEEE Trans. Power Electron.*, vol. 26, no. 12, pp. 3666–3679, Dec. 2011.

[89] T. Campi, S. Cruciani, and M. Feliziani, "Magnetic shielding of wireless power transfer systems," in *Proc. Int. Symp. Electromagn. Compat.*, Tokyo, Japan, May 2014, pp. 422–425.

[90] M. Mohammad, E. T. Wodajo, S. Choi, and M. E. Elbuluk, "Modeling and design of passive shield to limit EMF emission and to minimize shield loss in unipolar wireless charging system for EV," *IEEE Trans. Power Electron.*, vol. 34, no. 12, pp. 12235–12245, Dec. 2019.

[91] H. Zhao, K. Liu, S. Li, F. Yang, S. Cheng, H. H. Eldeeb, J. Kang, and G. Xu, "Shielding optimization of IPT system based on genetic algorithm for efficiency promotion in EV wireless charging applications," *IEEE Trans. Ind. Appl.*, vol. 58, no. 1, pp. 1190–1200, Jan. 2022.

[92] B. Zhang, R. B. Carlson, V. P. Galigekere, O. C. Onar and J. L. Pries, "Electromagnetic shielding design for 200 kW stationary wireless charging of light-duty EV," *Proc. IEEE Energy Convers. Congr. Expo.*, Oct. 2020, pp. 5185–5192.

[93] M. Lu and K. D. T. Ngo, "Attenuation of stray magnetic field in inductive power transfer by controlling phases of windings' currents," *IEEE Trans. Magn.*, vol. 53, no. 9, pp. 1–8, Sep. 2017.

[94] J. Kim, J. Kim, S. Kong, H. Kim, I.-S. Suh, N. P. Suh, D.-H. Cho, J. Kim, and S. Ahn, "Coil design and shielding methods for a magnetic resonant wireless power transfer system," *Proc. IEEE*, vol. 101, no. 6, pp. 1332–1342, Jun. 2013.

[95] S. Ahn and J. Kim, "Magnetic field design for high efficient and low EMF wireless power transfer in on-line electric vehicle," in *Proc. 5th Eur. Conf. Antennas Propag.*, Rome, Italy, 2011, pp. 3979–3982.

[96] S. Ahn, J. Pak, T. Song, H. Lee, J.-G. Byun, D. Kang, C.-S. Choi, E. Kim, J. Ryu, M. Kim, Y. Cha, Y. Chun, C.-T. Rim, J.-H. Yim, D.-H. Cho, and J. Kim, "Low frequency electromagnetic field reduction techniques for the on-line electric vehicle (OLEV)," in *Proc. IEEE Int. Symp. Electromagn. Compat.*, Jul. 2010, pp. 625–630.

[97] L. Gu, G. Zulauf, A. Stein, P. A. Kyaw, T. Chen, and J. M. R. Davila, "6.78-MHz wireless power transfer with self-resonant coils at 95% DC–DC efficiency," *IEEE Trans. Power Electron.*, vol. 36, no. 3, pp. 2456–2460, Mar. 2021.

[98] R. Qin, J. Li and D. Costinett, "A high frequency wireless power transfer system for electric vehicle charging using multi-layer nonuniform self-resonant coil at MHz," in *Proc. IEEE Energy Convers. Congr. Expo.*, Oct. 2020, pp. 5487–5494.

[99] R. Qin, J. Li, and D. Costinett, "A 6.6-kW high-frequency wireless power transfer system for electric vehicle charging using multilayer nonuniform self-resonant coil at MHz," *IEEE Trans. Power Electron.*, vol. 37, no. 4, pp. 4842–4856, Apr. 2022.

[100] J. Sun, R. Qin, J. Li, D. J. Costinett, and L. M. Tolbert, "Design of a resonant reactive shielding coil for wireless power transfer system," in *Proc. IEEE Appl. Power Electron. Conf. Expo.*, Jun. 2021, pp. 1565–1572.

[101] R. Qin, J. Li, J. Sun, and D. Costinett, "Shielding design for high-frequency wireless power transfer system for EV charging with self-resonant coils," *IEEE Trans. Power Electron.*, vol. 38, no. 6, pp. 7900–7909, Jun. 2023, doi: 10.1109/TPEL.2023.3251990.

[102] R. Qin, J. Li, and D. Costinett, "A high frequency wireless power transfer system for electric vehicle charging using multi-layer nonuniform self-resonant coil at MHz," in *Proc. IEEE Energy Convers. Congr. Expo. (ECCE)*, Detroit, MI, USA, Oct. 2020, pp. 5487–5494, doi: 10.1109/ECCE44975.2020.9236415.

[103] S. Bandyopadhyay, V. Prasanth, L. R. Elizondo, and P. Bauer, "Design considerations for a misalignment tolerant wireless inductive power system for electric vehicle (EV) charging," in *Proc. 19th Eur. Conf. Power Electron. Appl. (EPE ECCE Europe)*, Sep. 2017, pp. P.1–P.10, doi: 10.23919/EPE17ECCEEurope.2017.8099320.

[104] J. Villa, J. Sanz, R. Acerete, and M. Perie, "Design considerations for WPT dynamic charging applications," in *Proc. AEIT Int. Conf. Electr. Electron. Technol. Automot. (AEIT AUTOMOTIVE)*, Jul. 2019, pp. 1–6, doi: 10.23919/EETA.2019.8804508.

[105] C.-S. Wang, G. A. Covic, and O. H. Stielau, "Investigating an LCL load resonant inverter for inductive power transfer applications," *IEEE Trans. Power Electron.*, vol. 19, no. 4, pp. 995–1002, Jul. 2004, doi: 10.1109/TPEL.2004.830098.

[106] N. A. Keeling, G. A. Covic, and J. T. Boys, "A unity-power-factor IPT pickup for high-power applications," *IEEE Trans. Ind. Electron.*, vol. 57, no. 2, pp. 744–751, Feb. 2010, doi: 10.1109/TIE.2009.2027255.

[107] W. Zhang, S.-C. Wong, C. K. Tse, and Q. Chen, "Analysis and comparison of secondary series- and parallel-compensated inductive power transfer systems operating for optimal efficiency and load-independent voltage-transfer ratio," *IEEE Trans. Power Electron.*, vol. 29, no. 6, pp. 2979–2990, Jun. 2014, doi: 10.1109/TPEL.2013.2273364.

[108] M. Pinuela, D. C. Yates, S. Lucyszyn, and P. D. Mitcheson, "Maximizing DC-to-load efficiency for inductive power transfer," *IEEE Trans. Power Electron.*, vol. 28, no. 5, pp. 2437–2447, May 2013, doi: 10.1109/TPEL.2012.2215887.

[109] C.-S. Wang, G. A. Covic, and O. H. Stielau, "Power transfer capability and bifurcation phenomena of loosely coupled inductive power transfer systems," *IEEE Trans. Ind. Electron.*, vol. 51, no. 1, pp. 148–157, Feb. 2004, doi: 10.1109/TIE.2003.822038.

[110] Z. Pantic, S. Bai, and S. M. Lukic, "ZCS *LCC*-compensated resonant inverter for inductive-power-transfer application," *IEEE Trans. Ind. Electron.*, vol. 58, no. 8, pp. 3500–3510, Aug. 2011, doi: 10.1109/TIE.2010.2081954.

[111] W. Zhang, S.-C. Wong, C. K. Tse, and Q. Chen, "An optimized track length in roadway inductive power transfer systems," *IEEE J. Emerg. Sel. Topics Power Electron.*, vol. 2, no. 3, pp. 598–608, Sep. 2014, doi: 10.1109/JESTPE.2014.2301460.

[112] I. Nam, R. Dougal, and E. Santi, "Optimal design method to achieve both good robustness and efficiency in loosely-coupled wireless charging system employing series-parallel resonant tank with asymmetrical magnetic coupler," in *Proc. IEEE Energy Convers. Congr. Expo.*, Sep. 2013, pp. 3266–3276, doi: 10.1109/ECCE.2013.6647129.

[113] I. Nam, R. Dougal, and E. Santi, "General optimal design method for series–series resonant tank in loosely-coupled wireless power transfer applications," in *Proc. IEEE Appl. Power Electron. Conf. Expo.*, Mar. 2014, pp. 857–866, doi: 10.1109/APEC.2014.6803408.

[114] A. Khaligh and S. Dusmez, "Comprehensive topological analysis of conductive and inductive charging solutions for plug-in electric vehicles," *IEEE Trans. Veh. Technol.*, vol. 61, no. 8, pp. 3475–3489, Oct. 2012, doi: 10.1109/TVT.2012.2213104.

[115] J. L. Villa, J. Sallán, J. F. S. Osorio, and A. Llombart, "High-misalignment tolerant compensation topology for ICPT systems," *IEEE Trans. Ind. Electron.*, vol. 59, no. 2, pp. 945–951, Feb. 2012, doi: 10.1109/TIE.2011.2161055.

[116] W. Zhang, S.-C. Wong, C. K. Tse, and Q. Chen, "Design for efficiency optimization and voltage controllability of series–series compensated inductive power transfer systems," *IEEE Trans. Power Electron.*, vol. 29, no. 1, pp. 191–200, Jan. 2014, doi: 10.1109/TPEL.2013.2249112.

[117] W. Zhang, S.-C. Wong, C. K. Tse, and Q. Chen, "Load-independent duality of current and voltage outputs of a series- or parallel-compensated inductive power transfer converter with optimized efficiency," *IEEE J. Emerg. Sel. Topics Power Electron.*, vol. 3, no. 1, pp. 137–146, Mar. 2015, doi: 10.1109/JESTPE.2014.2348558.

[118] J. Hou, Q. Chen, S.-C. Wong, C. K. Tse, and X. Ruan, "Analysis and control of series/series-parallel compensated resonant converter for contactless power transfer," *IEEE J. Emerg. Sel. Topics Power Electron.*, vol. 3, no. 1, pp. 124–136, Mar. 2015, doi: 10.1109/JESTPE.2014.2336811.

[119] R. Ota, N. Hoshi, and J. Haruna, "Design of compensation capacitor in S/P topology of inductive power transfer system with buck or boost converter on secondary side," *IEEJ J. Ind. Appl.*, vol. 4, no. 4, pp. 476–485, 2015, doi: 10.1541/ieejjia.4.476.

[120] Z. U. Zahid, C. Zheng, R. Chen, W. E. Faraci, J. J. Lai, M. Senesky, and D. Anderson, "Design and control of a single-stage large air-gapped transformer isolated battery charger for wide-range output voltage for EV applications," in *Proc. IEEE Energy Convers. Congr. Expo.*, Sep. 2013, pp. 5481–5487, doi: 10.1109/ECCE.2013.6647445.

[121] A. J. Moradewicz and M. P. Kazmierkowski, "Contactless energy transfer system with FPGA-controlled resonant converter," *IEEE Trans. Ind. Electron.*, vol. 57, no. 9, pp. 3181–3190, Sep. 2010, doi: 10.1109/TIE.2010.2051395.

[122] R. Bosshard, U. Badstübner, J. W. Kolar, and I. Stevanovic, "Comparative evaluation of control methods for inductive power transfer," in *Proc. Int. Conf. Renew. Energy Res. Appl. (ICRERA)*, Nov. 2012, pp. 1–6, doi: 10.1109/ICRERA.2012.6477400.

[123] S. Nutwong, A. Sangswang, and S. Naetiladdanon, "Output voltage control of the SP topology IPT system using a primary side controller," in *Proc. 13th Int. Conf. Electr. Eng./Electron., Comput., Telecommun. Inf. Technol. (ECTI-CON)*, Jun. 2016, pp. 1–5, doi: 10.1109/ECTI-Con.2016.7561393.

[124] S. Nutwong, A. Sangswang, S. Naetiladdanon, and E. Mujjalinvimut, "Load monitoring and output voltage control for SP topology IPT system using a single-side controller without any output measurement," in *Proc. 18th Eur. Conf. Power Electron. Appl. (EPE ECCE Europe)*, Sep. 2016, doi: 10.1109/EPE.2016.7695458.

[125] D. Patil, M. K. McDonough, J. M. Miller, B. Fahimi, and P. T. Balsara, "Wireless power transfer for vehicular applications: Overview and challenges," *IEEE Trans. Transport. Electrific.*, vol. 4, no. 1, pp. 3–37, Mar. 2018, doi: 10.1109/TTE.2017.2780627.

[126] V. Shevchenko, O. Husev, B. Pakhaliuk, and I. Kondratenko, "Design and simulation verification of low power wireless charging battery system for electric bicycle," in *Proc. IEEE 3rd Int. Conf. Intell. Energy Power Syst. (IEPS)*, Sep. 2018, pp. 22–27, doi: 10.1109/IEPS.2018.8559531.

[127] H. Hong, D. Yang, and S. Won, "The analysis for selecting compensating capacitances of two-coil resonant wireless power transfer system," in *Proc. IEEE Int. Conf. Energy Internet (ICEI)*, Apr. 2017, pp. 220–225, doi: 10.1109/ICEI.2017.46.

[128] W. Zhang and C. C. Mi, "Compensation topologies of high-power wireless power transfer systems," *IEEE Trans. Veh. Technol.*, vol. 65, no. 6, pp. 4768–4778, Jun. 2016, doi: 10.1109/TVT.2015.2454292.

[129] X. Mou, D. T. Gladwin, R. Zhao, and H. Sun, "Survey on magnetic resonant coupling wireless power transfer technology for electric vehicle charging," *IET Power Electron.*, vol. 12, no. 12, pp. 3005–3020, Oct. 2019, doi: 10.1049/iet-pel.2019.0529.

[130] K. Aditya and S. S. Williamson, "Design considerations for loosely coupled inductive power transfer (IPT) system for electric vehicle battery charging—A comprehensive review," in *Proc. IEEE Transp. Electrific. Conf. Expo (ITEC)*, Jun. 2014, pp. 1–6, doi: 10.1109/ITEC.2014.6861764.

[131] K. Li, S.-C. Tan, and S. Y. R. Hui, "Dynamic response and stability margin improvement of wireless power receiver systems via right-half-plane zero elimination," *IEEE Trans. Power Electron.*, vol. 36, no. 10, pp. 11196–11207, Oct. 2021, doi: 10.1109/TPEL.2021.3074324.

[132] J. Sallán, J. L. Villa, A. Llombart, and J. F. Sanz, "Optimal design of ICPT systems applied to electric vehicle battery charge," *IEEE Trans. Ind. Electron.*, vol. 56, no. 6, pp. 2140–2149, Jun. 2009, doi: 10.1109/TIE.2009.2015359.

[133] M. Fu, Z. Tang, and C. Ma, "Analysis and optimized design of compensation capacitors for a megahertz WPT system using full-bridge rectifier," *IEEE Trans. Ind. Informat.*, vol. 15, no. 1, pp. 95–104, Jan. 2019, doi: 10.1109/TII.2018.2833209.

[134] B. Ni, C. Y. Chung, and H. L. Chan, "Design and comparison of parallel and series resonant topology in wireless power transfer," in *Proc. IEEE 8th Conf. Ind. Electron. Appl. (ICIEA)*, Jun. 2013, pp. 1832–1837, doi: 10.1109/ICIEA.2013.6566666.

[135] M. Ishihara, K. Umetani, and E. Hiraki, "Strategy of topology selection based on quasi-duality between series–series and series–parallel topologies of resonant inductive coupling wireless power transfer systems," *IEEE Trans. Power Electron.*, vol. 35, no. 7, pp. 6785–6798, Jul. 2020, doi: 10.1109/TPEL.2019.2956732.

[136] C. Wang, R. Lu, C. Zhu, G. Wei, and K. Song, "Characteristics comparison of typical secondary-side compensation topologies in wireless powering systems with constant-current primary-side," in *Proc. IEEE Transp. Electrific. Conf. Expo, Asia–Pacific (ITEC Asia–Pacific)*, Aug. 2017, pp. 1–6, doi: 10.1109/ITEC-AP.2017.8080828.

[137] Y. H. Sohn, B. H. Choi, E. S. Lee, G. C. Lim, G.-H. Cho, and C. T. Rim, "General unified analyses of two-capacitor inductive power transfer systems: Equivalence of current-source SS and SP compensations," *IEEE Trans. Power Electron.*, vol. 30, no. 11, pp. 6030–6045, Nov. 2015, doi: 10.1109/TPEL.2015.2409734.

[138] U. Pratik, B. J. Varghese, A. Azad, and Z. Pantic, "Optimum design of decoupled concentric coils for operation in double-receiver wireless power transfer systems," *IEEE J. Emerg. Sel. Topics Power Electron.*, vol. 7, no. 3, pp. 1982–1998, Sep. 2019, doi: 10.1109/JESTPE.2018.2871150.

[139] Z. Zhang, K. T. Chau, C. Liu, F. Li, and T. W. Ching, "Quantitative analysis of mutual inductance for optimal wireless power transfer via magnetic resonant coupling," *IEEE Trans. Magn.*, vol. 50, no. 11, pp. 1–4, Nov. 2014, doi: 10.1109/TMAG.2014.2329298.

[140] D. H. Tran, V. B. Vu, and W. Choi, "Design of a high-efficiency wireless power transfer system with intermediate coils for the on-board chargers of electric vehicles," *IEEE Trans. Power Electron.*, vol. 33, no. 1, pp. 175–187, Jan. 2018, doi: 10.1109/TPEL.2017.2662067.

[141] J. Pries, V. P. N. Galigekere, O. C. Onar, and G.-J. Su, "A 50-kW three-phase wireless power transfer system using bipolar windings and series resonant networks for rotating magnetic fields," *IEEE Trans. Power Electron.*, vol. 35, no. 5, pp. 4500–4517, May 2020, doi: 10.1109/TPEL.2019.2942065.

[142] S. Samanta and A. K. Rathore, "A new inductive power transfer topology using direct AC–AC converter with active source current waveshaping," *IEEE Trans. Power Electron.*, vol. 33, no. 7, pp. 5565–5577, Jul. 2018, doi: 10.1109/TPEL.2017.2750081.

[143] C. Park, S. Lee, S. Y. Jeong, G.-H. Cho, and C. T. Rim, "Uniform power I-type inductive power transfer system with DQ-power supply rails for on-line electric vehicles," *IEEE Trans. Power Electron.*, vol. 30, no. 11, pp. 6446–6455, Nov. 2015, doi: 10.1109/TPEL.2015.2420372.

[144] A. Zakerian, S. Vaez-Zadeh, and A. Babaki, "A dynamic WPT system with high efficiency and high power factor for electric vehicles," *IEEE Trans. Power Electron.*, vol. 35, no. 7, pp. 6732–6740, Jul. 2020, doi: 10.1109/TPEL.2019.2957294.

[145] B. Esteban, M. Sid-Ahmed, and N. C. Kar, "A comparative study of power supply architectures in wireless EV charging systems," *IEEE Trans. Power Electron.*, vol. 30, no. 11, pp. 6408–6422, Nov. 2015, doi: 10.1109/TPEL.2015.2440256.

[146] A. Zaheer, M. Neath, H. Z. Z. Beh, and G. A. Covic, "A dynamic EV charging system for slow moving traffic applications," *IEEE Trans. Transport. Electrific.*, vol. 3, no. 2, pp. 354–369, Jun. 2017, doi: 10.1109/TTE.2016.2628796.

[147] D. J. Thrimawithana and U. K. Madawala, "A generalized steady-state model for bidirectional IPT systems," *IEEE Trans. Power Electron.*, vol. 28, no. 10, pp. 4681–4689, Oct. 2013, doi: 10.1109/TPEL.2012.2237416.

[148] U. K. Madawala and D. J. Thrimawithana, "A bidirectional inductive power interface for electric vehicles in V2G systems," *IEEE Trans. Ind. Electron.*, vol. 58, no. 10, pp. 4789–4796, Oct. 2011, doi: 10.1109/TIE.2011.2114312.

[149] R. Mai, Y. Chen, Y. Li, Y. Zhang, G. Cao, and Z. He, "Inductive power transfer for massive electric bicycles charging based on hybrid topology switching with a single inverter," *IEEE Trans. Power Electron.*, vol. 32, no. 8, pp. 5897–5906, Aug. 2017, doi: 10.1109/TPEL.2017.2654360.

[150] Q. Zhu, Y. Guo, L. Wang, C. Liao, and F. Li, "Improving the misalignment tolerance of wireless charging system by optimizing the compensate capacitor," *IEEE Trans. Ind. Electron.*, vol. 62, no. 8, pp. 4832–4836, Aug. 2015, doi: 10.1109/TIE.2015.2397882.

[151] Y. Lim, H. Tang, S. Lim, and J. Park, "An adaptive impedance-matching network based on a novel capacitor matrix for wireless power transfer," *IEEE Trans. Power Electron.*, vol. 29, no. 8, pp. 4403–4413, Aug. 2014, doi: 10.1109/TPEL.2013.2292596.

[152] T. Kan, T.-D. Nguyen, J. C. White, R. K. Malhan, and C. C. Mi, "A new integration method for an electric vehicle wireless charging system using LCC compensation topology: Analysis and design," *IEEE Trans. Power Electron.*, vol. 32, no. 2, pp. 1638–1650, Feb. 2017, doi: 10.1109/TPEL.2016.2552060.

[153] Y. Chen, Z. Kou, Y. Zhang, Z. He, R. Mai, and G. Cao, "Hybrid topology with configurable charge current and charge voltage output-based WPT charger for massive electric bicycles," *IEEE J. Emerg. Sel. Topics Power Electron.*, vol. 6, no. 3, pp. 1581–1594, Sep. 2018, doi: 10.1109/JESTPE.2017.2782269.

[154] J. Deng, W. Li, T. D. Nguyen, S. Li, and C. C. Mi, "Compact and efficient bipolar coupler for wireless power chargers: Design and analysis," *IEEE Trans. Power Electron.*, vol. 30, no. 11, pp. 6130–6140, Nov. 2015, doi: 10.1109/TPEL.2015.2417115.

[155] W. Shi, J. Deng, Z. Wang, and X. Cheng, "The start-up dynamic analysis and one cycle control-PD control combined strategy for primary-side controlled wireless power transfer system," *IEEE Access*, vol. 6, pp. 14439–14450, 2018, doi: 10.1109/ACCESS.2018.2811179.

[156] Y. Li, Q. Xu, T. Lin, J. Hu, Z. He, and R. Mai, "Analysis and design of load-independent output current or output voltage of a three-coil wireless power transfer system," *IEEE Trans. Transport. Electrific.*, vol. 4, no. 2, pp. 364–375, Jun. 2018, doi: 10.1109/TTE.2018.2808698.

[157] L. Yang, X. Li, Z. Xu, S. Liu, Z. Dong, and Y. Wu, "Analysis and design of a high-efficiency three-coil WPT system with constant current output," *IET Electr. Power Appl.*, vol. 14, no. 10, pp. 1933–1943, Oct. 2020, doi: 10.1049/iet-epa.2019.0967.

[158] N. Hatchavanich, M. Konghirun, and A. Saengswang, "LCL—LCCL voltage source inverter with phase shift control for wireless EV charger," in *Proc. IEEE 12th Int. Conf. Power Electron. Drive Syst. (PEDS)*, Dec. 2017, pp. 297–301, doi: 10.1109/PEDS.2017.8289137.

[159] W. Li, H. Zhao, J. Deng, S. Li, and C. C. Mi, "Comparison study on SS and double-sided LCC compensation topologies for EV/PHEV wireless chargers," *IEEE Trans. Veh. Technol.*, vol. 65, no. 6, pp. 4429–4439, Jun. 2016, doi: 10.1109/TVT.2015.2479938.

[160] J. Hou, Q. Chen, K. Yan, X. Ren, S.-C. Wong, and C. K. Tse, "Analysis and control of S/SP compensation contactless resonant converter with constant voltage gain," in *Proc. IEEE Energy Convers. Congr. Expo.*, Sep. 2013, pp. 2552–2558, doi: 10.1109/ECCE.2013.6647030.
[161] J. Hou, Q. Chen, X. Ren, X. Ruan, S.-C. Wong, and C. K. Tse, "Precise characteristics analysis of series/series-parallel compensated contactless resonant converter," *IEEE J. Emerg. Sel. Topics Power Electron.*, vol. 3, no. 1, pp. 101–110, Mar. 2015, doi: 10.1109/JESTPE.2014.2320524.
[162] Z. Xu, L. Yang, X. Li, S. Liu, Z. Dong, and Y. Wu, "Analysis and design of a S/PS compensated IPT system with constant current output," *IET Electr. Power Appl.*, vol. 14, no. 14, pp. 2739–2749, Dec. 2020, doi: 10.1049/iet-epa.2020.0626.
[163] G. Rituraj, E. R. Joy, B. K. Kushwaha, and P. Kumar, "Analysis and comparison of series–series and series-parallel topology of contactless power transfer systems," in *Proc. IEEE Region 10 Conf. (TENCON)*, Oct. 2014, pp. 1–6, doi: 10.1109/TENCON.2014.7022440.
[164] A. Ridge, K. K. Ahamad, R. McMahon, and J. Miles, "Development of a 50 kW wireless power transfer system," in *Proc. IEEE PELS Workshop Emerg. Technol., Wireless Power Transf. (WoW)*, Jun. 2019, pp. 406–409, doi: 10.1109/WoW45936.2019.9030672.
[165] A. Sagar, A. Kumar, M. Bertoluzzo, and R. K. Jha, "Analysis and design of a two-winding wireless power transfer system with higher system efficiency and maximum load power," in *Proc. 48th Annu. Conf. IEEE Ind. Electron. Soc. (IECON)*, Oct. 2022, pp. 1–6, doi: 10.1109/IECON49645.2022.9968858.
[166] R. Singh, P. Sanjeevikumar, D. S. Kumar, M. Molinas, and F. Blaabjerg, Eds., *Cable Based and Wireless Charging Systems for Electric Vehicles: Technology and Control, Management and Grid Integration*. Edison, NJ, USA: Institution of Engineering and Technology, 2021, doi: 10.1049/PBTR032E.
[167] G. R. Nagendra, G. A. Covic, and J. T. Boys, "Sizing of inductive power pads for dynamic charging of EVs on IPT highways," *IEEE Trans. Transport. Electrific.*, vol. 3, no. 2, pp. 405–417, Jun. 2017, doi: 10.1109/TTE.2017.2666554.
[168] H. Feng, T. Cai, S. Duan, J. Zhao, X. Zhang, and C. Chen, "An LCC-compensated resonant converter optimized for robust reaction to large coupling variation in dynamic wireless power transfer," *IEEE Trans. Ind. Electron.*, vol. 63, no. 10, pp. 6591–6601, Oct. 2016, doi: 10.1109/TIE.2016.2589922.
[169] A. Kamineni, M. J. Neath, A. Zaheer, G. A. Covic, and J. T. Boys, "Interoperable EV detection for dynamic wireless charging with existing hardware and free resonance," *IEEE Trans. Transport. Electrific.*, vol. 3, no. 2, pp. 370–379, Jun. 2017, doi: 10.1109/TTE.2016.2631607.
[170] F. Lu, H. Zhang, H. Hofmann, and C. C. Mi, "A dynamic charging system with reduced output power pulsation for electric vehicles," *IEEE Trans. Ind. Electron.*, vol. 63, no. 10, pp. 6580–6590, Oct. 2016, doi: 10.1109/TIE.2016.2563380.
[171] L. Zhao, D. J. Thrimawithana, U. K. Madawala, A. P. Hu, and C. C. Mi, "A misalignment-tolerant series-hybrid wireless EV charging system with integrated magnetics," *IEEE Trans. Power Electron.*, vol. 34, no. 2, pp. 1276–1285, Feb. 2019, doi: 10.1109/TPEL.2018.2828841.
[172] L. Chen, G. R. Nagendra, J. T. Boys, and G. A. Covic, "Double-coupled systems for IPT roadway applications," *IEEE J. Emerg. Sel. Topics Power Electron.*, vol. 3, no. 1, pp. 37–49, Mar. 2015.
[173] G. A. Covic, J. T. Boys, M. L. G. Kissin, and H. G. Lu, "A three-phase inductive power transfer system for roadway-powered vehicles," *IEEE Trans. Ind. Electron.*, vol. 54, no. 6, pp. 3370–3378, Dec. 2007.
[174] M. L. G. Kissin, J. T. Boys, and G. A. Covic, "Interphase mutual inductance in polyphase inductive power transfer systems," *IEEE Trans. Ind. Electron.*, vol. 56, no. 7, pp. 2393–2400, Jul. 2009.
[175] M. L. G. Kissin, H. Hao, and G. A. Covic, "A practical multiphase IPT system for AGV and roadway applications," in *Proc. IEEE Energy Convers. Congr. Expo.*, Atlanta, GA, USA, Sep. 2010, pp. 1844–1850.
[176] M. L. G. Kissin, G. A. Covic, and J. T. Boys, "Steady-state flat-pickup loading effects in polyphase inductive power transfer systems," *IEEE Trans. Ind. Electron.*, vol. 58, no. 6, pp. 2274–2282, Jun. 2011.
[177] Z. Dang and J. A. A. Qahouq, "Modeling and investigation of magnetic resonance coupled wireless power transfer system with lateral misalignment," in *Proc. IEEE Appl. Power Electron. Conf. Expo. (APEC)*, Fort Worth, TX, USA, Mar. 2014, pp. 1317–1322.
[178] Z. Dang and J. A. A. Qahouq, "Elimination method for the transmission efficiency valley of death in laterally misaligned wireless power transfer systems," in *Proc. IEEE Appl. Power Electron. Conf. Expo. (APEC)*, Charlotte, NC, USA, Mar. 2015, pp. 1644–1649.
[179] S. G. Lee, H. Hoang, Y. H. Choi, and F. Bien, "Efficiency improvement for magnetic resonance based wireless power transfer with axial-misalignment," *Electron. Lett.*, vol. 48, no. 6, pp. 339–340, Mar. 2012.
[180] K. Fotopoulou and B. W. Flynn, "Wireless power transfer in loosely coupled links: Coil misalignment model," *IEEE Trans. Magn.*, vol. 47, no. 2, pp. 416–430, Feb. 2011.
[181] D. Patil, M. Sirico, L. Gu, and B. Fahimi, "Maximum efficiency tracking in wireless power transfer for battery charger: Phase shift and frequency control," in *Proc. IEEE Energy Convers. Congr. Expo. (ECCE)*, Milwaukee, WI, USA, Sep. 2016, pp. 1–8.
[182] R. Jegadeesan and Y. X. Guo, "A study on the inductive power links for implantable biomedical devices," in *Proc. IEEE Antennas Propag. Soc. Int. Symp.*, Jul. 2010, pp. 1–4, doi: 10.1109/APS.2010.5562122.
[183] Y.-X. Guo, D. Zhu, and R. Jegadeesan, "Inductive wireless power transmission for implantable devices," in *Proc. Int. Workshop Antenna Technol. (iWAT)*, Mar. 2011, pp. 445–448, doi: 10.1109/IWAT.2011.5752354.
[184] M. J. Karimi, A. Schmid, and C. Dehollain, "Wireless power and data transmission for implanted devices via inductive links: A systematic review," *IEEE Sensors J.*, vol. 21, no. 6, pp. 7145–7161, Mar. 2021, doi: 10.1109/JSEN.2021.3049918.
[185] M. Haerinia and R. Shadid, "Wireless power transfer approaches for medical implants: A review," *Signals*, vol. 1, no. 2, pp. 209–229, Dec. 2020, doi: 10.3390/signals1020012.
[186] M. Rehman, P. Nallagownden, and Z. Baharudin, "Efficiency investigation of SS and SP compensation topologies for wireless power transfer," *Int. J. Power Electron. Drive Syst.*, vol. 10, no. 4, p. 2157, Dec. 2019, doi: 10.11591/ijpeds.v10.i4.pp2157-2164.
[187] D. Ahn and S. Hong, "Wireless power transmission with self-regulated output voltage for biomedical implant," *IEEE Trans. Ind. Electron.*, vol. 61, no. 5, pp. 2225–2235, May 2014, doi: 10.1109/TIE.2013.2273472.
[188] T. Campi, S. Cruciani, F. Maradei, and M. Feliziani, "Near-field reduction in a wireless power transfer system using LCC compensation," *IEEE Trans. Electromagn. Compat.*, vol. 59, no. 2, pp. 686–694, Apr. 2017, doi: 10.1109/TEMC.2016.2641383.
[189] S. Cui, Z. Z. Liu, Y. J. Hou, H. Zeng, Z. K. Yue, and L. H. Liang, "Study on efficiency of different topologies of magnetic coupled resonant wireless charging system," *IOP Conf. Ser., Earth Environ. Sci.*, vol. 93, Nov. 2017, Art. no. 012064, doi: 10.1088/1755-1315/93/1/012064.
[190] A. Vulfovich, D. Baimel, and A. Kuperman, "Modified first harmonic approximation-based modeling of SN-compensated inductive power transfer links operating at load-independent-voltage-output frequency," *Simul. Model. Pract. Theory*, vol. 111, Sep. 2021, Art. no. 102340, doi: 10.1016/j.simpat.2021.102340.
[191] M. Borage, S. Tiwari, and S. Kotaiah, "Analysis and design of an LCL-T resonant converter as a constant-current power supply," *IEEE Trans. Ind. Electron.*, vol. 52, no. 6, pp. 1547–1554, Dec. 2005, doi: 10.1109/TIE.2005.858729.
[192] C. Liu, S. Ge, Y. Guo, H. Li, and G. Cai, "Double-LCL resonant compensation network for electric vehicles wireless power transfer: Experimental study and analysis," *IET Power Electron.*, vol. 9, no. 11, pp. 2262–2270, Sep. 2016, doi: 10.1049/iet-pel.2015.0186.
[193] C. Liu, Y. Guo, S. Ge, G. Cai, and F. Zhou, "Characteristics analysis and experimental verification of the double LCL resonant compensation network for electrical vehicles wireless power transfer," *Diangong Jishu Xuebao/Trans. China Electrotech. Soc.*, vol. 30, no. 15, pp. 127–135, 2015.
[194] Y. Zhang, Z. Yan, Z. Liang, S. Li, and C. C. Mi, "A high-power wireless charging system using LCL-N topology to achieve a compact and low-cost receiver," *IEEE Trans. Power Electron.*, vol. 35, no. 1, pp. 131–137, Jan. 2020, doi: 10.1109/TPEL.2019.2914363.
[195] D. Baimel, M. Mellincovsky, M. Sitbon, Y. Darhovsky, and A. Kuperman, "Modeling and analysis of none-series compensation for inductive wireless power transfer links," in *Proc. IEEE 29th Int. Symp. Ind. Electron. (ISIE)*, Jun. 2020, pp. 1623–1627, doi: 10.1109/ISIE45063.2020.9152534.
[196] A. Vulfovich, S. Kolesnik, D. Baimel, E. Cohen, M. Gutman, A. Geftler, and A. Kuperman, "Output characteristics of none-series compensated inductive wireless power transfer link operating at load-independent-voltage-output frequency," *Simul. Model. Pract. Theory*, vol. 115, Feb. 2022, Art. no. 102424, doi: 10.1016/j.simpat.2021.102424.

[197] K. Song, Z. Li, J. Jiang, and C. Zhu, "Constant current/voltage charging operation for series–series and series–parallel compensated wireless power transfer systems employing primary-side controller," *IEEE Trans. Power Electron.*, vol. 33, no. 9, pp. 8065–8080, Sep. 2018, doi: 10.1109/TPEL.2017.2767099.

[198] B. H. Choi, E. S. Lee, J. H. Kim, and C. T. Rim, "7m-off-long-distance extremely loosely coupled inductive power transfer systems using dipole coils," in *Proc. IEEE Energy Convers. Congr. Expo. (ECCE)*, Sep. 2014, pp. 858–563, doi: 10.1109/ECCE.2014.6953487.

[199] Z. Huang, S.-C. Wong, and C. K. Tse, "Comparison of basic inductive power transfer systems with linear control achieving optimized efficiency," *IEEE Trans. Power Electron.*, vol. 35, no. 3, pp. 3276–3286, Mar. 2020, doi: 10.1109/TPEL.2019.2932100.

[200] Y. Zhang, S. Chen, X. Li, Z. She, F. Zhang, and Y. Tang, "Coil comparison and downscaling principles of inductive wireless power transfer systems," in *Proc. IEEE PELS WoW*, Nov. 2020, pp. 116–122.

[201] K. Song, G. Yang, Y. Guo, Y. Lan, S. Dong, J. Jiang, and C. Zhu, "Design of DD coil with high misalignment tolerance and low EMF emissions for wireless electric vehicle charging systems," *IEEE Trans. Power Electron.*, vol. 35, no. 9, pp. 9034–9045, Sep. 2020.

[202] J. Mai, Y. Wang, Y. Yao, M. Sun, and D. Xu, "High-misalignment-tolerant IPT systems with solenoid and double D pads," *IEEE Trans. Ind. Electron.*, vol. 69, no. 4, pp. 3527–3535, Apr. 2022.

[203] Y. Zhang, S. Chen, X. Li, and Y. Tang, "Design methodology of free-positioning nonoverlapping wireless charging for consumer electronics based on antiparallel windings," *IEEE Trans. Ind. Electron.*, vol. 69, no. 1, pp. 825–834, Jan. 2022.

[204] W.-S. Lee, W.-I. Son, K.-S. Oh, and J.-W. Yu, "Contactless energy transfer systems using antiparallel resonant loops," *IEEE Trans. Ind. Electron.*, vol. 60, no. 1, pp. 350–359, Jan. 2013.

[205] W. Zhao, X. Qu, J. Lian, and C. K. Tse, "A family of hybrid IPT couplers with high tolerance to pad misalignment," *IEEE Trans. Power Electron.*, vol. 37, no. 3, pp. 3617–3625, Mar. 2022.

[206] Y. Chen, B. Yang, X. Zhou, Q. Li, Z. He, R. Mai, and J.-S. Lai, "A hybrid inductive power transfer system with misalignment tolerance using quadruple-D quadrature pads," *IEEE Trans. Power Electron.*, vol. 35, no. 6, pp. 6039–6049, Jun. 2020.

[207] L. Zhao, D. J. Thrimawithana, and U. K. Madawala, "Hybrid bidirectional wireless EV charging system tolerant to pad misalignment," *IEEE Trans. Ind. Electron.*, vol. 64, no. 9, pp. 7079–7086, Sep. 2017.

[208] C. Xia, W. Wang, S. Ren, X. Wu, and Y. Sun, "Robust control for inductively coupled power transfer systems with coil misalignment," *IEEE Trans. Power Electron.*, vol. 33, no. 9, pp. 8110–8122, Sep. 2018.

[209] T.-S. Lee, S.-J. Huang, S.-H. Dai, and J.-L. Su, "Design of misalignment-insensitive inductive power transfer via interoperable coil module and dynamic power control," *IEEE Trans. Power Electron.*, vol. 35, no. 9, pp. 9024–9033, Sep. 2020.

[210] F. P. Wijaya, T. Shimotsu, T. Saito, and K. Kondo, "A simple active power control for a high-power wireless power transmission system considering coil misalignment and its design method," *IEEE Trans. Power Electron.*, vol. 33, no. 11, pp. 9989–10002, Nov. 2018.

[211] Y. Zhang, W. Pan, H. Wang, Z. Shen, Y. Wu, J. Dong, and X. Mao, "Misalignment-tolerant dual-transmitter electric vehicle wireless charging system with reconfigurable topologies," *IEEE Trans. Power Electron.*, vol. 37, no. 8, pp. 8816–8819, Aug. 2022, doi: 10.1109/TPEL.2022.3160868.

[212] R. Mai, B. Yang, Y. Chen, N. Yang, Z. He, and S. Gao, "A misalignment tolerant IPT system with intermediate coils for constant-current output," *IEEE Trans. Power Electron.*, vol. 34, no. 8, pp. 7151–7155, Aug. 2019.

[213] Z. Liu, M. Su, Q. Zhu, L. Zhao, and A. P. Hu, "A dual frequency tuning method for improved coupling tolerance of wireless power transfer system," *IEEE Trans. Power Electron.*, vol. 36, no. 7, pp. 7360–7365, Jul. 2021.

[214] W. Xiong, Q. Yu, Z. Liu, Q. Zhu, M. Su, L. Zhao, and A. P. Hu, "A dual-frequency-detuning method for improving the coupling tolerance of wireless power transfer," *IEEE Trans. Power Electron.*, vol. 38, no. 6, pp. 6923–6928, Jun. 2023, doi: 10.1109/TPEL.2023.3253904.

[215] W. Zhong, S. Zhang, M. Chen, and M. D. Xu, "Reconfigurable resonant topology linking two-, three-, and four-coil modes for WPT with large coupling range and fixed frequency," *IEEE Trans. Power Electron.*, vol. 37, no. 7, pp. 8713–8725, Jul. 2022, doi: 10.1109/TPEL.2022.3148001.

[216] A. Hossain, P. Darvish, S. Mekhilef, K. S. Tey, and C. W. Tong, "A new coil structure of dual transmitters and dual receivers with integrated decoupling coils for increasing power transfer and misalignment tolerance of wireless EV charging system," *IEEE Trans. Ind. Electron.*, vol. 69, no. 8, pp. 7869–7878, Aug. 2022.

[217] P. Darvish, S. Mekhilef, and H. A. B. Illias, "A novel S–S–*LCLCC* compensation for three-coil WPT to improve misalignment and energy efficiency stiffness of wireless charging system," *IEEE Trans. Power Electron.*, vol. 36, no. 2, pp. 1341–1355, Feb. 2021.

[218] Y. Chen, S. He, B. Yang, S. Chen, Z. He, and R. Mai, "Reconfigurable rectifier-based detuned series–series compensated IPT system for anti-misalignment and efficiency improvement," *IEEE Trans. Power Electron.*, vol. 38, no. 2, pp. 2720–2729, Feb. 2023, doi: 10.1109/TPEL.2022.3204592.

[219] Y. Zhang, Z. Shen, C. Liu, X. Mao, Y. Zhuang, S. Chen, and Y. Tang, "A quadrupole receiving coil with series-connected diode rectifiers for interoperability of nonpolarized and polarized transmitting coils," *IEEE Trans. Power Electron.*, vol. 38, no. 7, pp. 8000–8004, Jul. 2023, doi: 10.1109/TPEL.2023.3264295.

[220] Y. Zhang, T. Kan, Z. Yan, and C. C. Mi, "Frequency and voltage tuning of series–series compensated wireless power transfer system to sustain rated power under various conditions," *IEEE J. Emerg. Sel. Topics Power Electron.*, vol. 7, no. 2, pp. 1311–1317, Jun. 2019, doi: 10.1109/JESTPE.2018.2871636.

[221] P. Si, A. P. Hu, S. Malpas, and D. Budgett, "A frequency control method for regulating wireless power to implantable devices," *IEEE Trans. Biomed. Circuits Syst.*, vol. 2, no. 1, pp. 22–29, Mar. 2008, doi: 10.1109/TBCAS.2008.918284.

[222] Y. Zhang and Z. Zhao, "Frequency splitting analysis of two-coil resonant wireless power transfer," *IEEE Antennas Wireless Propag. Lett.*, vol. 13, pp. 400–402, 2014, doi: 10.1109/LAWP.2014.2307924.

[223] K. Hata, T. Imura, and Y. Hori, "Dynamic wireless power transfer system for electric vehicles to simplify ground facilities—Power control and efficiency maximization on the secondary side," in *Proc. IEEE Appl. Power Electron. Conf. Expo. (APEC)*, Mar. 2016, pp. 1731–1736, doi: 10.1109/APEC.2016.7468101.

[224] C.-C. Huang, C.-L. Lin, and Y.-K. Wu, "Simultaneous wireless power/data transfer for electric vehicle charging," *IEEE Trans. Ind. Electron.*, vol. 64, no. 1, pp. 682–690, Jan. 2017, doi: 10.1109/TIE.2016.2608765.

[225] S. Aldhaher, P. C. Luk, and J. F. Whidborne, "Electronic tuning of misaligned coils in wireless power transfer systems," *IEEE Trans. Power Electron.*, vol. 29, no. 11, pp. 5975–5982, Nov. 2014, doi: 10.1109/TPEL.2014.2297993.

[226] Z. Huang, S.-C. Wong, and C. K. Tse, "Control design for optimizing efficiency in inductive power transfer systems," *IEEE Trans. Power Electron.*, vol. 33, no. 5, pp. 4523–4534, May 2018, doi: 10.1109/TPEL.2017.2724039.

[227] A. Smagulova, M. Lu, A. Darabi, and M. Bagheri, "Simulation analysis of PI and fuzzy controller for dynamic wireless charging of electric vehicle," in *Proc. IEEE Int. Conf. Environ. Electr. Eng. IEEE Ind. Commercial Power Syst. Eur. (EEEIC/ICPS Europe)*, Jun. 2020, pp. 1–6, doi: 10.1109/EEEIC/ICPSEurope49358.2020.9160851.

[228] H. H. Wu, A. Gilchrist, K. D. Sealy, and D. Bronson, "A high efficiency 5 kW inductive charger for EVs using dual side control," *IEEE Trans. Ind. Informat.*, vol. 8, no. 3, pp. 585–595, Aug. 2012, doi: 10.1109/TII.2012.2192283.

[229] H. Li, J. Li, K. Wang, W. Chen, and X. Yang, "A maximum efficiency point tracking control scheme for wireless power transfer systems using magnetic resonant coupling," *IEEE Trans. Power Electron.*, vol. 30, no. 7, pp. 3998–4008, Jul. 2015, doi: 10.1109/TPEL.2014.2349534.

[230] X. Zhang, T. Cai, S. Duan, H. Feng, H. Hu, J. Niu, and C. Chen, "A control strategy for efficiency optimization and wide ZVS operation range in bidirectional inductive power transfer system," *IEEE Trans. Ind. Electron.*, vol. 66, no. 8, pp. 5958–5969, Aug. 2019, doi: 10.1109/TIE.2018.2871794.

[231] H. Chen, C. Chen, M. Jiang, S. Jia, and X. Huang, "Dual-side three-stage asymmetric phase shift strategy for bidirectional inductive power transfer system with SiC power module," in *Proc. IEEE Workshop Wide Bandgap Power Devices Appl. Asia (WiPDA Asia)*, Aug. 2021, pp. 459–461, doi: 10.1109/WiPDAAsia51810.2021.9656027.

[232] Y. Liu, U. K. Madawala, R. Mai, and Z. He, "An optimal multivariable control strategy for inductive power transfer systems to improve efficiency," *IEEE Trans. Power Electron.*, vol. 35, no. 9, pp. 8998–9010, Sep. 2020, doi: 10.1109/TPEL.2020.2970780.

[233] F. Xu, S.-C. Wong, and C. K. Tse, "Overall loss compensation and optimization control in single-stage inductive power transfer converter delivering constant power," *IEEE Trans. Power Electron.*, vol. 37, no. 1, pp. 1146–1158, Jan. 2022, doi: 10.1109/TPEL.2021.3098914.

[234] S. Chen, H. Li, and Y. Tang, "A burst mode pulse density modulation scheme for inductive power transfer systems without communication modules," in *Proc. IEEE Appl. Power Electron. Conf. Expo. (APEC)*, Mar. 2018, pp. 1071–1075, doi: 10.1109/APEC.2018.8341148.

[235] G. Guidi and J. A. Suul, "Minimizing converter requirements of inductive power transfer systems with constant voltage load and variable coupling conditions," *IEEE Trans. Ind. Electron.*, vol. 63, no. 11, pp. 6835–6844, Nov. 2016, doi: 10.1109/TIE.2016.2582459.

[236] A. C. Bagchi, A. Kamineni, R. A. Zane, and R. Carlson, "Review and comparative analysis of topologies and control methods in dynamic wireless charging of electric vehicles," *IEEE J. Emerg. Sel. Topics Power Electron.*, vol. 9, no. 4, pp. 4947–4962, Aug. 2021, doi: 10.1109/JESTPE.2021.3058968.

[237] Y. Zhang, S. Chen, X. Li, and Y. Tang, "Design of high-power static wireless power transfer via magnetic induction: An overview," *CPSS Trans. Power Electron. Appl.*, vol. 6, no. 4, pp. 281–297, Dec. 2021, doi: 10.24295/CPSSTPEA.2021.00027.

[238] G. de Freitas Lima and R. B. Godoy, "Modeling and prototype of a dynamic wireless charging system using LSPS compensation topology," *IEEE Trans. Ind. Appl.*, vol. 55, no. 1, pp. 786–793, Jan. 2019, doi: 10.1109/TIA.2018.2871035.

[239] V.-B. Vu, M. Dahidah, V. Pickert, and V.-T. Phan, "A high-power multiphase wireless dynamic charging system with low output power pulsation for electric vehicles," *IEEE J. Emerg. Sel. Topics Power Electron.*, vol. 8, no. 4, pp. 3592–3608, Dec. 2020, doi: 10.1109/JESTPE.2019.2932302.

[240] J. M. Arteaga, S. Aldhaher, G. Kkelis, D. C. Yates, and P. D. Mitcheson, "Multi-MHz IPT systems for variable coupling," *IEEE Trans. Power Electron.*, vol. 33, no. 9, pp. 7744–7758, Sep. 2018, doi: 10.1109/TPEL.2017.2768244.

[241] A. Kumar, M. Bertoluzzo, R. K. Jha, and A. Sagar, "Analysis of losses in two different control approaches for S-S wireless power transfer systems for electric vehicle," *Energies*, vol. 16, no. 4, p. 1795, Feb. 2023, doi: 10.3390/EN16041795.

[242] Z. Huang, C.-S. Lam, P.-I. Mak, R. P. D. S. Martins, S.-C. Wong, and C. K. Tse, "A single-stage inductive-power-transfer converter for constant-power and maximum-efficiency battery charging," *IEEE Trans. Power Electron.*, vol. 35, no. 9, pp. 8973–8984, Sep. 2020, doi: 10.1109/TPEL.2020.2969685.

[243] M. Turzyński, S. Bachman, M. Jasiński, S. Piasecki, M. Ryłko, H.-J. Chiu, S.-H. Kuo, and Y.-C. Chang, "Analytical estimation of power losses in a dual active bridge converter controlled with a single-phase shift switching scheme," *Energies*, vol. 15, no. 21, p. 8262, Nov. 2022, doi: 10.3390/EN15218262.

[244] A. N. Azad, A. Echols, V. A. Kulyukin, R. Zane, and Z. Pantic, "Analysis, optimization, and demonstration of a vehicular detection system intended for dynamic wireless charging applications," *IEEE Trans. Transport. Electrific.*, vol. 5, no. 1, pp. 147–161, Mar. 2019, doi: 10.1109/TTE.2018.2870339.

[245] D. Patil, J. M. Miller, B. Fahimi, P. T. Balsara, and V. Galigekere, "A coil detection system for dynamic wireless charging of electric vehicle," *IEEE Trans. Transport. Electrific.*, vol. 5, no. 4, pp. 988–1003, Dec. 2019, doi: 10.1109/TTE.2019.2905981.

[246] Y. Huang, C. Liu, Y. Zhou, Y. Xiao, and S. Liu, "Power allocation for dynamic dual-pickup wireless charging system of electric vehicle," *IEEE Trans. Magn.*, vol. 55, no. 7, pp. 1–6, Jul. 2019, doi: 10.1109/TMAG.2019.2894163.

[247] L. Xiang, X. Li, J. Tian, and Y. Tian, "A crossed DD geometry and its double-coil excitation method for electric vehicle dynamic wireless charging systems," *IEEE Access*, vol. 6, pp. 45120–45128, 2018, doi: 10.1109/ACCESS.2018.2864999.

[248] S. Y. Choi, S. Y. Jeong, B. W. Gu, G. C. Lim, and C. T. Rim, "Ultraslim S-type power supply rails for roadway-powered electric vehicles," *IEEE Trans. Power Electron.*, vol. 30, no. 11, pp. 6456–6468, Nov. 2015, doi: 10.1109/TPEL.2015.2444894.

[249] A. Kamineni, M. J. Neath, G. A. Covic, and J. T. Boys, "A mistuning-tolerant and controllable power supply for roadway wireless power systems," *IEEE Trans. Power Electron.*, vol. 32, no. 9, pp. 6689–6699, Sep. 2017, doi: 10.1109/TPEL.2016.2622300.

[250] R. Tavakoli and Z. Pantic, "Analysis, design, and demonstration of a 25-kW dynamic wireless charging system for roadway electric vehicles," *IEEE J. Emerg. Sel. Topics Power Electron.*, vol. 6, no. 3, pp. 1378–1393, Sep. 2018, doi: 10.1109/JESTPE.2017.2761763.

[251] S. Wang, J. Chen, Z. Hu, C. Rong, and M. Liu, "Optimisation design for series–series dynamic WPT system maintaining stable transfer power," *IET Power Electron.*, vol. 10, no. 9, pp. 987–995, Jul. 2017, doi: 10.1049/iet-pel.2016.0839.

[252] A. C. Bagchi, A. Kamineni, R. Zane, and R. B. Carlson, "Comparative analysis of DWPT topologies and regulation schemes for improved controllability," in *Proc. IEEE Energy Convers. Congr. Expo. (ECCE)*, Oct. 2020, pp. 5199–5206, doi: 10.1109/ECCE44975.2020.9235424.

[253] X. Dai, J.-C. Jiang, and J.-Q. Wu, "Charging area determining and power enhancement method for multiexcitation unit configuration of wirelessly dynamic charging EV system," *IEEE Trans. Ind. Electron.*, vol. 66, no. 5, pp. 4086–4096, May 2019, doi: 10.1109/TIE.2018.2860537.

[254] A. Babaki, S. Vaez-Zadeh, and A. Zakerian, "Performance optimization of dynamic wireless EV charger under varying driving conditions without resonant information," *IEEE Trans. Veh. Technol.*, vol. 68, no. 11, pp. 10429–10438, Nov. 2019, doi: 10.1109/TVT.2019.2944153.

[255] S. Zhou and C. C. Mi, "Multi-paralleled LCC reactive power compensation networks and their tuning method for electric vehicle dynamic wireless charging," *IEEE Trans. Ind. Electron.*, vol. 63, no. 10, pp. 6546–6556, Oct. 2016, doi: 10.1109/TIE.2015.2512236.

[256] S. Y. Jeong, J. H. Park, G. P. Hong, and C. T. Rim, "Autotuning control system by variation of self-inductance for dynamic wireless EV charging with small air gap," *IEEE Trans. Power Electron.*, vol. 34, no. 6, pp. 5165–5174, Jun. 2019, doi: 10.1109/TPEL.2018.2866412.

[257] J. Liu, Z. Liu, W. Chen, X. Sun, and H. Su, "An optimized coil array and passivity-based control for receiving side multilevel connected DC–DC converter of dynamic wireless charging," *IEEE Trans. Veh. Technol.*, vol. 71, no. 4, pp. 3715–3726, Apr. 2022, doi: 10.1109/TVT.2022.3146636.

[258] A. Ong, P. K. S. Jayathuathnage, J. H. Cheong, and W. L. Goh, "Transmitter pulsation control for dynamic wireless power transfer systems," *IEEE Trans. Transport. Electrific.*, vol. 3, no. 2, pp. 418–426, Jun. 2017, doi: 10.1109/TTE.2017.2703173.

[259] Y. Guo, L. Wang, Q. Zhu, C. Liao, and F. Li, "Switch-on modeling and analysis of dynamic wireless charging system used for electric vehicles," *IEEE Trans. Ind. Electron.*, vol. 63, no. 10, pp. 6568–6579, Oct. 2016, doi: 10.1109/TIE.2016.2557302.

[260] F. Farajizadeh, D. M. Vilathgamuwa, D. Jovanovic, P. Jayathurathnage, G. Ledwich, and U. Madawala, "Expandable N-legged converter to drive closely spaced multitransmitter wireless power transfer systems for dynamic charging," *IEEE Trans. Power Electron.*, vol. 35, no. 4, pp. 3794–3806, Apr. 2020, doi: 10.1109/TPEL.2019.2939848.

[261] Y. Shin, K. Hwang, J. Park, D. Kim, and S. Ahn, "Precise vehicle location detection method using a wireless power transfer (WPT) system," *IEEE Trans. Veh. Technol.*, vol. 68, no. 2, pp. 1167–1177, Feb. 2019, doi: 10.1109/TVT.2018.2885942.

[262] X. Liu, C. Liu, and P. W. T. Pong, "TMR-sensor-array-based misalignment-tolerant wireless charging technique for roadway electric vehicles," *IEEE Trans. Magn.*, vol. 55, no. 7, pp. 1–7, Jul. 2019, doi: 10.1109/TMAG.2019.2903895.

[263] A. Brecher and D. Arthur, "Review and evaluation of wireless power transfer (WPT) for electric transit applications," FTA Res., Washington, DC, USA, FTA Rep. 0060, 2014.

[264] *Product Overview Inductive Power Transfer—IPT*, Conductix-Wampfler, Germany, 2005. [Online]. Available: https://www.conductix.com/sites/default/files/downloads/KAT9000-0001-E_Product_Overview_IPT.pdf

[265] Z. Bi, T. Kan, C. C. Mi, Y. Zhang, Z. Zhao, and G. A. Keoleian, "A review of wireless power transfer for electric vehicles: Prospects to enhance sustainable mobility," *Appl. Energy*, vol. 179, pp. 413–425, Oct. 2016, doi: 10.1016/j.apenergy.2016.07.003.

[266] M. Amjad, M. Farooq-i-Azam, Q. Ni, M. Dong, and E. A. Ansari, "Wireless charging systems for electric vehicles," *Renew. Sustain. Energy Rev.*, vol. 167, Oct. 2022, Art. no. 112730, doi: 10.1016/J.RSER.2022.112730.

[267] H. Feng, R. Tavakoli, O. C. Onar, and Z. Pantic, "Advances in high-power wireless charging systems: Overview and design considerations," *IEEE Trans. Transport. Electrific.*, vol. 6, no. 3, pp. 886–919, Sep. 2020, doi: 10.1109/TTE.2020.3012543.

[268] D. H. Cho, G. H. Jung, U. Yoon, and B. Lee, "Development & implementation of electric tram system with wireless charging technology," *ICT Exp.*, vol. 1, no. 1, pp. 34–38, 2015, doi: 10.1016/S2405-9595(15)30019-9.

[269] S.-H. Lee, B.-S. Lee, and J.-H. Lee, "A new design methodology for a 300-kW, low flux density, large air gap, online wireless power transfer system," *IEEE Trans. Ind. Appl.*, vol. 52, no. 5, pp. 4234–4242, Sep. 2016, doi: 10.1109/TIA.2016.2583407.

[270] J. R. Bailey and M. E. Hairr, "Wayside charging and hydrogen hybrid bus: Extending the range of electric shuttle buses," Center Energy, Univ. Tennessee Chattanooga, Chattanooga, TN, USA, Tech. Rep. 0028, Sep. 2012, doi: 10.21949/1503565.

[271] R. Bosshard and J. W. Kolar, "Multi-objective optimization of 50 kW/85 kHz IPT system for public transport," *IEEE J. Emerg. Sel. Topics Power Electron.*, vol. 4, no. 4, pp. 1370–1382, Dec. 2016, doi: 10.1109/JESTPE.2016.2598755.

[272] W. Shi, J. Dong, T. B. Soeiro, C. Riekerk, F. Grazian, G. Yu, and P. Bauer, "Design of a highly efficient 20-kW inductive power transfer system with improved misalignment performance," *IEEE Trans. Transport. Electrific.*, vol. 8, no. 2, pp. 2384–2399, Jun. 2022, doi: 10.1109/TTE.2021.3133759.

[273] K. Kusaka, R. Kusui, J.-I. Itoh, D. Sato, S. Obayashi, and M. Ishida, "A 22 kW-85 kHz three-phase wireless power transfer system with 12 coils," in *Proc. IEEE Energy Convers. Congr. Expo. (ECCE)*, Sep. 2019, pp. 3340–3347, doi: 10.1109/ECCE.2019.8913006.

[274] Q. Deng, P. Sun, W. Hu, D. Czarkowski, M. K. Kazimierczuk, and H. Zhou, "Modular parallel multi-inverter system for high-power inductive power transfer," *IEEE Trans. Power Electron.*, vol. 34, no. 10, pp. 9422–9434, Oct. 2019, doi: 10.1109/TPEL.2019.2891064.

[275] T. Shijo, K. Ogawa, M. Suzuki, Y. Kanekiyo, M. Ishida, and S. Obayashi, "EMI reduction technology in 85 kHz band 44 kW wireless power transfer system for rapid contactless charging of electric bus," in *Proc. IEEE Energy Convers. Congr. Expo. (ECCE)*, Sep. 2016, pp. 1–6, doi: 10.1109/ECCE.2016.7855077.

[276] S. Obayashi, T. Shijo, M. Suzuki, F. Moritsuka, K. Ogawa, K. Ogura, Y. Kanekiyo, M. Ishida, T. Takanaka, N. Tada, F. Takeuchi, S. Take, Y. Yamauchi, W.-H. Yang, and Y. Kamiya, "85 kHz band 44 kW wireless rapid charging system for field test and public road operation of electric bus," *World Electr. Vehicle J.*, vol. 10, no. 2, p. 26, May 2019, doi: 10.3390/wevj10020026.

[277] *INTIS—Integrated Infrastructure Solutions*. Accessed: Mar. 28, 2023. [Online]. Available: https://intis.de/wireless-power-transfer.html

[278] J. Pries, V. P. Galigekere, O. C. Onar, G.-J. Su, R. Wiles, L. Seiber, J. Wilkins, S. Anwar, and S. Zou, "Coil power density optimization and trade-off study for a 100 kW electric vehicle IPT wireless charging system," in *Proc. IEEE Energy Convers. Congr. Expo. (ECCE)*, Sep. 2018, pp. 1196–1201, doi: 10.1109/ECCE.2018.8557490.

[279] *A Joint Stock Limited Company Incorporated in the People's Republic of China With Limited Liability, Announcement Launch of the First Pre-Commercial Bus Route in China Deploying Buses With High-Power Wireless-Charging System*, ZTE Corp., Shenzhen, China, 2014.

[280] A. Calabro, B. Cohen, A. Daga, J. Miller, and F. McMahon, "Performance of 200-kW inductive charging system for range extension of electric transit buses," in *Proc. IEEE Transp. Electrific. Conf. Expo (ITEC)*, Jun. 2019, pp. 1–5, doi: 10.1109/ITEC.2019.8790490.

[281] *ENRX I Revolutionizing Smart Energy Transfer*. Accessed: Mar. 28, 2023. [Online]. Available: https://www.enrx.com/?x-redirected=1

[282] *ENRX I Electric Roadway: Dynamic Wireless Charging*. Accessed: Mar. 28, 2023. [Online]. Available: https://www.enrx.com/Products/Charge-and-power-products/Electric-roadway?x-redirected=1

[283] H. T. Nguyen, J. Y. Alsawalhi, K. A. Hosani, A. S. Al-Sumaiti, K. A. A. Jaafari, Y.-J. Byon, and M. S. E. Moursi, "Review map of comparative designs for wireless high-power transfer systems in EV applications: Maximum efficiency, ZPA, and CC/CV modes at fixed resonance frequency independent from coupling coefficient," *IEEE Trans. Power Electron.*, vol. 37, no. 4, pp. 4857–4876, Apr. 2022, doi: 10.1109/TPEL.2021.3124293.

[284] V. Shevchenko, O. Husev, R. Strzelecki, B. Pakhaliuk, N. Poliakov, and N. Strzelecka, "Compensation topologies in IPT systems: Standards, requirements, classification, analysis, comparison and application," *IEEE Access*, vol. 7, pp. 120559–120580, 2019, doi: 10.1109/ACCESS.2019.2937891.

[285] M. Petersen and F. W. Fuchs, "Investigation on power electronics topologies for inductive power transfer (IPT) systems in high power low voltage applications," in *Proc. 17th Eur. Conf. Power Electron. Appl. (EPE ECCE-Europe)*, Sep. 2015, pp. 1–10, doi: 10.1109/EPE.2015.7309132.

[286] C. Zheng, J.-S. Lai, R. Chen, W. E. Faraci, Z. U. Zahid, B. Gu, L. Zhang, G. Lisi, and D. Anderson, "High-efficiency contactless power transfer system for electric vehicle battery charging application," *IEEE J. Emerg. Sel. Topics Power Electron.*, vol. 3, no. 1, pp. 65–74, Mar. 2015, doi: 10.1109/JESTPE.2014.2339279.

[287] H. Movagharnejad and A. Mertens, "Design metrics of compensation methods for contactless charging of electric vehicles," in *Proc. 19th Eur. Conf. Power Electron. Appl. (EPE ECCE Europe)*, Sep. 2017, pp. P.1–P.10, doi: 10.23919/EPE17ECCEEurope.2017.8099403.

[288] V.-T. Nguyen, V.-B. Vu, G. Gohil, and B. Fahimi, "Efficiency optimization of double-sided LCC topology for inductive power transfer systems," in *Proc. IEEE Appl. Power Electron. Conf. Expo. (APEC)*, Jun. 2021, pp. 1610–1617, doi: 10.1109/APEC42165.2021.9487207.

[289] V.-T. Nguyen, V.-B. Vu, G. Gohil, and B. Fahimi, "Coil-to-coil efficiency optimization of double-sided LCC topology for electric vehicle inductive chargers," *IEEE Trans. Ind. Electron.*, vol. 69, no. 11, pp. 11242–11252, Nov. 2022, doi: 10.1109/TIE.2021.3118343.

[290] *Wireless Power Transfer for Light-Duty Plug-In EVs and Alignment Methodology*, SAE Int., Warrendale, PA, USA, 2017.

[291] *Wireless Power Transfer for Light-Duty Plug-In/Electric Vehicles and Alignment Methodology*, Apr. 2019, doi: 10.4271/J2954_201904.

[292] *Electric Vehicle Wireless Power Transfer (WPT) Systems—Part 3: Specific*, Standard IEC TS 61980-3:2019. Accessed: Mar. 28, 2023. [Online]. Available: https://standards.iteh.ai/catalog/standards/iec/f269b49e-bb9c-4ef1-996c-c60b08fb20da/iec-ts-61980-3-2019

[293] *Homepage | Wireless Power Consortium*. Accessed: Mar. 28, 2023. [Online]. Available: https://www.wirelesspowerconsortium.com/

[294] M. A. Houran, X. Yang, and W. Chen, "Magnetically coupled resonance WPT: Review of compensation topologies, resonator structures with misalignment, and EMI diagnostics," *Electronics*, vol. 7, no. 11, p. 296, Nov. 2018, doi: 10.3390/electronics7110296.

[295] G. Ziegelberger, R. Croft, M. Feychting, A. C. Green, A. Hirata, G. d'Inzeo, K. Jokela, S. Loughran, C. Marino, S. Miller, G. Oftedal, T. Okuno, E. van Rongen, M. Röösli, Z. Sienkiewicz, J. E. H. Tattersall, and S. Watanabe, "Guidelines for limiting exposure to electromagnetic fields (100 kHz to 300 GHz)," *Health Phys.*, vol. 118, no. 5, pp. 483–524, 2020, doi: 10.1097/HP.0000000000001210.

[296] *IEEE Standard for Military Workplaces—Force Health Protection Regarding Personnel Exposure to Electric, Magnetic, and Electromagnetic Fields, 0 Hz to 300 GHz*, IEEE Standard PC95.1-2345/D6.9, Mar. 2014, pp. 1–78.

[297] I.-S. Suh and J. Kim, "Electric vehicle on-road dynamic charging system with wireless power transfer technology," in *Proc. Int. Electr. Mach. Drives Conf.*, May 2013, pp. 234–240, doi: 10.1109/IEMDC.2013.6556258.

[298] C. Li, X. Dong, L. M. Cipcigan, M. A. Haddad, M. Sun, J. Liang, and W. Ming, "Economic viability of dynamic wireless charging technology for private EVs," *IEEE Trans. Transport. Electrific.*, vol. 9, no. 1, pp. 1845–1856, Mar. 2023, doi: 10.1109/TTE.2022.3163823.

[299] P. Lazzeroni, V. Cirimele, and A. Canova, "Economic and environmental sustainability of dynamic wireless power transfer for electric vehicles supporting reduction of local air pollutant emissions," *Renew. Sustain. Energy Rev.*, vol. 138, Mar. 2021, Art. no. 110537, doi: 10.1016/j.rser.2020.110537.

[300] S. Jeong, Y. J. Jang, and D. Kum, "Economic analysis of the dynamic charging electric vehicle," *IEEE Trans. Power Electron.*, vol. 30, no. 11, pp. 6368–6377, Nov. 2015, doi: 10.1109/TPEL.2015.2424712.

[301] J. M. Miller, P. T. Jones, J.-M. Li, and O. C. Onar, "ORNL experience and challenges facing dynamic wireless power charging of EV's," *IEEE Circuits Syst. Mag.*, vol. 15, no. 2, pp. 40–53, 2nd Quart., 2015, doi: 10.1109/MCAS.2015.2419012.

[302] P. Jain and T. Jain, "Impacts of G2V and V2G power on electricity demand profile," in *Proc. IEEE Int. Electric Vehicle Conf. (IEVC)*, Dec. 2014, pp. 1–8, doi: 10.1109/IEVC.2014.7056148.

[303] S. Ruddell, U. K. Madawala, and D. J. Thrimawithana, "Dynamic WPT system for EV charging with integrated energy storage," *IET Power Electron.*, vol. 12, no. 10, pp. 2660–2668, Aug. 2019, doi: 10.1049/iet-pel.2018.5848.
[304] T. Kan, R. Mai, P. P. Mercier, and C. Mi, "A three-phase wireless charging system for lightweight autonomous underwater vehicles," in *Proc. IEEE Appl. Power Electron. Conf. Expo. (APEC)*, Mar. 2017, pp. 1407–1411, doi: 10.1109/APEC.2017.7930881.
[305] T. Kan, R. Mai, P. P. Mercier, and C. C. Mi, "Design and analysis of a three-phase wireless charging system for lightweight autonomous underwater vehicles," *IEEE Trans. Power Electron.*, vol. 33, no. 8, pp. 6622–6632, Aug. 2018, doi: 10.1109/TPEL.2017.2757015.
[306] S. Aldhaher, P. D. Mitcheson, J. M. Arteaga, G. Kkelis, and D. C. Yates, "Light-weight wireless power transfer for mid-air charging of drones," in *Proc. 11th Eur. Conf. Antennas Propag. (EUCAP)*, Mar. 2017, pp. 336–340, doi: 10.23919/EuCAP.2017.7928799.
[307] K. Mainali, R. Wang, J. Sabate, Y. Veer Singh, and S. Klopman, "Design of gate drive power supply with air core transformer for high dv/dt switching," in *Proc. IEEE Energy Convers. Congr. Expo. (ECCE)*, Sep. 2018, pp. 5479–5484, doi: 10.1109/ECCE.2018.8558054.
[308] Z. Kashani, S. J. Ilham, and M. Kiani, "Design and optimization of ultrasonic links with phased arrays for wireless power transmission to biomedical implants," *IEEE Trans. Biomed. Circuits Syst.*, vol. 16, no. 1, pp. 64–78, Feb. 2022, doi: 10.1109/TBCAS.2022.3140591.
[309] W. Zhou and K. Jin, "Optimal photovoltaic array configuration under Gaussian laser beam condition for wireless power transmission," *IEEE Trans. Power Electron.*, vol. 32, no. 5, pp. 3662–3672, May 2017, doi: 10.1109/TPEL.2016.2583502.
[310] M. Meng and M. Kiani, "Design and optimization of ultrasonic wireless power transmission links for millimeter-sized biomedical implants," *IEEE Trans. Biomed. Circuits Syst.*, vol. 11, no. 1, pp. 98–107, Feb. 2017, doi: 10.1109/TBCAS.2016.2583783.
[311] V. Cirimele, R. Torchio, A. Virgillito, F. Freschi, and P. Alotto, "Challenges in the electromagnetic modeling of road embedded wireless power transfer," *Energies*, vol. 12, no. 14, p. 2677, Jul. 2019, doi: 10.3390/en12142677.
[312] F. Chen, N. Taylor, R. Balieu, and N. Kringos, "Dynamic application of the inductive power transfer (IPT) systems in an electrified road: Dielectric power loss due to pavement materials," *Construct. Building Mater.*, vol. 147, pp. 9–16, Aug. 2017, doi: 10.1016/j.conbuildmat.2017.04.149.
[313] R. Tavakoli, A. Echols, U. Pratik, Z. Pantic, F. Pozo, A. Malakooti, and M. Maguire, "Magnetizable concrete composite materials for road-embedded wireless power transfer pads," in *Proc. IEEE Energy Convers. Congr. Expo. (ECCE)*, Oct. 2017, pp. 4041–4048, doi: 10.1109/ECCE.2017.8096705.
[314] Y. Yamada, S. Hasegawa, T. Imura, and Y. Hori, "Design method of coreless coil considering power, efficiency and magnetic field leakage in wireless power transfer," in *Proc. 48th Annu. Conf. IEEE Ind. Electron. Soc. (IECON)*, Oct. 2022, pp. 1–6, doi: 10.1109/IECON49645.2022.9968782.
[315] D. Trinko, N. Horesh, R. Zane, Z. Song, A. Kamineni, T. Konstantinou, K. Gkritza, C. Quinn, T. H. Bradley, and J. C. Quinn, "Economic feasibility of in-motion wireless power transfer in a high-density traffic corridor," *eTransportation*, vol. 11, Feb. 2022, Art. no. 100154, doi: 10.1016/j.etran.2021.100154.
[316] B. Marmiroli, G. Dotelli, and E. Spessa, "Life cycle assessment of an on-road dynamic charging infrastructure," *Appl. Sci.*, vol. 9, no. 15, p. 3117, Aug. 2019, doi: 10.3390/app9153117.
[317] B. J. Limb, Z. D. Asher, T. H. Bradley, E. Sproul, D. A. Trinko, B. Crabb, R. Zane, and J. C. Quinn, "Economic viability and environmental impact of in-motion wireless power transfer," *IEEE Trans. Transport. Electrific.*, vol. 5, no. 1, pp. 135–146, Mar. 2019, doi: 10.1109/TTE.2018.2876067.
[318] W. Zhang, J. C. White, A. M. Abraham, and C. C. Mi, "Loosely coupled transformer structure and interoperability study for EV wireless charging systems," *IEEE Trans. Power Electron.*, vol. 30, no. 11, pp. 6356–6367, Nov. 2015, doi: 10.1109/TPEL.2015.2433678.
[319] W. C. Brown, "The history of power transmission by radio waves," *IEEE Trans. Microw. Theory Techn.*, vol. MTT-32, no. 9, pp. 1230–1242, Sep. 1984.

AMRITANSH SAGAR (Student Member, IEEE) was born in Saharsa, India. He received the B.Tech. degree in electrical and electronics engineering from the Birla Institute of Technology, Mesra, Jharkhand, India, in 2011, and the M.Tech. degree in power electronics and drives from the Sardar Vallabhbhai National Institute of Technology, Surat, India, in 2017. He is currently pursuing the Ph.D. degree with the Department of Industrial Engineering, University of Padua, Padua, Italy.

From August 2017 to December 2018, he was an Assistant Professor with Silver Oak University, Ahmedabad. From March 2019 to June 2020, he was a Junior Research Fellow with VIT, Vellore, India. He joined the University of Padua, in October 2020. His research interests include wireless power transfer, and modeling, design, and control of power.

ARUN KASHYAP was born in Kashipur, Uttarakhand, India, in March 1983. He received the B.Tech. degree in computer science and engineering from Uttar Pradesh Technical University, India, in 2007, and the M.Tech. degree in computer science and engineering from Teerthankar Mahaveer University, Uttar Pradesh, India, in 2013. He was an Assistant Professor in different universities and colleges across India. He has collaborated actively with researchers in several other disciplines of computer science and engineering. His research interests include electrical vehicles and artificial intelligence techniques.

MORTEZA AZIMI NASAB (Member, IEEE) received the B.Sc. and M.Sc. degrees in electrical power engineering from Islamic Azad University, Tehran Branch, Tehran, Iran, in 2014 and 2017, respectively. He is currently a University Lecturer with the University of Applied Sciences and Technology, Tehran, and an External Researcher with the Department of Electrical Engineering, Information Technology and Cybernetic, University of South-Eastern Norway, Norway. He has authored or coauthored more than 25 scientific papers in international journals and conferences. He has also published a book and coauthored ten book chapters. His main research interests include renewable energy technologies, partial shaded PV, MPPT algorithms, smart cities, smart grids, electric vehicles, and fault location. Since June 2020, he has been a reviewer of several high-quality journals.

SANJEEVIKUMAR PADMANABAN (Senior Member, IEEE) received the Ph.D. degree in electrical engineering from the University of Bologna, Bologna, Italy, in 2012.

He is a Full Professor in Electrical Power Engineering with the Department of Electrical Engineering, Information Technology, and Cybernetics, University of South-Eastern Norway, Norway. He has authored over 750+ scientific papers. He is a Fellow of the Institution of Engineers, India, the Institution of Electronics and Telecommunication Engineers, India, and the Institution of Engineering and Technology, U.K. He received a lifetime achievement award from Marquis Who's Who - USA 2017 for contributing to power electronics and renewable energy research. He is listed among the world's top 2 scientists (from 2019) by Stanford University USA. He received the Best Paper cum Most Excellence Research Paper Award from IET-SEISCON'13, IET-CEAT'16, IEEE-EECSI'19, IEEE-CENCON'19, and five best paper awards from ETAEERE'16 sponsored Lecture Notes in Electrical Engineering, Springer book. He is an Editor/Associate Editor/Editorial Board for refereed journals, in particular the IEEE Systems Journal, IEEE Transaction on Industry Applications, IEEE Access,

IET Power Electronics, *IET Electronics Letters*, and Wiley-*International Transactions on Electrical Energy Systems*, Subject Editorial Board Member–*Energy Sources–Energies Journal, MDPI*, and the Subject Editor for the *IET Renewable Power Generation, IET Generation, Transmission and Distribution, and FACETS Journal* (Canada).

Dr. Padmanaban is a fellow of the Institution of Engineers, India, the Institution of Electronics and Telecommunication Engineers, India, and the Institution of Engineering and Technology, U.K. He received the Best Paper cum Most Excellence Research Paper Award from IET-SEISCON 2013, IET-CEAT 2016, IEEE-EECSI 2019, and IEEE-CENCON 2019, and five best paper awards from ETAEERE 2016 sponsored *Lecture Notes in Electrical Engineering*, Springer book. He received the Lifetime Achievement Award from Marquis Who's Who-USA 2017 for contributing to power electronics and renewable energy research. He is listed among the world's top 2% scientists (since 2019) by Stanford University, USA.

MANUELE BERTOLUZZO received the M.S. degree in electronic engineering and the Ph.D. degree in industrial electronics and computer science from the University of Padua, Padua, Italy, in 1993 and 1997, respectively.

In 2000, he joined the Scientific Disciplines' Group Electric Converters, Machines, and Drives, Department of Industrial Engineering, University of Padua, as a Researcher. Since 2015, he has been an Associate Professor and holds the lectureship of road electric vehicles and systems for automation for the master's degree in electric engineering. He is involved in the analysis and design of power electronics systems, especially for wireless charging of electric vehicle batteries.

ABHAY KUMAR received the B.Tech. degree in electrical engineering from DRIEMS, Cuttack, India, in 2012, and the M.E. degree in electrical engineering with specialization in power electronics from the BIT Mesra, Ranchi, India, in 2014. He is currently pursuing the Ph.D. degree with the University of Padua, Italy.

He was an Assistant Professor with NPSEI, Pithoragarh, India, from 2014 to 2019. His research interests include power electronics and control systems for power electronics converters, and wireless charging of electric vehicles.

FREDE BLAABJERG (Fellow, IEEE) received the Ph.D. degree in electrical engineering from Aalborg University, in 1995.

He was with ABB-Scandia, Randers, Denmark, from 1987 to 1988. He became an Assistant Professor, in 1992, an Associate Professor, in 1996, and a Full Professor of power electronics and drives at the Department of Energy, Aalborg University, Aalborg, Denmark, in 1998. Since 2017, he has been a Villum Investigator. He is currently an Honoris Causa with Politehnica University Timisoara (UPT), Romania, and Tallinn Technical University (TTU), Estonia. He has published more than 600 journal articles in the fields of power electronics and its applications. He is the coauthor of four monographs and the editor of ten books on power electronics and its applications. His current research interests include power electronics and its applications, such as wind turbines, PV systems, reliability, harmonics, and adjustable speed drives.

Dr. Blaabjerg has received 32 IEEE prize paper awards, the IEEE PELS Distinguished Service Award, in 2009, the EPE-PEMC Council Award, in 2010, the IEEE William E. Newell Power Electronics Award, in 2014, the Villum Kann Rasmussen Research Award, in 2014, the Global Energy Prize, in 2019, and the 2020 IEEE Edison Medal. From 2019 to 2020, he was the President of the IEEE Power Electronics Society. He is the Vice-President of the Danish Academy of Technical Sciences. He was nominated in 2014–2019 by Thomson Reuters to be among the most 250 cited researchers in engineering in the world. He was the Editor-in-Chief of the IEEE TRANSACTIONS ON POWER ELECTRONICS, from 2006 to 2012. He has been a Distinguished Lecturer of the IEEE Power Electronics Society, from 2005 to 2007, and the IEEE Industry Applications Society, from 2010 to 2011 as well as from 2017 to 2018.

Open Access funding provided by 'Università degli Studi di Padova' within the CRUI CARE Agreement